



<https://theses.gla.ac.uk/>

Theses Digitisation:

<https://www.gla.ac.uk/myglasgow/research/enlighten/theses/digitisation/>

This is a digitised version of the original print thesis.

Copyright and moral rights for this work are retained by the author

A copy can be downloaded for personal non-commercial research or study,  
without prior permission or charge

This work cannot be reproduced or quoted extensively from without first  
obtaining permission in writing from the author

The content must not be changed in any way or sold commercially in any  
format or medium without the formal permission of the author

When referring to this work, full bibliographic details including the author,  
title, awarding institution and date of the thesis must be given

Enlighten: Theses

<https://theses.gla.ac.uk/>  
[research-enlighten@glasgow.ac.uk](mailto:research-enlighten@glasgow.ac.uk)

High Energy Photoproton Investigations Using  
a Counter-Controlled Cloud Chamber

by

Robert McI. Turnbull

Department of Natural Philosophy,

University of Glasgow.

Presented as a thesis for the degree of Ph.D. in the University  
of Glasgow, November, 1960.

ProQuest Number: 10656235

All rights reserved

INFORMATION TO ALL USERS

The quality of this reproduction is dependent upon the quality of the copy submitted.

In the unlikely event that the author did not send a complete manuscript and there are missing pages, these will be noted. Also, if material had to be removed, a note will indicate the deletion.



ProQuest 10656235

Published by ProQuest LLC (2017). Copyright of the Dissertation is held by the Author.

All rights reserved.

This work is protected against unauthorized copying under Title 17, United States Code  
Microform Edition © ProQuest LLC.

ProQuest LLC.  
789 East Eisenhower Parkway  
P.O. Box 1346  
Ann Arbor, MI 48106 – 1346

Preface.

This thesis describes an investigation by the author of the production of high energy photoprotons from oxygen gas by a triggered cloud chamber technique. An experiment in which this technique is applied to the measurement of the polarization of the photoprotons from carbon is also included.

When the author started his research in October 1957 he joined Mr J.M. Reid and Mr B. Lalovic in work on the development of a triggered cloud chamber for use with the 300 MeV electron synchrotron at Glasgow University. At that time, although most of the instrumentation and cloud chamber equipment had been constructed, no complete experiment had been attempted and many improvements still had to be made. In December 1957 and again in March 1958 the author assisted Mr Reid and Mr Lalovic in experiments on the photodisintegration of helium, neon and nitrogen. Although the equipment was capable of yielding results, experiments could only be performed with difficulty. The author therefore spent considerable time on modifications which are described in Chapter II.

The experiment on the photodisintegration of oxygen in March 1959 which is described in Chapter III was carried out solely by the author who was also entirely responsible for the scanning of the cloud chamber photographs as well as the

analysis and interpretation of the results obtained. The computer programme used for the routine calculations, and given in the Appendix, was written by the author.

In April 1960 an experiment to measure the polarization of photoprotons from carbon by scattering the protons in a carbon block inside the chamber was performed. This experiment, described in Chapter IV, which had been suggested by Dr. J.G. Rutherglen, enabled the angle of scatter to be determined very accurately while still achieving a reasonable counting rate. The author built four of the five scintillation counters used in this experiment and was also responsible for the operation of the cloud chamber. The counter electronics were supplied and operated by Dr. J.G. Rutherglen, Mr J.K. Walker and Mr J.M. Paterson. The analysis of the cloud chamber photographs for this experiment was performed entirely by the author and the interpretation of results was shared with Mr Paterson.

Acknowledgments.

The author is greatly indebted to Mr J.M. Reid for his close supervision throughout this period of research, to Mr B. Lalovic for much advice during the first year and also to Mr A. McLeod who assisted with the apparatus preceding and during the polarization experiment. He would also like to express his appreciation of the collaboration of Dr. Rutherglen, Mr Walker and Mr Paterson in the work on polarization.

Thanks are also due to Dr. W. McFarlane and his staff for operating the synchrotron during the experimental runs and to Mr Lloyd and his technical staff who provided valuable assistance on various occasions.

The author is grateful to Professor P.I. Dee for his interest and encouragement during the above research.

Finally the author would like to express his appreciation to the Trustees of Sir James Caird's Travelling Scholarships Trust for the award of a scholarship for the period of his research and also a travel grant to enable him to visit the 1960 Karlsruhe Photonuclear Conference where many valuable discussions with other workers in the same field of research took place.

# Contents.

## Section A High Energy Photodisintegration and the "Quasi-Deuteron" Model.

### Page

Chapter I	Introduction	1
1.1.	Historical	1
1.2.	Experimental Results for $E_{\gamma} < 30$ MeV	4
1.2.a.	General	4
1.2.b.	Photodisintegration of Oxygen	6
1.3.	Theories of the Nuclear Photoeffect for $E_{\gamma} < 30$ MeV	8
1.4.	High Energy Photodisintegration	13
	Preliminary Discussion	13
1.4.A.	Photodisintegration of the Deuteron	15
1.4.A.1.	Experimental Investigations	16
1.4.A.2.	Experimental and Theoretical Results	17
1.4.B.	Photodisintegration of Complex Nuclei at High Energies	24
1.4.B.1.	Photoproton Production	24
1.4.B.2.	Photostar Production	27
1.4.B.3.	Photoneutron Production	29
1.4.B.4.	The "Quasi-Deuteron" Model	31
1.4.B.5.	Experimental Evidence for the "Quasi-Deuteron" Model	34
1.4.B.6.	Proton-Proton Coincidences	37
1.4.B.7.	Photodeuteron Production	38

## Contents (Contd.)

	<u>Page</u>
I.4.B.8. Further Theoretical Investigations of the High Energy Photoeffect.	39
I.4.B.9. Extension of the "Quasi-Deuteron" Model to the Region below 150 MeV.	42
I.4.B.10. Limitations of the Previous Experiments.	45
Chapter II. Instrumentation	49
II.1. The Cloud Chamber and Related Equipment.	49
II.1.1. The Operation of a Wilson Expansion Chamber	49
II.1.2. The Cloud Chamber	51
II.1.3. Illumination	52
II.1.4. Clearing Field Grids.	53
II.1.5. Expansion Mechanism	54
II.1.6. Trigger Unit for Three-Electrode Spark Gap.	56
II.1.7. High Voltage Unit for Three-Electrode Spark Gap.	57
II.1.8. Speed of Expansion.	58
II.1.9. Resetting of the Expansion Valve.	59
II.1.10. Cameras and Photography.	60
II.2. Counters and Associated Electronics Used in the Experiment on photo-disintegration of oxygen.	62
II.2.1. Counters.	62
II.2.2. Coincidence Circuits.	62
II.2.3. Counter Electronics.	62

Contents (Contd.)

	<u>Page</u>
Chapter III	The Photodisintegration of Oxygen. 64
III.1.	Experimental Arrangement. 64
III.2.	Measurement of the Cloud Chamber Tracks. 65
III.3.	Beam Monitor. 66
III.4.	Calculation of Results. 66
III.5.	Experimental Results. 68
III.5.1.	Classification of Events. 68
III.5.2.	Proton Angular Distributions. 81
III.5.3.	Neutron Angular Distributions. 84
III.5.4.	Gamma-Ray Energy Distributions. 85
III.5.5.	Excitation Energy Distributions. 87
III.5.6.	Neutron Energy Distributions. 90
III.5.7.	Recoil Range Distribution. 93
III.5.8.	Possible Proton-Proton Coincidences. 94
	Concluding Remarks. 95
Chapter IV.	Discussion of Photodisintegration Results. 96
IV.1.	The Impulse and Closure Approximations. 96
(a)	The Impulse Approximation. 96
(b)	The Closure Approximation. 97
IV.2.	( $\gamma, p$ ) Events. 98
IV.3.	Emission of Two Fast Particles. 100

Contents (Contd.)

	<u>Page</u>
Chapter IV.4.	Internal Nucleon Scattering. 102
IV.5.	Momentum of "Quasi-Deuterons". 106
IV.6.	Future Experiments. 111
Section B.	The Polarization of Photonucleons.
Chapter V.	Introduction 113
V.1.	Polarization Effects in Nucleon-Nucleus Scattering. 113
V.2.	The Polarization of Photonucleons Emitted in Non-Mesonic Processes - Theoretical Investigations. 116
V.3.	The Polarization of Nucleons Emitted in Meson Production. 123
	(a) The Fermi-Yang Solutions. 123
	(b) The Wilson-Peierls Ambiguity 124
V.4.	Experimental Investigations. 125
V.5.	Information Obtainable from Polarization Measurements. 127
Chapter VI.	The Polarization of Photoprotons from Carbon. 128
VI.1.	The Measurement of Polarization. 128
VI.2.	Experimental Arrangement. 130
VI.3.	Cloud Chamber Modifications and Operation. 130
VI.4.	Counters. 132
VI.5.	Counter Electronics. 132
VI.6.	Counter Alignment. 133
VI.7.	Mathematical Analysis of Results. 135
	(a) Maximum Likelihood Calculation. 135
	(b) Carbon Polarization Data. 136

## Contents (Contd.)

	<u>Page</u>
Chapter VI.8.      Experimental Analysis of Events.	137
(a) Measurement System.	137
(b) Reflection Criterion.	137
(c) Track Displacement.	138
(d) Track Distortion.	138
VI.9.            Testing of the Experimental Equipment.	139
VI.10.          Results.	140
VI.11.          Errors.	143
VI.12.          Discussion.	144
Appendix 1      Computer Programme.	A1
Appendix 2      Cloud Chamber Photographs.	A11
References.	

Section A.

High Energy Photodisintegration and the "quasi-deuteron"  
Model.

I.1. Historical:

In the history of the world, the development of the human mind has been a continuous process. It has been shaped by the environment, by the needs of the community, and by the individual's quest for knowledge. The history of the human mind is a story of discovery, of exploration, and of the triumph of the human spirit over the limitations of nature.

Chapter I Introduction.

The history of the human mind is a story of discovery, of exploration, and of the triumph of the human spirit over the limitations of nature. It is a story of the quest for knowledge, of the search for truth, and of the pursuit of the good. The human mind has always been a restless creature, always seeking to understand the world around it, always striving to improve itself and its community. The history of the human mind is a story of the triumph of the human spirit over the limitations of nature.

## Chapter I.

### Introduction.

#### I.1. Historical.

In the development of atomic physics the interaction of electromagnetic radiation with atoms played an indispensable role in the understanding of the structure of the atom. In the case of nuclei, the relevant wavelengths of the electromagnetic radiation are much shorter and the energy determination very inaccurate by spectroscopic standards. Consequently, the interaction of electromagnetic radiation with nuclei has been of less importance than in the corresponding atomic case. However, in spite of this fact there has been considerable research on the subject.

In this thesis only the absorption of gamma-rays by nuclei will be considered. The research described will be concerned with gamma-rays of energy greater than 100 MeV where the low absorption cross-section hinders investigation. In this region data is not extensive, and in addition we are compelled, almost without exception, to use a bremsstrahlung spectrum of gamma-rays, thus resulting in many ambiguities. Our present knowledge of the entire field is illustrated, initially, by a brief description of the low energy

results obtained.

Let us consider the absorption by a nucleus of a gamma-ray or, in the quantum-mechanical interpretation, a light quantum. If the quantum energy,  $h\omega$ , is larger than the separation energy of a constituent of the nucleus such as a proton, a neutron, or an alpha-particle then a  $(\gamma, p)$ ,  $(\gamma, n)$  or  $(\gamma, \alpha)$  process will occur. This is called photodisintegration.

Little advance was seen in the ten years following the discovery of photodisintegration in 1934 by Chadwick and Goldhaber (1) who observed the disintegration of deuterium using the naturally emitted 2.62 MeV gamma-rays from thorium C". In that very year, Szilard and Chalmers (2) observed photoneutrons produced from beryllium by the same source.

Neutron emission from more stable elements requires higher energy gamma-rays and in 1937 Bothe and Gentner (3) achieved this by using protons from an electrostatic generator to excite the 440 KeV resonance in  $\text{Li}^7$  so producing the 17.6 MeV gamma-rays from the  $\text{Li}^7(p, \gamma)\text{Be}^8$  reaction.

The development by Kerst (4) of the betatron provided a much more intense source of photons and a greater range of gamma-ray energies than had been

available from the naturally occurring radioactive elements and so led to more rapid progress in the field. However, the advent of electron accelerators introduced a disadvantage in that only a bremsstrahlung spectrum of gamma-rays could be produced by them in contrast to the line spectra used in all previous experiments.

Photoprotons other than those from deuterium were first observed by Huber et al. (5) in 1944. The absorption of photons by nuclei was demonstrated by Baldwin and Klaiber (6,7) to result in the emission, of not only neutrons and protons but also various aggregates of nucleons such as deuterons, tritons, and alpha-particles. They used a cloud chamber to observe ( $\gamma, \alpha$ ) and multi-particle events and were the first to measure the variation of cross-section with energy. A broad maximum was observed in the ( $\gamma, n$ ) cross-section at about 20 MeV. Weinstock and Halpern (8) later showed that this "giant resonance" always occurred in photon-induced reactions in this low energy region. Examples of this "resonance" can be seen in figure 1.1 which is taken from Jones and Terwilliger (148).

For a gamma-ray energy,  $E_\gamma$ , of less than 25 MeV the wavelength is long compared with the nuclear size

and classical radiation theory will apply. The only transitions of importance will be dipole and quadrupole. The increase in cross-section towards the "resonance" was interpreted as being due to the onset of electric dipole absorption. This was assumed to occur when the excitation of nuclear vibrations resulted in the displacement of the centre of mass from the centre of charge.

## I.2. Experimental Results for $E_\gamma < 30$ MeV.

### I.2.a. General.

The properties of the "giant resonance" vary from element to element. There is some evidence that the width of these maxima is related to the number of neutrons and protons in the nucleus, and Okamoto (9,10) illustrated this by plotting the width against neutron number. A series of minima appear which coincide with the neutron and proton magic numbers. Using a neutron counting technique, Ferrero et al. (11) showed that the relationship between abnormally large "resonance" widths and deformed nuclei may be due to the existence of a double peak. However, as demonstrated by Carver and Turchinets (12) the second maximum may be caused by the

onset of the  $(\gamma, 2n)$  reaction.

The value of gamma-ray energy at which peak cross-section occurs ranges from 11 MeV for Bi (13) to 26 MeV for He (14) and varies approximately as  $A^{-1/3}$  (15).

The total photon absorption cross-section is of the order of several tens of millibarns for the light elements at the peak of the "resonance" and falls to a few millibarns in the region beyond the maximum.

The integrated cross-section is found to be approximately proportional to  $A$ .

The photonuclear cross-section is largely accounted for by the emission of single nucleons in the region below 30 MeV. In the case of the light elements, neutrons and protons are emitted with approximately equal probabilities but for the heavier elements ( $A > 30$ ), neutron emission predominates. Multi-particle emission is much more probable for gamma-ray energies of greater than 50 MeV.

For the light elements, a smaller resonance in photon absorption is occasionally found at a lower energy than that of the "giant resonance" and may be attributed to quadrupole as distinct from dipole

absorption.

In the  $(\gamma, n)$  work using betatrons, well-defined discontinuities in the slope of the activation curve were obtained. This fine structure was interpreted as resulting from absorption of photons into well-defined levels of the target nucleus. The reactions may be regarded as being the inverse of the radiative capture of light particles by light nuclei. The energy spectra of emitted photonucleons also exhibits this fine structure. Groups of photonucleons with energies corresponding to the excitation of various levels in the residual nucleus have been observed.

#### I.2.b. The Photodisintegration of Oxygen.

Many of these phenomena are observed in the photodisintegration of oxygen which has been the subject of considerable theoretical and experimental investigation and is one of the most interesting nuclei that can be studied. The fact that  $O^{16}$  is doubly magic offers simplicities to the theoretician. Furthermore, none of the nuclei  $O^{16}$ ,  $O^{15}$ , or  $N^{15}$  (the last two being the final nuclei from the  $O^{16}(\gamma, n)$  and the  $O^{16}(\gamma, p)$  reactions) have excited states below 5 MeV. The experimenter thus gains some practical advantage.

Since the early work of Waffler and Younis (16) who used the emulsion technique to examine the  $(\gamma, p)$ ,  $(\gamma, n)$  and  $(\gamma, \alpha)$  reactions in oxygen for gamma-ray energies up to 20 MeV, considerable effort (17-52) has been expended in examining the various possible disintegrations of the oxygen nucleus in the "giant resonance" region.

Almost without exception, the photographic plate method has been used for the investigation of the reaction  $O^{16}(\gamma, p)N^{15}$  (17-29). Much of this work indicated several peaks in the  $(\gamma, p)$  excitation function in the region below the main "resonance" in a manner similar to that described in the previous section.

Corresponding resonances are also obtained when the  $(\gamma, n)$  cross-section curve is determined either by measuring the  $\beta^+$  activity in the residual  $O^{15}$  nucleus or by counting neutrons with a  $BF_3$  counter embedded in paraffin wax (30-41). Of these two methods, the former is probably more reliable since, using a neutron detector, the  $(\gamma, 2n)$ ,  $(\gamma, pn)$ ,  $(\gamma, p2n)$ ,  $(\gamma, 3n)$  etc. reactions, may give rise to spurious effects.

Recently, the  $N^{15}(p, \gamma)O^{16}$  reaction has been employed (42, 43) to observe the fine structure in the "resonance" region. Protons of well-defined energy give

rise to preferential emission of gamma-rays, which are detected by NaI crystals, at specific proton energies. The results correspond reasonably with those of the  $(\gamma, p)$  reactions.

The  $O^{16}(\gamma, \alpha)C^{12}$  (25, 44-46) and the  $O^{16}(\gamma, 4\alpha)$  (47-49) reactions have been studied using emulsions.

Using NaI crystals to detect the gamma-rays from the  $O^{16}(\gamma, p\gamma')N^{15}$  and  $O^{16}(\gamma, n\gamma')O^{15}$  reactions, the states of the  $O^{15}$  and  $N^{15}$  nuclei have been examined (50, 51). Recently Jones et al. (52) have used the  $N^{15}(p, n)O^{15}$  reaction to find the location and spin of the excited states of  $O^{16}$ . The latter method gives results in moderate agreement with those obtained from the  $(\gamma, n)$  approach.

### I.3. Theories of the Nuclear Photo-effect for $E_\gamma < 30$ MeV.

As long as the wavelength,  $\lambda$ , for the incident photons is long compared with the nuclear diameter, classical radiation theory may be applied to the nuclear photon absorption. We would then expect magnetic multipole absorption to be reduced in intensity in relation to electric multipole absorption of the same

order in the ratio  $\sim \left(\frac{\hbar}{McR}\right)^2$  and multipole absorption to be small compared with dipole absorption. Thus electric dipole absorption should account for almost all the observed effects in the "giant resonance" region. However, for gamma-ray energies of less than about 10 MeV for heavy nuclei and about 15 MeV for light nuclei the strong correlations between nucleons inside the nucleus make it difficult to effect the separation between the nuclear centres of mass and of charge which is necessary for dipole absorption to occur. In this region quadrupole absorption may be expected to take place.

Levinger and Bethe (54-57) have shown that, if the forces between nucleons can be described by a potential with no particular exchange properties then, by applying the electromagnetic sum rules, the total integrated cross-section for electric dipole absorption is represented by

$$\int_0^{\infty} \sigma(k) dk = \frac{2\pi^2 e^2 \hbar}{Mc} \cdot \frac{NZ}{A} \text{ mev - barns.}$$

This formula requires modification when exchange forces between nucleons are assumed. Levinger finds that the above result must be multiplied by a factor  $(1 + 0.8x)$  where  $x$  is the fraction of exchange force

in the neutron-proton interaction when an independent particle model of the nucleus is taken. The calculated result is of the same order of magnitude as the experimental value. It therefore seems reasonable to assume that electric dipole absorption predominates.

In order to account for the detailed variation of cross-section with energy some correlation between the nucleons in the nucleus is necessary and various models have been proposed.

Goldhaber and Teller (58) suggested a model in which all the protons in the nucleus were assumed to move collectively in one direction while all the neutrons moved in the opposite direction. The displacement of the neutron and proton centres of gravity resulted in dipole oscillations with fixed resonance frequencies. The value of  $E_{\max}$  corresponding to the resonance frequency, determined by the magnitude of the restoring force, was estimated to be proportional to  $A^{-1/6}$  and the result for the integrated cross-section was similar to that of Levinger and Bethe with no exchange force. The width of the resonance was interpreted as a frictional effect between the nucleons.

Steinwedel and Jensen (59), and Danos (60-62) have studied the Goldhaber and Teller collective model

in greater detail and regard the neutrons and protons as compressible fluids constrained within the nucleus. The value of  $E_{\max}$  is then found to vary as  $A^{-1/3}$ .

A reasonably complete description of the photo-effect in light nuclei has been given by Wilkinson (63,64) using an independent particle model, in which bonds between the nucleons are weak, and relating the absorption to shell model states in the nucleus.

When a nucleon in a free orbit in the ground state of the target nucleus absorbs a gamma-ray quantum it is elevated to a higher shell model orbit. The excited nucleon remains in its orbit until a collision with other nucleons causes it to share its energy with the whole nucleus. If the nucleons are emitted before the interaction takes place a direct photoprocess occurs; otherwise a compound nucleus formation results.

A previous calculation by Courant (65) gave a smaller value for the ratio of direct to compound nucleus effects than the shell model theory but was particularly successful in accounting for the relatively large number of high energy photoprotons emitted in comparison with photoneutrons.

Both the collective model and the shell model explain several general features of the nuclear photo-

effect. Each can forecast the values of

- (a)  $E_m$ , the gamma-ray energy at peak cross-section
- (b)  $\Gamma$ , the total width of the resonance at half of the peak value.
- (c)  $\int \sigma(k) dk$ , the integrated cross-section.

The prediction of cross-section is not unexpected since this may be derived from the sum rules alone and is not sensitive to the nuclear model chosen. The shell model is more successful in predicting the angular distributions of photonucleons and emission processes at higher energy.

Brink (66) has demonstrated that the collective model and shell model are identical if the nuclear potential is described by a harmonic oscillator potential. In this case the independent particle model wavefunction already includes collective motion. The relationship between the two models has also been discussed by Levinger (67).

Theoretical work on the  $O^{16}$  nucleus in the "giant resonance" region by Elliott and Flowers (53) provides support for Wilkinson's theory. Agreement with Wilkinson is also achieved by Brown and Levinger (68) using dispersion theory.

#### I.4. High Energy Photodisintegration.

##### Preliminary Discussion.

At energies greater than about 40 MeV both the collective model and shell model lose their usefulness. As seen in the work of Sugarman and Peters (69) who measured the activity of the product after irradiating Bi with 48 MeV and 86 MeV quanta, the disintegration of the nucleus into many particles becomes much more probable. As the energy increases the wavelength of the gamma-ray becomes short in comparison to the internucleon spacing and interaction with individual nucleons or small groups of nucleons is to be expected. When we consider conservation of energy and momentum the only possible reaction between a gamma-ray and a single nucleon (excluding meson production) is elastic scattering. The cross-section for this reaction is much smaller, however, than that for interaction with a two nucleon subunit. Levinger (70,71) proposed that, for gamma-ray energies greater than 150 MeV, the wavelength would be sufficiently short for the gamma-ray to interact with a two-nucleon subunit in the nucleus. It was well known that electric dipole absorption predominated in the nuclear photoeffect at

these energies; the two nucleon subunit had therefore to be a proton-neutron group as neither a proton-proton nor a neutron-neutron system has a dipole moment. The postulate did not infer that these two nucleon systems existed in the nucleus as deuterons. The only implication was that a strong probability of a proton and a neutron coming together for a time long enough for the gamma-ray to interact with them existed. Such a model would lead one to expect emission from complex nuclei of protons and neutrons in coincidence and at angles governed by the kinematics of deuteron photodisintegration. The correlation will be slightly different from that for deuteron photodisintegration due to the internal momentum of the "quasi-deuterons" in the nucleus and the possibility of the photonucleons interacting with the residual nucleus on their way to the surface. Levinger calculated the cross-section for "quasi-deuteron" photodisintegration in relation to that for the deuteron and showed that they were proportional to each other for small separations of the neutron and proton.

Before examining this model in detail it is therefore convenient to consider the photodisintegration

of the deuteron.

#### I.4.A. Photodisintegration of the Deuteron.

The electron accelerator is the sole source of photons available for experimental investigations of photodisintegration beyond a gamma-ray energy of 30 MeV. As these machines produce a bremsstrahlung spectrum it is preferable to have some means of measuring the gamma-ray energy. In the photodisintegration of the deuteron, as distinct from complex nuclei, the photon energy may be calculated if the angle and energy of one of the emitted nucleons are known. The emitted proton has been the detected photonucleon in nearly all high energy investigations of this particular process.

In the region below 100 MeV the protons are most readily detected using photographic plates. Due to the short range of protons at these energies counter telescopes are not so simple to use.

Above 150 MeV meson production can occur and the kinematics become complicated owing to the existence of a three-body final state. Detectors must therefore be capable of distinguishing protons and mesons and in addition must be situated at angles beyond the kinematic limits of the three-body state for a given value of the maximum energy of the bremsstrahlung

spectrum. Any ambiguity is eliminated by alteration of the maximum photon energy (89).

#### I.4.A.1. Experimental Investigations.

Various combinations of target and detector system have been employed in the many experiments (72-91) performed to investigate photodisintegration of the deuteron.

Probably the best system for investigation of the region below 100 MeV was used by Allen et al. (85, 86) who placed emulsions round a gas target.

Outstanding in the region 150 MeV to 450 MeV are the results of Keck and Tollestrup (89). Indeed, they provide the only measurements above 300 MeV. Because of inelastic scattering of the protons the largest correction to the data occurred in defining the energy of the proton by its range. The use of a gas target considerably reduced this uncertainty in proton energy.

More recently Tatro et al. (91) have extended the measurements of the differential cross-section to  $11^\circ$  in the forward direction and to  $76^\circ$  at backward angles. The cross-section at forward angles agrees with previous measurements or extrapolation of these measurements but an increase occurs in the backward direction (see figure 1.6).

I.4.A.2. Experimental and Theoretical Results.

$$(1) \quad 0 \leq E_{\gamma} \leq 10 \text{ MeV}$$

In the energy range between threshold and 10 MeV the experimental results agree very well with the predictions of theory.

Magnetic dipole transitions between  $^3S$  and  $^1S$  states reach a maximum probability at 65 KeV above threshold and are dominant below 3 MeV. In this region the neutron and proton angular distributions are isotropic. Electric dipole transitions become more frequent just beyond this attaining their maximum at 2.2 MeV above threshold. The angular distribution of the disintegration products is proportional to  $\sin^2\theta$  in the centre of mass system at these energies.

Up to 10 MeV the angular distribution is described by

$$f(\theta) = a + b \sin^2\theta \quad (A)$$

The early calculation of the cross-section by Bethe and Peierls (92) predicted a value of  $1.6 \times 10^{-27} \text{ cm}^2$  for gamma-ray energies of a few MeV. Their calculation has subsequently formed the basis of all more sophisticated discussions of the nuclear photoeffect. The experimentally determined values can be seen in figure 1.2 which is taken from Levinger (100) and it

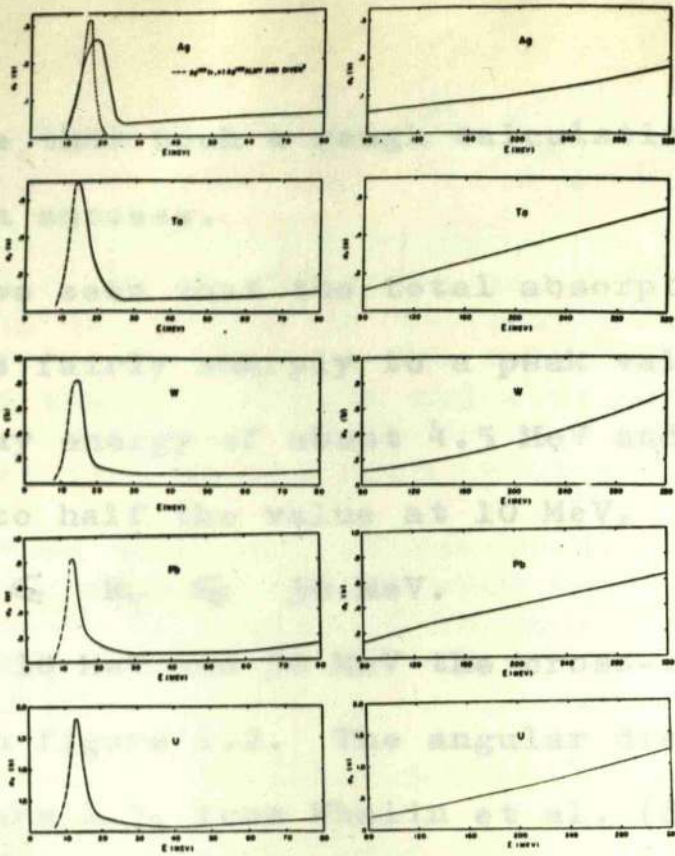
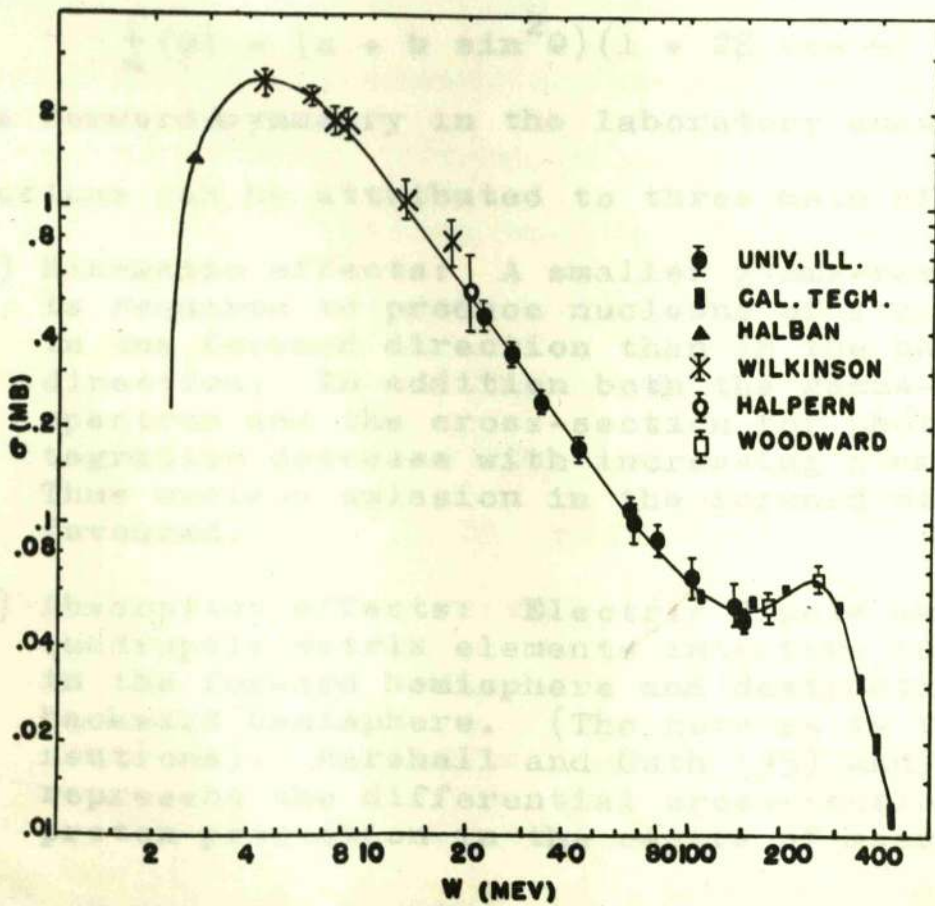


FIG. 1.1.



Experimental measurements of the total cross section, in millibarns, for photodisintegration of the deuteron as a function of photon energy  $W$  (laboratory system).

FIG. 1.2.

is remarkable that such a rough calculation should have achieved such success.

It can be seen that the total absorption cross-section rises fairly sharply to a peak value of  $25 \times 10^{-28} \text{ cm}^2$  at a gamma-ray energy of about 4.5 MeV and drops steadily beyond this to half the value at 10 MeV.

$$(11) \quad 10 \text{ MeV} \leq E_\gamma \leq 50 \text{ MeV}.$$

Between 10 MeV and 50 MeV the cross-section continues to fall as in figure 1.2. The angular distributions, as shown in figure 1.3, from Whalin et al. (83), become peaked at forward angles and can be represented as a function of centre of mass angle by

$$f(\theta) = (a + b \sin^2 \theta)(1 + 2\beta \cos \theta) \quad (B)$$

The forward asymmetry in the laboratory angular distributions can be attributed to three main effects:

- (a) Kinematic effects: A smaller gamma-ray energy is required to produce nucleons of a given energy in the forward direction than in the backward direction. In addition both the gamma-ray spectrum and the cross-section for photodisintegration decrease with increasing gamma-ray energy. Thus nucleon emission in the forward direction is favoured.
- (b) Absorption effects: Electric dipole and electric quadrupole matrix elements interfere constructively in the forward hemisphere and destructively in the backward hemisphere. (The reverse is true for neutrons). Marshall and Guth (95) and Schiff (96) represent the differential cross-section for proton production in the centre of mass system by

$$\frac{d\sigma}{d\Omega} = \frac{3}{8\pi} \sigma_1(\omega) \sin^2 \theta_c \left\{ 1 + \left( 20 \frac{\sigma_2}{\sigma_1} \right)^{1/2} \cos \theta_c + 5 \frac{\sigma_2}{\sigma_1} \cos^2 \theta_c \right\}$$

where  $\theta_c$  is the angle which the proton makes with the photon in the centre of mass system;  $\sigma_1$  and  $\sigma_2$  are the total cross-sections for the electric dipole and electric quadrupole terms respectively. This effect is included in the last term in equation (B).

- (c) Motion of centre of mass: The forward motion of the centre of mass system relative to the laboratory system of co-ordinates due to the photon momentum will shift the angular distribution forward.

In this region the experiments are in substantial agreement with the calculations of Marshall and Guth (93-95) and Schiff (96) who use effective range theory.

$$(111) \quad 50 \text{ MeV} \leq E_\gamma \leq 100 \text{ MeV}.$$

Beyond 50 MeV the trends indicated above continue. Reasonable experimental agreement is achieved on the form of the angular distributions but the absolute values obtained for the cross-sections frequently differ. These variations can be accounted for by uncertain beam calibrations at the various laboratories.

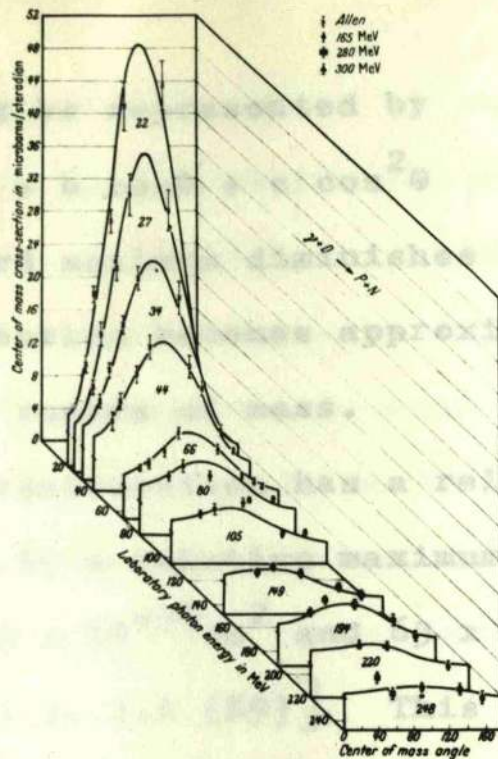
Marshall and Guth (93-95) and Schiff (96) assumed only electric dipole, electric quadrupole and magnetic dipole terms to be involved, and derived the angular distribution and cross-section for gamma-rays between 10 MeV and 160 MeV. The electric dipole contribution was shown to account for more than 90% of the total

cross-section; the magnetic dipole contribution, which could not be obtained reliably without explicit reference to a meson theory of nuclear forces, had little effect on the general trend of the curves.

As the total cross-section derived experimentally is already more than twice the value obtained by Schiff, and Marshall and Guth at 100 MeV further calculations of the cross-section and angular distribution have been made (97-104) to modify the absolute values. Austern (97,98) and Meyer (101) advocate the introduction of meson effects to obtain better agreement with experiment but De Swart and Marshak (103) find it possible to obtain a detailed understanding of the photodisintegration of the deuteron for  $E_\gamma \leq 80$  MeV without introducing virtual meson effects. By assuming a 7% contribution of D-state to the ground state of the deuteron, they can explain the large isotropic term in the angular distributions at these energies. It is usually reckoned that the deuteron spends about 4% of its time in the D-state.

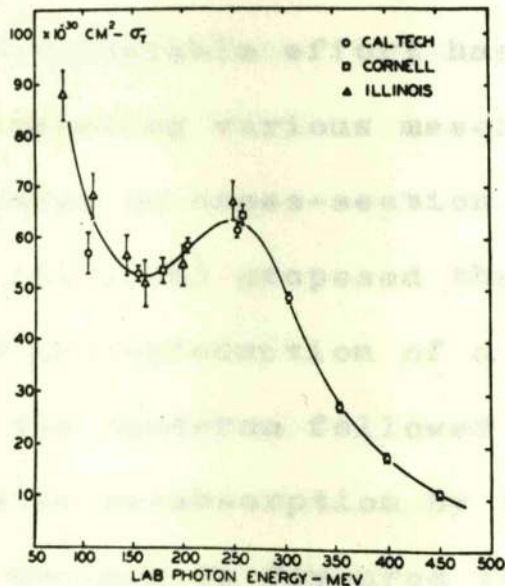
(1V)  $E_\gamma > 100$  MeV.

At gamma-ray energies greater than 100 MeV, where virtual meson effects become important, the angular distribution in the centre of mass system no longer



The differential cross section for the photodisintegration of the deuteron as a function of the center-of-mass angle and the photon energy in the laboratory. The curves are an attempt to fit the data to an angular dependence of the form  $(A + B \sin^2 \theta)(1 + 2.5 \cos \theta)$ .

FIG. 1.3.



Total cross sections for photodisintegration of the deuteron as a function of laboratory energy.

FIG. 1.4.

fits (B) and must be represented by

$$f(\theta) = a + b \cos\theta + c \cos^2\theta \quad (c)$$

The strong forward maximum diminishes at higher energies until the distribution becomes approximately symmetrical about  $90^\circ$  in the centre of mass.

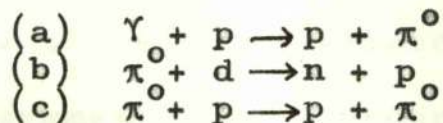
The total cross-section has a relative minimum at 150 MeV followed by a relative maximum at 250 MeV where the values are  $53 \times 10^{-30} \text{ cm}^2$  and  $63 \times 10^{-30} \text{ cm}^2$  respectively. [ Figures 1.2, 1.4 (89) ]. This is the same order of magnitude as the photomeson production cross-section. Beyond this there is a gradual fall to 450 MeV which is at present the upper limit of the experimental results.

No theory can account for all the results in this energy range. Considerable effort has been expended (105-120) in postulating various mesonic models to explain the increase in cross-section in the 250 MeV region. Wilson (117,118) proposed that disintegration is caused by the photoproduction of a meson on one of the nucleons of the deuteron followed by either escape from the nucleus or re-absorption by the two nucleons. Escape from the nucleus is favoured if the two nucleons are greater than a meson Compton wavelength ( $\hbar/\mu c$ ) apart. Wilson's results can be seen in figure 1.5. It can be seen that reasonable agreement has been

achieved, but, due to the nature of the calculation, this may only be regarded as partial success.

Bruno and Depken (108) considered various processes for emission, and re-absorption of a single meson and by a superposition of these could obtain agreement with experiment. In particular, they consider a process whereby a meson which is emitted by one nucleon, absorbs the photon and is then itself absorbed by the other nucleon.

Austern (109,110) and Feld (111) independently considered the emission and re-absorption to proceed via an intermediate nucleon resonance state with total angular momentum  $J = 3/2$  and isotopic spin  $T = 3/2$ . The nucleon is assumed to have been excited to its isobar state by magnetic dipole absorption. The same intermediate state would exist in the reactions



The cross-section for photodisintegration is then calculated from the cross-sections for the processes (a), (b) and (c) by detailed balancing. It is given by

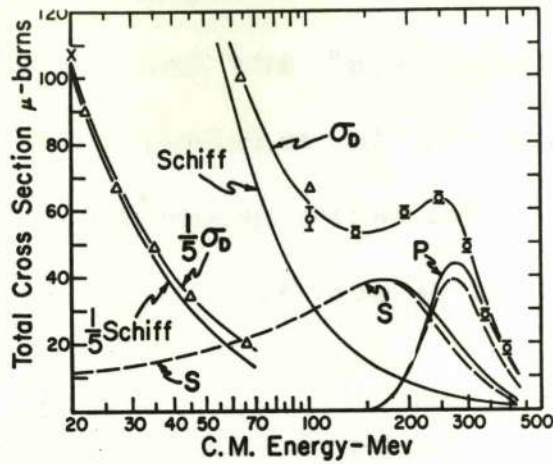
$$\sigma = \sigma_a \left( \frac{\sigma_b}{\sigma_c} \right)$$

where  $\sigma_a$  is the cross-section for photoproduction of

the isobar state, and  $\left(\sigma_b/\sigma_c\right)$  is proportional to the probability that the isobar will decay by photodisintegration of the deuteron. The calculated cross-section is found to be half the observed value.

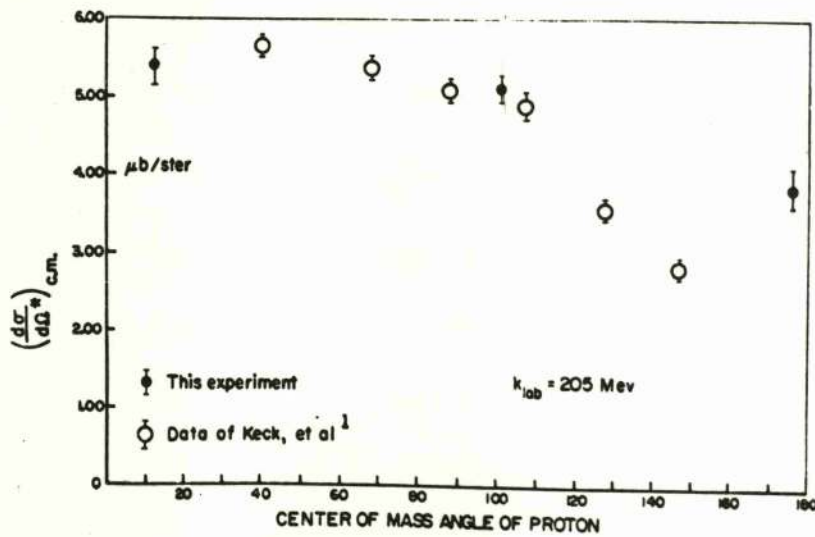
Zachariasen (119) has applied the Chew meson theory to account for the resonance at 250 MeV and succeeded in qualitatively explaining the total cross-section; however, neither Austern nor Zachariasen can reach even qualitative agreement with experiment in the energy region between 50 MeV and 200 MeV.

The increase in differential cross-section at far backward angles, obtained by Tatro et al. (91), which is clearly seen in figure 1.6, is taken as evidence that higher powers of  $\cos \theta$  should appear in  $f(\theta)$ . The cross-section may be regarded as coming partly from the pick-up of the forward pion in the reaction  $\gamma + d \longrightarrow (\pi^+ + n) + n$  by the "spectator" neutron. Due to the forward asymmetry for photoproduction of charged pions, this will give rise to a forward maximum in the angular distribution which is, however, hidden by the other contributions (a) - (c) mentioned previously in section (11). Similarly will the reaction  $\gamma + d \longrightarrow (\pi^- + p) + p$  give rise to a backward maximum because of the momentum



The curve marked *S* shows the contribution to the total cross section of the disintegration of the deuteron which results from the reabsorption of *S*-wave mesons. The curve marked *P* is the same but for *P*-wave mesons. The curve marked "Schiff" shows the result of the calculation which neglects specific meson effects. The curve  $\sigma_D$  is the sum of the other curves. The triangles show the Illinois measurements and the circles show the C.I.T. measurements.

FIG. 1.5.



Comparison of angular distributions for a photon energy of 205 Mev.

FIG. 1.6.

required by the detected proton to balance the forward motion of the  $\pi^-$  meson and the "spectator" proton.

In addition, the existence of the direct interaction term in meson photoproduction substantiates the necessity for including higher powers of  $\cos \theta$  in the angular distribution.

The calculations of Zernik et al. (120) (which will be discussed in greater detail when the polarization of photonucleons is considered) are in reasonable agreement with experiment up to 160 MeV. They apply Siegert's theorem (121) which states that one can ignore meson effects in electric dipole transitions and can use the conventional theory of nuclear forces for photon energies below 50 MeV. Their results would suggest that the theorem might be applicable and that mesonic effects would assume minor importance below 160 MeV.

#### I.4.B. Photodisintegration of Complex Nuclei at High Energies.

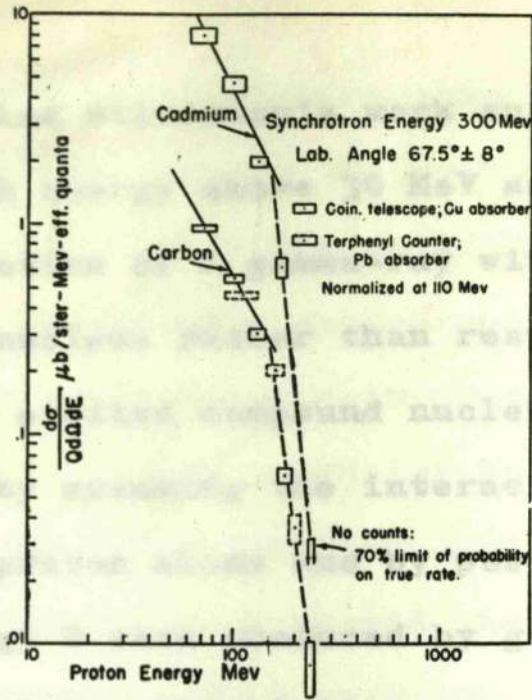
##### I.4.B.1. Photoproton Production.

By bombarding C, Cu and Pb targets with a 320 MeV gamma-ray beam and observing the ejected photoprotons with a proportional counter telescope Levinthal and Silverman (122) discovered that the protons of energy 30-40 MeV showed a distinct peaking at forward angles whereas the angular distribution for 10 MeV protons was

spherically symmetrical. These lower energy protons were attributed to evaporation processes. In addition, for protons with energies between 7 and 70 MeV the proton energy spectra at  $90^\circ$  fell approximately as  $E^{-2}$ , where  $E$  is the proton energy, and the cross-section per nucleus was proportional to  $Z$ .

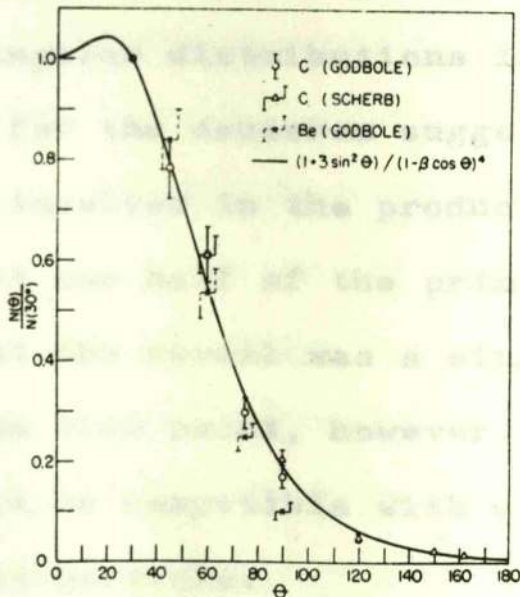
Walker (123-125) later confirmed these results for carbon using photographic plates and attained slightly higher proton energies where the spectra decreased more rapidly with increasing  $E$ .

Later work by Keck et al. (126,127), Weil and McDaniel (128-130), Rosengren and Dudley (131), Wattenberg et al. (132,133) and Murray et al. (134), who all used scintillation counter telescopes, and by Haxby et al. (135) using a cloud chamber with a magnetic field have confirmed and extended these results to higher energies, a larger number of elements, and a greater range of angles. The proton energy spectra fall as  $E^{-x}$  for  $1.7 \leq x \leq 2.2$  up to a photon energy of approximately 140 to 190 MeV, for a maximum gamma-ray energy of 300 MeV, beyond which they decrease much more rapidly. These results are to be seen in figures 1.7 and 1.8 which are taken from (126) and (133) respectively.



Differential energy spectra of protons at  $67.5^\circ$  produced by 300-Mev synchrotron photons on carbon and cadmium.

FIG. 1.7.



The angular distribution in the laboratory of 169-Mev photoprotons from beryllium and carbon. The data marked "Scherb" were obtained at a later date than that marked "Godbole." The data are normalized to the value at  $30^\circ$ . The curve is a semiempirical fit to the data with  $\beta = v/c$  of the protons.

FIG. 1.8.

Levinthal and Silverman's work suggested that the protons with energy above 30 MeV arose primarily from the interaction of a gamma-ray with some small subunit of the nucleus rather than resulting from the formation of an excited compound nucleus. The results were explained by assuming the interaction to take place with the proton alone and by postulating that protons of energy  $E$  were produced by gamma-rays of energy  $(E + 25)$  MeV. This latter assumption was later shown by Kikuchi to be wrong.

The results of Walker and of Keck which showed the sharp break in the proton energy spectra at about half the maximum gamma-ray energy and the forward peaking in the angular distributions in a manner similar to that for the deuteron suggested that the recoil particle involved in the production process carried off about one half of the primary photon energy. This implied that the recoil was a single nucleon. From the momentum view point, however, Walker saw that his results could be compatible with a sub-group as large as an alpha-particle.

The determination of the energy and angle of the emitted nucleon alone yields little information about the nature of the disintegration e.g. the proton could

be either one prong of a star or associated with meson production. In this respect the work of Weil and McDaniel helped to clarify the situation. These workers used an essentially monochromatic gamma-ray beam by taking a coincidence between the degraded electron, responsible for producing the gamma-ray which in turn caused the disintegration, and the detected proton. Their results also showed the break in the proton energy spectra. This technique is, however, of limited practical use because of the low beam intensity produced.

The cloud chamber work of Haxby et al. yielded only 236 protons with energies between 45 MeV and 105 MeV from a total of 6,800 photographs. This experiment must have consumed a considerable amount of synchrotron running time and involved laborious analysis of photographs.

#### I.4.B.2. Photostar Production.

The use of a visual technique such as a photographic emulsion method offers a more complete description of the nature of events than can the counter experiments although, in comparison, such a method is quantitatively poor.

Emulsions have been extensively employed by Kikuchi (136-140), Miller (141), and, more recently, by George (142)

and Peterson and Roos (143,144) to investigate star production by gamma-rays. These workers succeeded in separating the disintegrations into single protons, stars, and meson-associated stars. The relative numbers of events of each type produced at different maximum gamma-ray energies were studied.

Kikuchi showed that the protons observed by Levinthal and Silverman were a mixture of both single and star protons. It was seen that most of the star protons and half of the single protons were the product of gamma-quanta of energies greater than 150 MeV. In fact only a quarter of the total number of Levinthal and Silverman's protons originated from gamma-rays of energy below 150 MeV whereas these workers had deduced that almost all the protons which they had detected had come from gamma-rays in this energy region. Kikuchi's results also showed that nearly all Keck's protons were the product of gamma-quanta of energy greater than 150 MeV. No protons of energy larger than 160 MeV were found by Kikuchi for a maximum bremsstrahlung energy of 300 MeV. This was in accordance with the experiments of Keck in which few protons had been found to have energies above 150 MeV. In general the results obtained for the proton energy and angular distributions by Kikuchi were in agreement

with those of the counter experiments (122-127). In spite of poor statistics (only 34 protons of energy greater than 100 MeV were observed) these results did help to clarify the situation.

Although the relative numbers of different types of events as observed by Miller were consistent with those of Kikuchi, the absolute cross-sections of both these workers were in disagreement with each other and with previous workers. As in the case of deuteron photodisintegration this may be partly explained by uncertain beam calibrations.

The emulsion measurements were extended to 500 MeV by Peterson and Roos who found that very few of the photostars from silver nuclei in the emulsion could be accounted for by the Levinger model. These results will be more fully discussed after we have considered the Levinger model in greater detail.

#### I.4.B.3. Photoneutron Production.

The yields and angular distributions of photoneutrons from various elements have been investigated by Kerst et al. (145,146) and by Terwilliger et al. (147,148 and figure 1.1) using a neutron detector surrounded by a paraffin moderator.

1.4.B.4. The "Quasi-Deuteron" Model

For  $Z > 30$  the yield is proportional to  $Z^{1.4}$ .

The excitation functions showed a typical resonance shape in the 20 MeV region. Above this the cross-section is low and almost constant up to 80 MeV, beyond which there is a gradual increase to 300 MeV.

More recently Baranov and Goldanskii (149,150) compared the results obtained for peak energies of 170 MeV and 255 MeV for photoneutrons of energy greater than 20 MeV from deuterium and carbon. They found that the angular distributions shifted forward considerably for the higher energy experiment. Presumably this was due to the appearance of photoneutrons associated with meson production. Both sets of data gave

$$\frac{\sigma_{\text{carbon}}}{\sigma_{\text{deuterium}}} \doteq \frac{3NZ}{A} = 9$$

This substantiates the results of Feld et al. (156) discussed later. The results for the photodisintegration of the deuteron, agreed with the proton experiments.

Baranov and Goldanskii calculated that the upper limit of the probability for the re-absorption of a meson produced on one nucleon of the deuteron or "quasi-deuteron" by the other for 250 MeV gamma-rays was less than 0.1 and 0.5 for deuterium and carbon respectively.

Khoklov (153) and, independently, Levinger (70,71) used

I.4.B.4. The "Quasi-Deuteron" Model.

In the high energy nuclear photoeffect the proton has a high momentum in the final state, and, since it cannot gain much momentum during the gamma reaction, it must have had a high momentum in the ground state (assuming that momentum transfer between the nucleons does not take place after absorption). Now a proton will have a high momentum if acted upon by strong forces by virtue of its proximity to other nucleons. Thus any two nucleon model will become more effective for high energies of emitted proton<sup>s</sup>.

Bethe suggested that this may apply to many high energy nuclear reactions and the model was used by Tamor (151) for the production of protons from complex nuclei by the absorption of fast  $\pi^-$  mesons and by Heidmann (152) for the production of fast deuterons from nuclei bombarded by nucleons of about 100 MeV.

Furthermore, the early experimental results of Levinthal and Silverman and of Walker showing the forward peaking in the angular distributions and the break in the proton energy spectra at about one half of the peak photon energy suggested that such a two nucleon model might be used to explain the nuclear photoeffect. In this particular case, as explained earlier, the two nucleon model necessarily becomes a "quasi-deuteron" model.

Khoklov (153) and, independently, Levinger (70,71) used

the "quasi-deuteron" model in calculations of the high energy nuclear photoeffect.

Levinger assumed the ground state nuclear wave function to be given by

$$\psi(1, 2, \dots, A) = e^{i\mathbf{k} \cdot \mathbf{r}} \psi_k(r) \phi(3, 4, \dots, A).$$

where  $\psi_k(r)$  is the wave function for the proton-neutron subunit,  $\phi$  the wave function for the rest of the nucleus and  $e^{i\mathbf{k} \cdot \mathbf{r}}$  represents the motion of the centre of mass of the "quasi-deuteron". The function  $\phi$  was assumed to be the same for both initial and final states.

Then

$$\psi_k(r) = (4\pi)^{1/2} \left\{ \frac{\sin(kr + \delta)}{\sin \delta} - \chi \right\} (\alpha^2 + k^2)^{-1/2} v^{-1/2} r^{-1}$$

where  $k = 1/2 | \mathbf{k}_1 - \mathbf{k}_2 |$  is the wave number for relative motion of the neutron and proton,  $\delta$  the phase shift caused by the neutron-proton force,  $\alpha^{-1}$  the scattering length (found from effective range theory of nuclear forces),  $v$  the volume of the nucleons and  $\chi$  a function which can be ignored outside the range of nuclear forces.

By using the wave function for the ground state of the deuteron as given by Marshall and Guth (95) Levinger finds that

$$\frac{\sigma_{\text{quasi-deuteron absorption}}}{\sigma_{\text{deuteron}}} = \frac{(\psi_k)^2}{(\psi_d)^2} = \frac{2\pi(1 - \alpha^2 v)}{\alpha(\alpha^2 + k^2)v}.$$

out interaction is only 30% to the  
 example. In addition, the calculation of the deuteron

Since there are  $N$  choices for the neutron and  $Z$  for the proton

$$\sigma_{\text{quasi-deuteron}} = NZ \sigma_{\text{deuteron}}$$

Assuming Fermi momentum distributions for  $\underline{k}_1$  and  $\underline{k}_2$  and averaging  $(a^2 + k^2)^{-1}$  over all values of  $k$ , the cross-section for photon absorption by "quasi-deuterons" becomes

$$\sigma = 6.4 \frac{NZ}{A} \sigma_d \quad \text{when } r_0 = 1.4 \times 10^{-13} \text{ cm.}$$
$$a = 0.23 \times 10^{-13} \text{ cm.}^{-1}.$$

Levinger's calculations give qualitative agreement with the experimental results on the proton angular and energy distributions. It is not unexpected that the absolute values are at variance with experiment as the calculation has made many simplifying assumptions.

By taking into account the motion of the "quasi-deuteron" in the nucleus, Levinger shows that the angular distributions will be smoothed out and explains that this is also the reason for the large number of protons with energy greater than half the photon energy. A sharp cut-off at this energy would be expected for a "quasi-deuteron" at rest.

The paper neither takes account of meson emission and re-absorption nor scattering of the nucleons on their way out of the nucleus. This latter consideration is very important since the chance of both particles escaping without interaction is only 30% in the case of  $O^{16}$ , as an example. In addition, the calculation of the deuteron

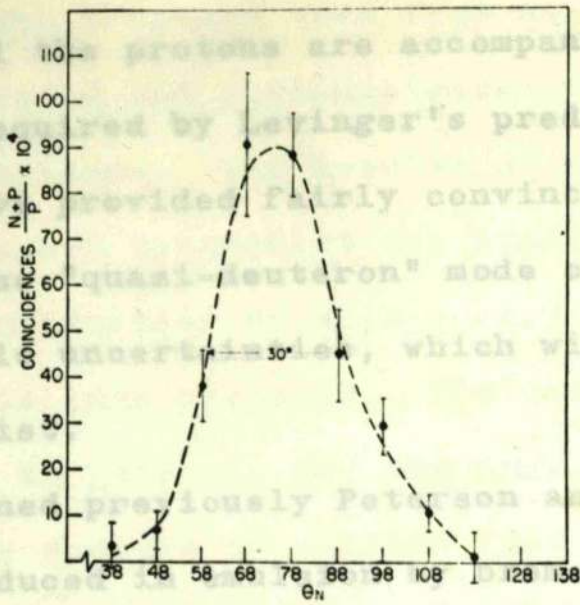
photodisintegration cross-section as given by Schiff, and Marshall and Guth was used and we have seen that this is inadequate. The use of the experimental values will help considerably. Furthermore Wilson (117) has shown that three nucleons and a meson will occasionally come close enough for a photon to interact with them. This process assumes greater significance at higher energies and should also be included in the calculation.

#### I.4.B.5. Experimental Evidence for the "Quasi-Deuteron" Model.

Single nucleon detection cannot give a direct test of the "quasi-deuteron" model. This can only be done by detecting protons and neutrons in coincidence and by examining the kinematical relationships between these emitted nucleons. Experiments of this nature have been performed by Wattenberg et al. (155-157) at M.I.T. and by Barton and Smith (158,159) at Illinois. Both groups used a similar procedure:- A proton scintillation counter telescope was set at a fixed angle to the gamma-ray beam and designed to accept protons in a certain fixed energy range. On the other side of the beam a neutron detector, capable of taking only neutrons with energy greater than a certain minimum value, was set in coincidence with the proton telescope and varied about that unique angle expected for deuteron photo-disintegration. In both experiments the proton telescope was set at  $75^\circ$  to the gamma-ray beam. This angle corresponds

to  $90^\circ$  in the centre of mass system of a deuteron at rest for a gamma-ray energy of 260 MeV. The M.I.T. group detected protons in the range 120 to 140 MeV from Li, C, and O using 340 MeV and 260 MeV gamma-rays whereas the Illinois workers accepted a series of proton energies ranging from 60 MeV to 125 MeV produced by 280 MeV and 265 MeV bremsstrahlung beams impinging on He and Li targets. The minimum neutron energy accepted in the two experiments was 15 MeV and 20 MeV respectively.

The neutron angular distribution was found to be represented by a gaussian curve centred at the unique angle which had been expected (see figures 1.9 and 1.10, from (157) and (159) respectively). The half-width of this gaussian for a complex target nucleus was greater than the instrumental half-width as given when a deuterium target was used and this varied for different nuclei. The spread in angular distribution was interpreted as being due to the motion of the "quasi-deuterons" in the nucleus and could give a relative measure of this effect for different target nuclei. The interpretation of the widths of the curves in terms of momentum of the nucleons assumes that a two-body process is involved. Barton and Smith find that about half the high energy protons are accompanied by high energy neutrons in the region of the expected direction. By considering effects of scattering and absorption they can conclude



..... Neutron-proton coincidences from lithium. The ratio of coincidences to total proton counts is plotted as a function of the angle of the neutron counter. The curve is drawn so as to connect the experimental points.

FIG. 1. 9.

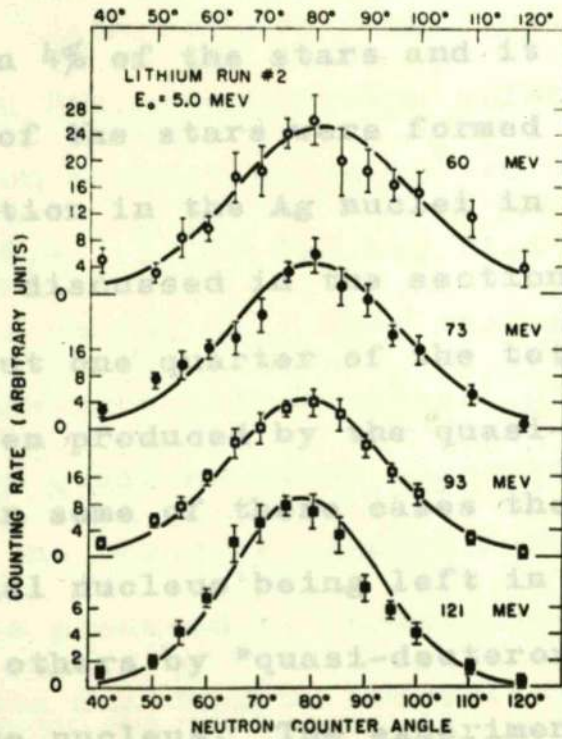


FIG. 1. 10.

that almost all the protons are accompanied by a neutron at the angle required by Levinger's prediction. These experiments have provided fairly convincing kinematic evidence for the "quasi-deuteron" mode of disintegration but considerable uncertainties, which will be discussed later, still exist.

As mentioned previously Peterson and Roos examined the photostars produced in emulsion by bremsstrahlung beams with energies in the range 250 MeV to 500 MeV. These workers found that the yield of photostars was large at 300 MeV and increased rapidly with energy. The results could not be accounted for by the "quasi-deuteron" model. It was estimated that the light nuclei in the emulsion contributed less than 4% of the stars and it is almost certain that the majority of the stars were formed by meson production and re-absorption in the Ag nuclei in the manner suggested by Wilson and discussed in the section on deuteron disintegration. About one quarter of the total number of stars could have been produced by the "quasi-deuteron" process. Presumably, in some of these cases the star would be formed by the residual nucleus being left in a highly excited state and in others by "quasi-deuteron" scattering on the way out of the nucleus. The experiments of Miller and of George suggest that only surface nucleons are effective in producing free mesons. This has also been stated by

- 57 -

Butler (160) who proposed that free meson production is strongly inhibited and photodisintegration intensified in the core nucleons. The results of these photostar experiments do not contradict the predictions of the model as the production of high energy nucleons by the pion process is less probable. The "quasi-deuteron" model does account, in general, for the angular distributions, and the energy spectra of emitted fast nucleons; the expected correlation in angle between coincident neutrons and protons is also observed.

#### I.4.B.6. Proton-Proton Coincidences.

Proton-proton coincidences have been detected by Weinstein et al. (161) at M.I.T. using two proton counter telescopes. These workers found that the ratio of the cross-section for proton-proton coincidences to that for proton-neutron production at  $90^\circ$  in the centre of mass system was  $(0.4 \pm 0.4) \%$  for Li,  $(2.2 \pm 2.0) \%$  for O,  $< 10\%$  for Al, and  $< 3\%$  for Cu. They estimated that the scattering of the neutrons with resultant production of recoil protons after "quasi-deuteron" absorption was sufficient to account for the observed results. Proton-proton coincidences could also be produced by formation of a meson on one nucleon in the nucleus followed by absorption by two nucleons or alternatively by quadrupole or higher order gamma-ray absorption. However, these workers looked for two protons

of roughly the same energy. For the experiments with O, Al, and Cu one proton telescope accepted proton energies between 106 and 114 MeV and the other took energies between 102 and 118 MeV. We shall see later that this may be the reason why so few coincidences were obtained.

#### I.4.B.7. Photodeuteron Production.

The "quasi-deuteron" model does not predict the direct emission of deuterons from the target nucleus but a surprisingly large number of these have been detected by De Wire et al. (162,163) using a NaI counter telescope. Some of the results obtained can be seen in figure 1.11. The angular distribution of 40 MeV deuterons was also found by these workers and is similar to those for protons. Targets of C, Cu, Ag, Pb, Be, Al, Mo, and W were bombarded with a 300 MeV  $\gamma$ -ray beam. The ratio of the number of 40 MeV deuterons to 40 MeV protons per unit energy interval at  $90^\circ$  was found to vary from 0.12 for C to 0.24 for Pb. These workers propose that the observed A and Z dependence of the ratios suggests a  $(\gamma, p)$  or  $(\gamma, n)$  reaction followed by a pick-up process. The author believes that the possibility of these deuterons arising from a secondary process, in which the residual nucleus, after proton-neutron emission, splits up with the ejection of a high energy deuteron, must also be considered.

I.4.B.8. Further Theoretical Investigations of the High Energy Photoeffect.

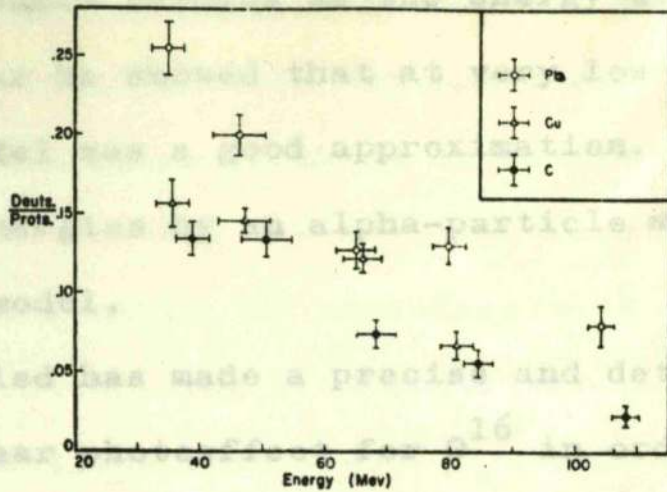
The calculations made by Levinger and Khoklov have been extended by Dedrick (164), by Yoshida (165), and by Gottfried (166).

Dedrick, applying Levinger's approach to the problem, performed more detailed calculations. Analytical results could be obtained by applying a random flight method and by assuming a Gaussian momentum distribution to average over all the "quasi-deuterons" in the nucleus. He considered the momentum vector,  $\underline{Q}$ , of a photoparticle in the laboratory to be given by

$$\underline{Q} = \underline{P} + \frac{1}{2} (\underline{p}_n + \underline{p}_p) + \frac{1}{2} \hbar \underline{k} \quad *$$

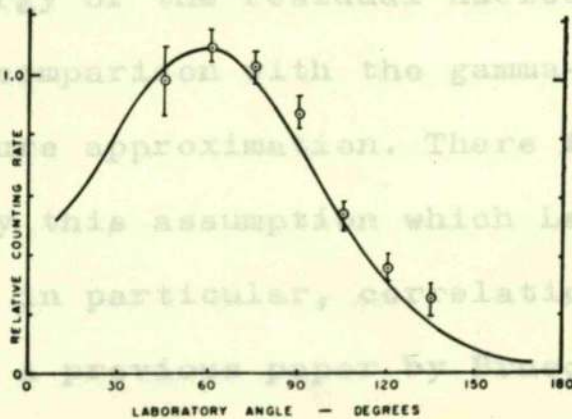
where  $\underline{P}$  is the momentum of the photonucleon in the centre of mass system,  $(\underline{p}_n + \underline{p}_p)$  is the momentum of the centre of mass of the "quasi-deuteron", and  $\hbar \underline{k}$  is the photon momentum. The probability  $W(\underline{Q}) d\underline{Q}$  that  $\underline{Q}$  lies in the range  $d\underline{Q}$  about  $\underline{Q}$  is derived by treating the four vectors in equation \* as random variables. Dedrick's calculations were performed for gamma-ray energies of 50, 75, 100 and 125 MeV. He considered only electric dipole and quadrupole absorption and made corrections for reflection of neutrons at the nuclear surface as well as Coulomb barrier effects on the protons. The results obtained are in reasonable agreement with experiment as can be seen in figure 1.12.

Yoshida assumed absorption to take place by an n-



The ratio of deuterons to protons produced by 310-Mev bremsstrahlung at 90° in the laboratory. The abscissa represents the energy of the product particles. The statistical errors are shown.

FIG. 1.11.



Experimental data of Johansson<sup>11</sup> showing the yield of photoprotons with energies greater than 14 Mev obtained from carbon irradiated by the bremsstrahlung beam from a betatron operating at 65 Mev. The smooth curve is the calculated yield of 13.3 Mev photoprotons from carbon irradiated by 50-Mev photons. The normalization is at 60°.

FIG. 1.12.

$$\frac{P_2(\xi_1, \xi_2)}{g(\xi_1 - \xi_2)^2} \quad \text{where } P_2 \text{ is the shell}$$

particle subunit followed by proton emission. He concluded that the subunit changes as the energy of gamma-ray varies. In particular he showed that at very low energies a single particle model was a good approximation. This was followed at higher energies by an alpha-particle model and later by a deuteron model.

Gottfried has made a precise and detailed calculation of the nuclear photoeffect for  $O^{16}$  in order to include effects unknown at the time of Levinger's work. The theory applies only to nuclei with completely closed shells. He ignored the effect of the remaining  $A-2$  nucleons during the absorption act but considered refraction of the outgoing "photonucleon wave" at the nuclear surface and attenuation of the photonucleons inside the nucleus. By assuming the excitation energy of the residual nucleus to be generally very small in comparison with the gamma-ray energy he could apply the closure approximation. There is no experimental data to justify this assumption which Levinger also made. He considered, in particular, correlation effects between the nucleons. A previous paper by Brueckner et al. (167) had shown that the experimental data provided strong evidence for correlations in the nuclear ground state wave function. Gottfried took the nuclear pair correlation function to be given by

$$\rho_s(\tau_1, \tau_2) |g(\tau_1 - \tau_2)|^2 \quad \text{where } \rho_s \text{ is the shell}$$

also calculated the cross-section for proton-proton

model correlation function. The function  $g$  contains the correlations due to nuclear forces and is a modification of  $\rho$  at small interparticle separations. The photodisintegration cross-section is shown to be proportional to the probability of finding two nucleons with total momentum in relative S states. He considers that only transitions from the  $^3S_1$  states are of importance. Levinger similarly ignored transitions from the  $^1S_0$  state of the "quasi-deuteron". Both authors justify this by the fact that the deuteron photoeffect proceeds almost entirely by electric dipole absorption and in addition there are three times as many pairs in triplet as in singlet states. The results obtained are compared with the M.I.T. results for  $C^{12}$  and reasonable agreement is achieved as can be seen in figure 1.13. In the counter experiments the neutron energy was undetermined. Gottfried therefore integrated over all neutron energies to obtain this curve although most of his calculations were made for discrete values of neutron energy. A better test of the theory will be obtained when both proton and neutron energies are determined. Wattenberg et al. did, in fact, obtain results for  $O^{16}$  but these are subject to large uncertainties as an  $H_2O$  target was used. Gottfried states that the angular correlation will probably agree with the momentum distribution computed from almost any set of shell-model wave functions with the correct r.m.s. radius. Gottfried also calculated the cross-section for proton-proton

resonance" region but above this energy it is possible that production and concurred with the experimental results of Weinstein et al.

I.4.B.9. Extension of the "Quasi-Deuteron" Model to the Region Below 150 MeV.

There have been some attempts to extend the applicability of the "quasi-deuteron" model to the region below 150 MeV, and in particular to the region just above the "giant resonance" where the collective and shell models are no longer useful.

Hendel (168) has measured the energy and angular distributions of photoprotons with energies between 20 MeV and 60 MeV from Be, C, Cu and Pb nuclei with a 150 MeV beam. The protons were detected in plates. His results are very similar to those obtained with a 300 MeV beam.

Johansson (169) bombarded C, Al, Mb and Ni targets with 65 MeV bremsstrahlung and examined the ejected neutrons and protons with counters. The accepted proton energies were those greater than 14 MeV. The results were consistent with an independent particle model. He also endeavoured to detect neutron-proton coincidences but achieved no success.

The photographic plate method has been used by Chuvilo and Shevchenko to investigate the angular and energy distributions of photo protons from  $\text{Be}^9$  and  $\text{C}^{12}$  with peak gamma-ray energies of 84 MeV, 64 MeV (170) and 44 MeV (171). For the low energy experiment, the results are explained by the resonance theory of the compound nucleus in the "giant

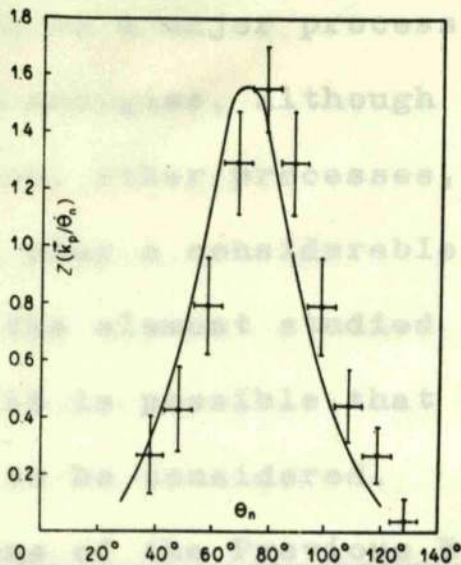
resonance" region but above this energy it is possible that interaction with substructures in the nucleus occurs. For the higher energy experiment the angular distributions show a marked forward asymmetry and the results for  $\text{Be}^9$  suggested that "quasi-deuteron" absorption might be taking place. The results for  $\text{C}^{12}$  were similar to those for  $\text{Be}^9$  for protons of energy between 26 MeV and 36 MeV but for proton energies between 18 MeV and 28 MeV a "quasi-alpha" model was more probable.

The angular distributions of photoprotons with energies between 15 and 65 MeV from Al and Ni and the energy distributions of those from Al at  $30^\circ$ ,  $90^\circ$  and  $130^\circ$  due to an 85 MeV beam have been measured by Bazhanov et al. (172) using scintillation counters. In the case of Al the angular distributions agree with those of the deuteron but for Ni the agreement is very poor and it is probable that a considerable contribution from the direct photoeffect is taking place.

Gorbunov and Spiridinov (173-175) have used a cloud chamber to study the photodisintegration of helium up to 170 MeV and find that both below and above 75 MeV the "quasi-deuteron" mechanism is responsible for the  $\text{He}^4 (\gamma, pn)d$  reaction. Although definite at the higher energies the correlation between the neutron and proton is masked by the momentum distributions of the nucleons in the nucleus at the lower values. They believe that the  $(\gamma, p)$  and  $(\gamma, n)$

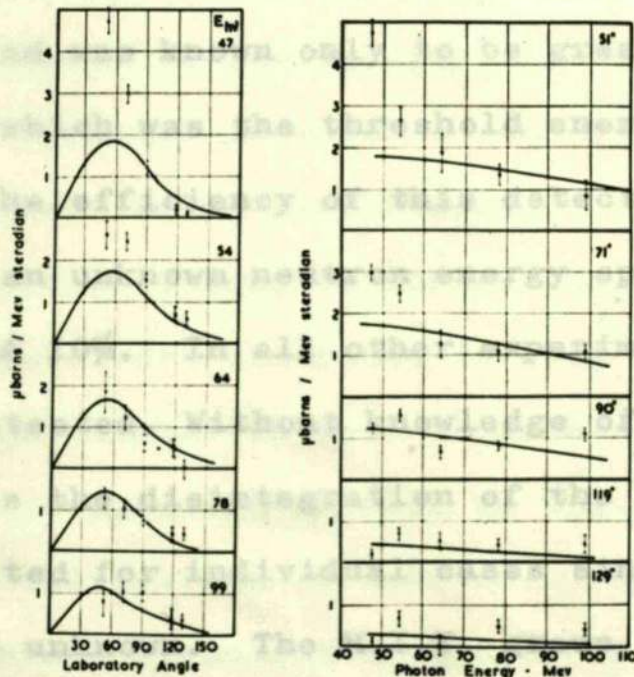
reactions proceed through single particle photon absorption and estimate that, over the whole energy range, two particle absorption accounts for about 12% of the total but above 75 MeV this is increased to about 30%. Their statistics in the high energy range are, of course, much poorer than in the region below 30 MeV.

The most convincing evidence that the "quasi-deuteron" mechanism contributes to the absorption in the region above the "giant resonance" has been given by Whitehead et al. (176) who detected neutron-proton coincidences with scintillation counters. They used peak gamma-ray energies between 40 MeV and 110 MeV and accepted protons of energy 37, 47, 55, 63, 73 and 78 MeV at angles  $36^\circ$ ,  $51^\circ$ ,  $71^\circ$ ,  $90^\circ$ ,  $119^\circ$  and  $129^\circ$  from C, Li, O, and Be targets. They compare their results (figure 1.14) for C with the predictions of Dedrick and, after adjustments to the theory to account for scattering of the photonucleons, they find that the cross-sections have only half of the expected magnitude. The fraction of protons accompanied by a neutron in the expected direction is found to be 0.012 for  $C^{12}$  and 0.027 for  $O^{16}$ . They explain that the lack of coincidences is not unexpected because of the severe scattering to be expected of such low energy particles on their way out of the nucleus. This scattering will prevent many particles from escaping and furthermore, many that do escape will no longer be correlated in angle to



The angular correlation function  $Z(\mathbf{k}_p, \Omega_n)$  when  $\epsilon_n$  is not determined,

FIG. 1.13.



Cross sections for the production of 37 Mev photoprotons from carbon. The curves shown are the quasi-deuteron calculations by Diederik

FIG. 1.14.

the proton. This could also explain the results of Johansson.

In conclusion we may say that the "quasi-deuteron" mechanism appears to be a major process in the region above 80 MeV but at lower energies, although it may make a substantial contribution, other processes, in particular the direct photoeffect, play a considerable part. The individual characteristics of the element studied seem to play an important role and it is possible that the isotopic spin selection rule has to be considered.

#### I.4.B.10. Limitations of the Previous Experiments.

In spite of the substantial support provided for the Levinger "quasi-deuteron" model by the coincidence experiments of Wattenberg et al. and of Barton and Smith many uncertainties still exist. In these experiments the neutron energy was undetermined and was known only to be greater than a certain minimum value which was the threshold energy of the detector. Furthermore, the efficiency of this detector had to be corrected for an unknown neutron energy spectrum and was only of the order of 10%. In all other experiments only a single nucleon was detected. Without knowledge of both neutron and proton energies the disintegration of the "quasi-deuteron" cannot be treated for individual cases since the gamma-ray energy is also unknown. The M.I.T. group (177) did start an experiment in 1956 in which neutron energies were also measured by a time of flight method but no results were

published. However, with the development of fast electronic techniques this seems to provide a feasible method of measuring the neutron energies.

Because of the low cross-section for such high energy processes, the use of a counter technique would seem to be imperative. Nuclear emulsions cannot be employed with much hope of success since the strong ionization produced by the gamma-ray must considerably limit the time of irradiation. The accuracy of low energy measurements in emulsion is, in addition, not very good and the presence of several target elements is also a disadvantage. As we have seen from the work of Haxby et al. the use of a cloud chamber with a magnetic field is restricted to the intermediate energy region because of the small number of high energy events obtained from a large number of photographs.

In any experiment in which a complex target nucleus is involved and where multi-particle emission is possible counters alone cannot hope to define the reaction completely.

In the experiment described in this thesis, in which a triggered cloud chamber is used to detect the recoiling nucleus or its fragments, as well as the proton, many of the previous difficulties are surmounted:

(a) The energy and direction of travel of any neutron which may be present in addition to the energy of the gamma-ray producing the disintegration can be calculated from the laws

of conservation of energy and momentum.

(b) In the counter experiments the exact role of processes other than "quasi-deuteron" absorption is left undetermined whereas the cloud chamber enables one to see whether direct single nucleon emission or absorption of gamma-rays by substructures other than proton-neutron pairs is taking place

(c) The state of excitation in which the residual nucleus is left after emission of a proton-neutron pair is still unknown and all existing theories assume it to be small compared with the gamma-ray energy. In the present experiment, by measuring the energies of all the fragments of this residual nucleus we can gain some measure of its excitation.

(d) In both the M.I.T. and Illinois experiments the values of "quasi-deuteron" momentum in the various nuclei obtained from the neutron angular distribution curves can only be regarded as relative values. The measurements were not taken to extreme angles and zero counting rates because of the considerable background experienced. In the Illinois experiments the accidental background provided 66% of the neutron-proton coincidences at  $40^\circ$  from Li. Appreciable uncertainty therefore exists in the absolute height, and consequently in the half-width, of the curves in figures 1.9 and 1.10. In the experiment described in this thesis, if we assume the "quasi-deuteron" mechanism to be responsible

for the ( $\gamma$ ,pn) events then, in those cases in which the recoiling nucleus does not disintegrate, the length of the recoil will give a direct measure of the internal momentum of the "quasi-deuteron" in the nucleus. We can plot the recoil range distribution and thus obtain the "quasi-deuteron" internal momentum distribution.

Chapter II.

Instrumentation.

II.1. The Cloud Chamber and Related Equipment.

II.1.1. The Operation of a Wilson Expansion Chamber.

When a visual technique, such as a Wilson chamber or bubble chamber, is used in conjunction with a large accelerator the conventional method of expanding the chamber is the use of a piston and bellows mechanism. This method is not suitable for the study of nuclear disintegrations produced by a single output pulse from a cyclotron. In the case of the cloud chamber, the chamber is expanded by means of a piston and bellows mechanism which is triggered by a pulse from the accelerator. The chamber is expanded to a volume of about 100 times its normal volume. The chamber is then passed through a series of grids which cause a further delay of about 0.1 sec. The chamber is then expanded and the ions are flashed and a photograph of the tracks is exposed. The pulse is taken. A series of 100 or more pulses are taken lasting a few minutes each. The cycle of operations is then repeated. The time intervals are usually equal to the case of a bubble chamber but usually the same procedure is followed.

Chapter II. Instrumentation.

When a triggered cloud chamber is used the accelerator is allowed to run continuously until the passage of a triggering particle through counters activates the expansion. The chamber is, of course, expanded after the passage of the beam pulse. Only a finite time (about 14 msecs) elapses before diffusion of the ions produced by the triggering particle

Chapter II.

Instrumentation.

II.1. The Cloud Chamber and Related Equipment.

II.1.1. The Operation of a Wilson Expansion Chamber.

When a visual technique, such as a cloud chamber or bubble chamber, is used in conjunction with a large accelerator the conventional method of operation involves examination of the nuclear disintegrations produced by a single output pulse from the machine. In practice, the cloud chamber, say, is first expanded then, after a delay of about 180 m.sec., a single output pulse from the machine is passed through or adjacent to the chamber. After a further delay of about 80 m.sec., to enable tracks to form, lamps are flashed and a photograph of the tracks produced by the pulse is taken. A series of cleaning operations, usually lasting a few minutes next occurs. The cycle of operations is then repeated. The time intervals are much smaller in the case of a bubble chamber but essentially the same procedure is followed.

When a triggered cloud chamber is used the accelerator is allowed to run continuously until the passage of a triggering particle through counters activates the expansion. The chamber is, of course, expanded after the passage of the beam pulse. Only a finite time (about 14 m.secs) elapses before diffusion of the ions produced by the triggering particle

goes beyond the limit of good photography (about 1 mm.).

In addition the electron background produced by the gamma-ray beam, in the present experiments, will grow very rapidly and tend to obscure short nuclear recoils in the same region of the chamber as the beam. Furthermore it becomes difficult to see fast lightly ionising particles against the large electron background.

These problems necessitated the use of a very fast expansion mechanism, described in this chapter, which produced supersaturation in the chamber only a few milliseconds after the passage of the triggering particle. This was followed by chamber illumination and photography after a delay of 30 m.secs.; a time much shorter than is conventional. Electron tracks seen in the photographs are therefore not fully grown and fast particle tracks are rather faint.

A high value of clearing field was maintained on the cloud chamber in the interval between successive synchrotron pulses. An electronic switch cut off the field during each beam pulse. This field was necessary to clear away unwanted ions produced by continuous pulsing of the accelerator. The system will be described in more detail later in this chapter.

which were activated in turn by a slow expansion control unit were connected through needle valves to this region. Thus a slow uniform flow of gas could be allowed to pass

### II.1.2. The Cloud Chamber.

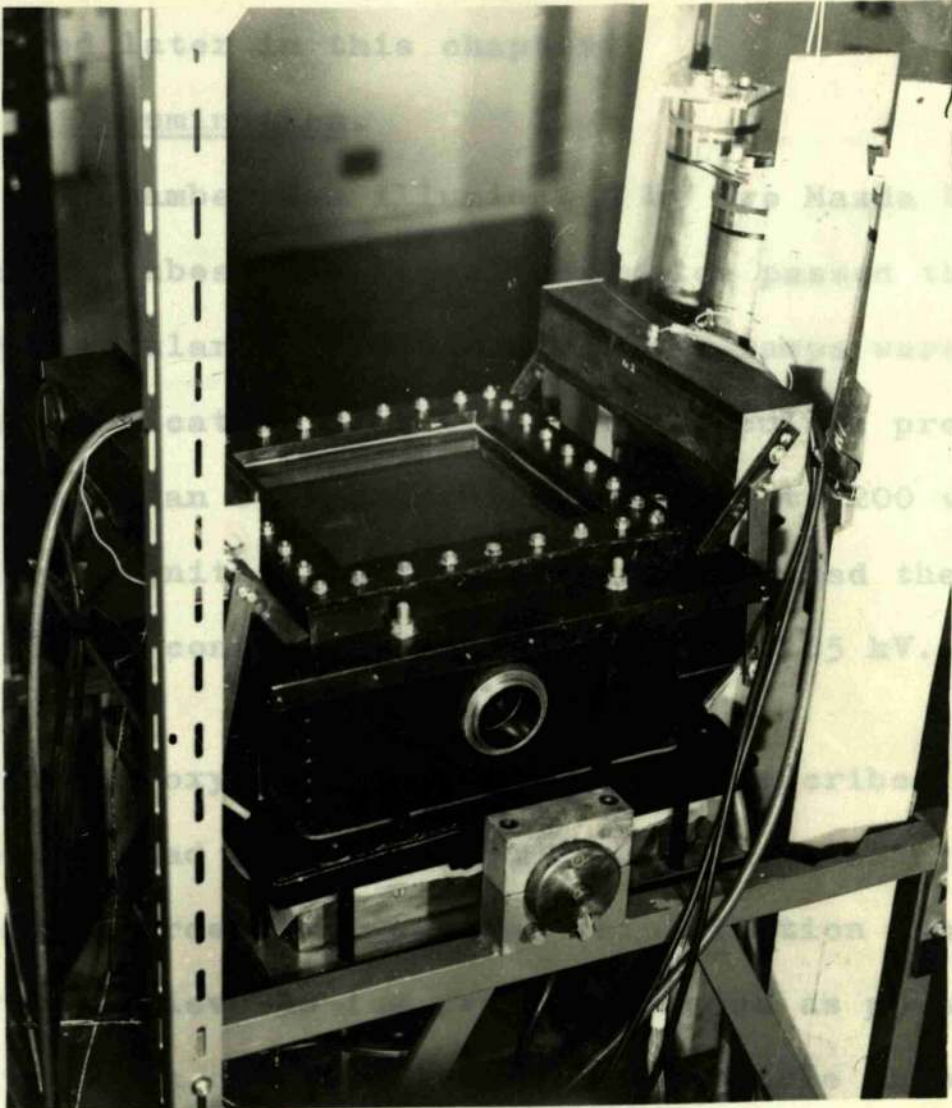
In both the experiments described in this thesis the same cloud chamber was used. A sectional view of the construction can be seen in figure II.1. It was a conventional square Wilson expansion chamber, the sensitive volume of 30 cm. x 30 cm. x 15 cm. being defined by a rubber diaphragm. Two opposite walls of the chamber each had a circular window 2" in diameter consisting of 0.0005" thick "mylar" for passage of the gamma-ray beam. These thin windows enabled background electrons produced by the beam to be kept to a minimum. The other two walls had perspex windows for illumination purposes. A small temperature gradient between top and bottom of the cloud chamber was produced by passing water through a collar attached to the heavy brass perforated plate immediately above the diaphragm. This also prevented condensation on the cloud chamber walls. The upper surface of this brass plate was covered with black velvet to serve as a photographic background and to trap any dust particles present. The compressed pressure in the sensitive volume was approximately 1.5 atmospheres. The compression was produced by the introduction of compressed air to the region below the diaphragm. Two magnetic valves which were activated in turn by a slow expansion control unit were connected through needle valves to this region. Thus a slow uniform flow of gas could be allowed to pass

Photograph II.1.

(Wilson Expansion Cloud Chamber).

either to or from the high pressure gas region in order to enable slow cleaning expansions to be made.

The operation of the fast expansion valve will be



solid material as uniform as possible, the lamps were positioned as in figure II.1 and mirrors were inserted. This arrangement can also be seen in photograph II.1. The positioning of the counters closer to the cloud chamber, thus increasing the solid angle of acceptance, was also facilitated.

By doubling the length of the perspex side windows the

either to or from the high pressure gas region in order to enable slow cleaning expansions to be made.

The operation of the fast expansion valve will be described later in this chapter.

### II.1.3. Illumination.

The chamber was illuminated by two Mazda L.S.D.16 discharge tubes, the flash from which passed through the two rectangular side windows. These lamps were triggered by the application of a high voltage pulse, produced by discharging an 8  $\mu\text{f}$  condenser, charged to 200 volts, through a 12 volt ignition coil. This pulse caused the discharge of a 300  $\mu\text{f}$  condenser bank, charged to 1.5 kV., through the lamps.

In the oxygen experiment, to be described, the triggering proton had to pass through one of the side walls of the chamber in order to reach the scintillation counters. In order to achieve as low proton energies as possible and to make the path of every triggering particle through external solid material as uniform as possible, the lamps were positioned as in figure II.1 and mirrors were inserted. This arrangement can also be seen in photograph II.1. The positioning of the counters closer to the cloud chamber, thus increasing the solid angle of acceptance, was also facilitated.

By doubling the length of the perspex side windows the

rather also succeeded in eliminating large areas of fog which had been present in each corner of the chamber in previous experiments. This improvement can be seen in a comparison of photographs II.2 and II.3.

II.1.4. Clearing Field

Two sets of grids were in the working position of the chamber and served to clear away stray ions after passage of the synchrotron beam and fiducial lines in the reconstruction of three dimensions. These were set above and below the synchrotron beam and carried 400v. with respect to the earthed aluminium walls of the chamber. The above values of clearing field were empirically found to be adequate to sweep away the ions from one burst of quanta before the arrival of the next burst 1/5 sec. later. The application of this clearing field allowed continuous pulsing of the synchrotron beam through the chamber. Dense fog would otherwise have been produced by the expansion eventually triggered by a high energy electron beam pulse and restoration of the voltage after the end of the output pulse. This switching prevented dragging of the tracks by the electrostatic field

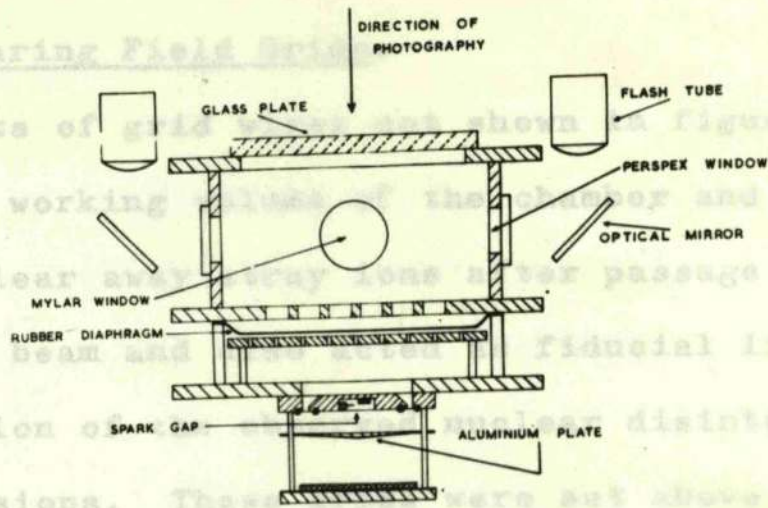


FIG. II 1.

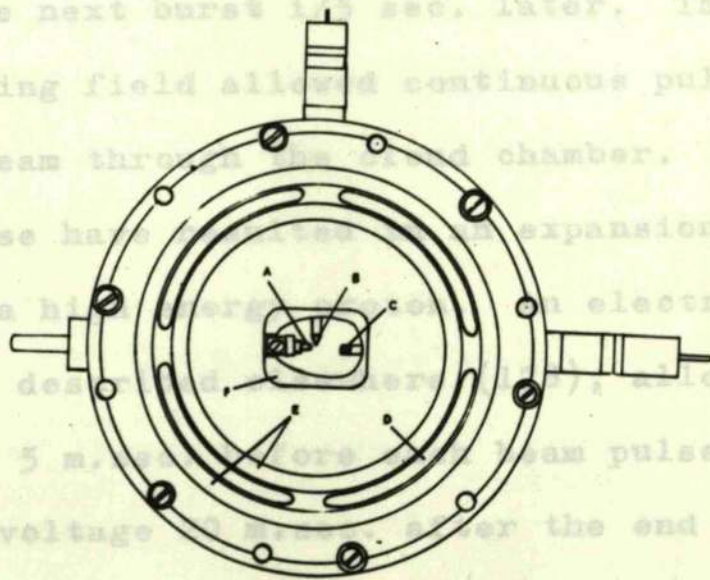
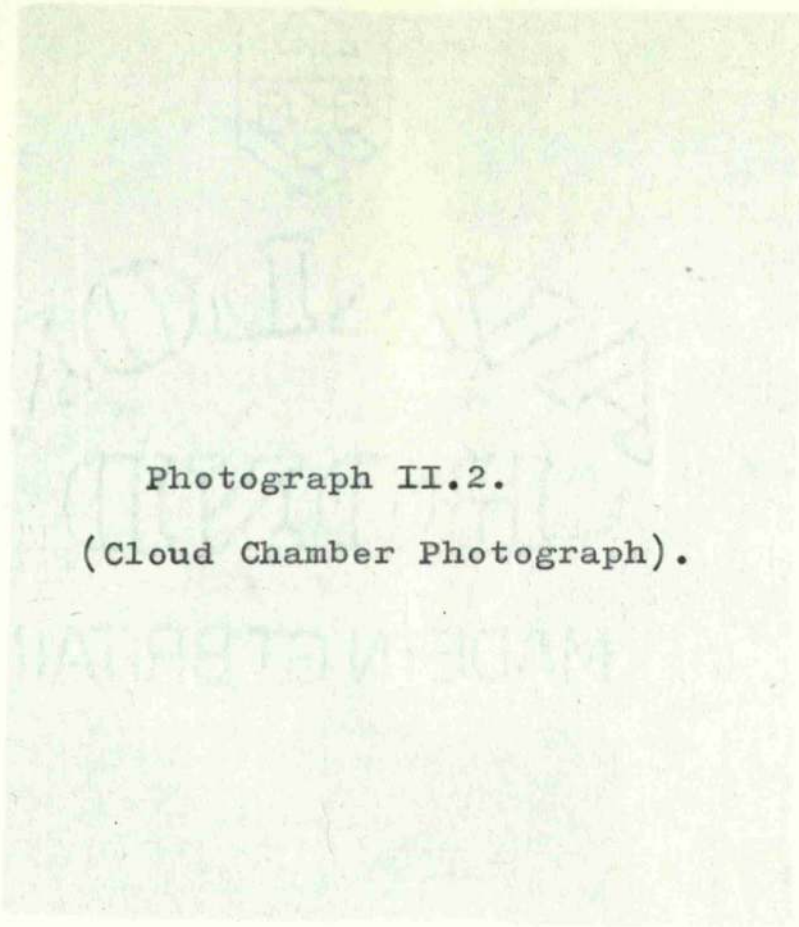


FIG. II 2.

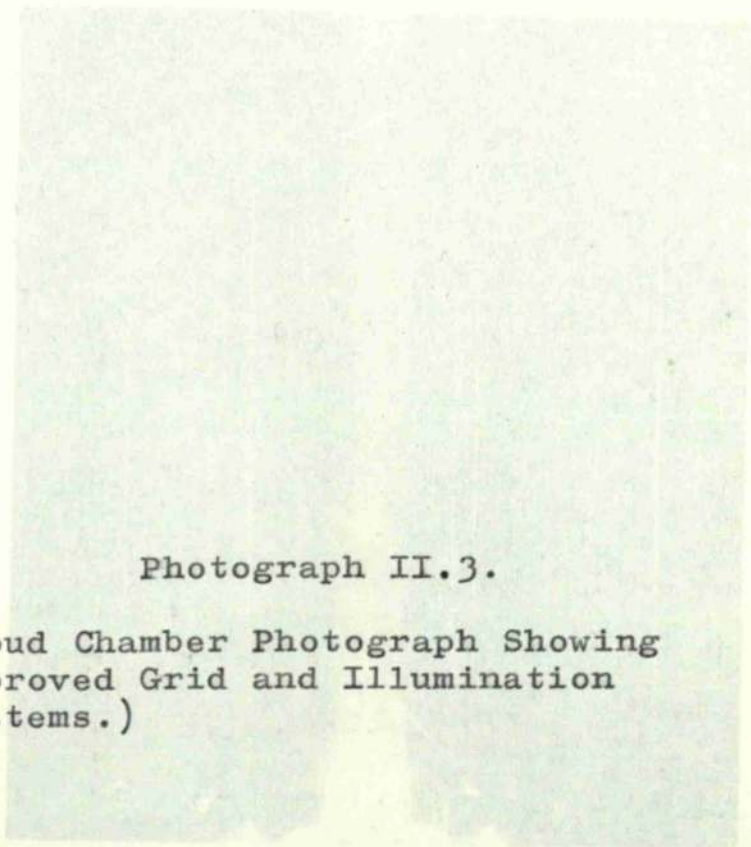
author also succeeded in eliminating large areas of darkness which had been present in each corner of the chamber in previous experiments. This improvement can be seen in a comparison of photographs II.2 and II.3.

#### II.1.4. Clearing Field Grids.

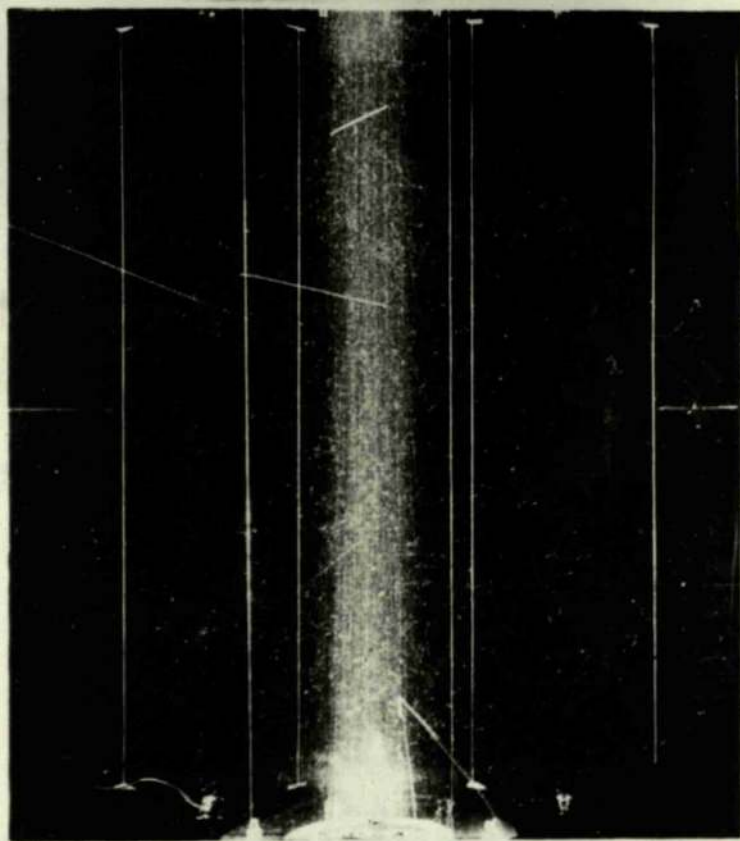
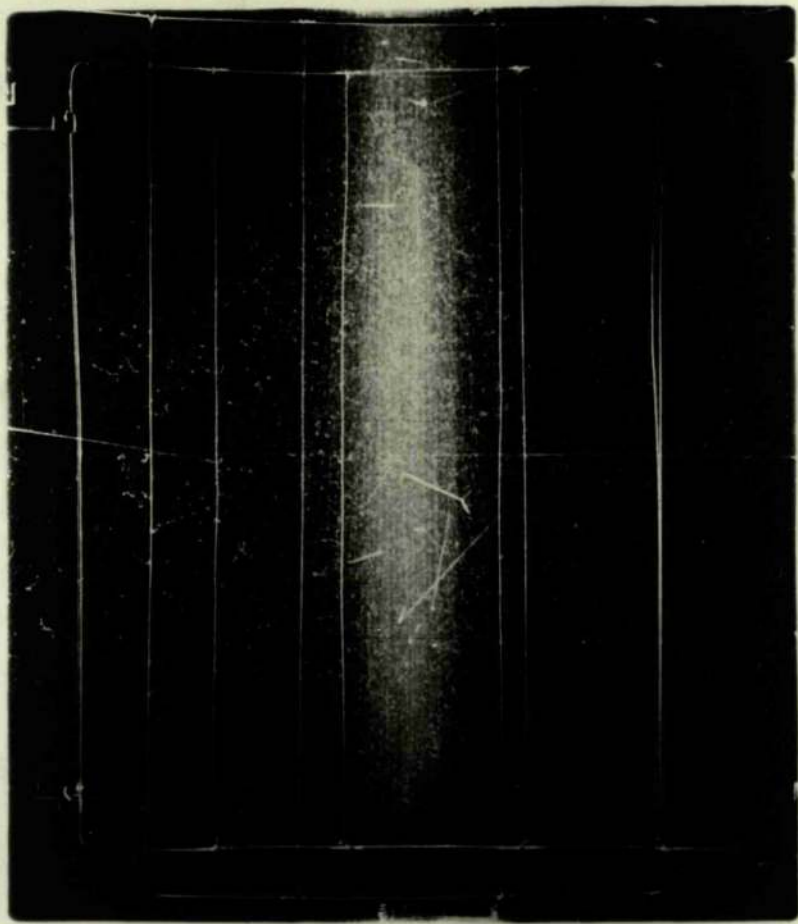
Two sets of grid wires not shown in figure II.1. which were in the working volume of the chamber and 10 cm. apart served to clear away stray ions after passage of the synchrotron beam and also acted as fiducial lines in the reconstruction of the observed nuclear disintegrations in three dimensions. These grids were set above and below the synchrotron beam and carried  $\pm 400\text{v.}$  with respect to the earthed aluminium walls of the chamber. The above values of clearing field were empirically found to be adequate to sweep away the ions from one burst of quanta before the arrival of the next burst  $1/5$  sec. later. The application of this clearing field allowed continuous pulsing of the synchrotron beam through the cloud chamber. Dense fog would otherwise have resulted in an expansion eventually triggered by a high energy proton. An electronic clearing field switch, described elsewhere (178), allowed both grids to be earthed 5 m.sec. before each beam pulse and restoration of the voltage 20 m.sec. after the end of the output pulse. This switching prevented dragging of the tracks by the electrostatic field.



Photograph II.2.  
(Cloud Chamber Photograph).



Photograph II.3.  
(Cloud Chamber Photograph Showing  
Improved Grid and Illumination  
Systems.)



Initially the grids consisted of wire frames which were partly superfluous and somewhat uneven. In three-dimensional reconstruction of the events these defects caused inconvenience and sometimes loss of information when an event was hidden behind part of the grid. The writer replaced this arrangement by rectangular paxolin frames fixed to the walls of the chamber. Strips of beryllium copper fixed to the paxolin frames provided springs for the stainless steel grid wires with the result that little strain was placed on the wire by the gas movement during expansion. The two grid systems can be compared from photographs II.2 and II.3.

#### II.1.5. Expansion Mechanism.

The expansion valve is similar to that described by Meyer and Stodiek ((179) and figures II.1 and II.2). The pressure,  $p$ , in the spark cavity and that under the rubber diaphragm,  $P$ , were so adjusted that atmospheric pressure was just sufficient to hold a "dural" disc on to two concentric "O" rings. The orifice,  $D$ , for escaping gas was thereby sealed. When the pressure balance was disturbed by activating a spark in the gap, the "dural" plate blew off very rapidly thus causing a fast expansion of the gas in the chamber. The two pressures  $p$  and  $P$  were set automatically by positioning electrical contacts in two mercury

obtained from B. This produces ionisation in the gap and

manometers so that activation of two electromagnetic valves on a vacuum line and an air line respectively could, by a suitable choice of pressures, produce a very critical balance of the plate.

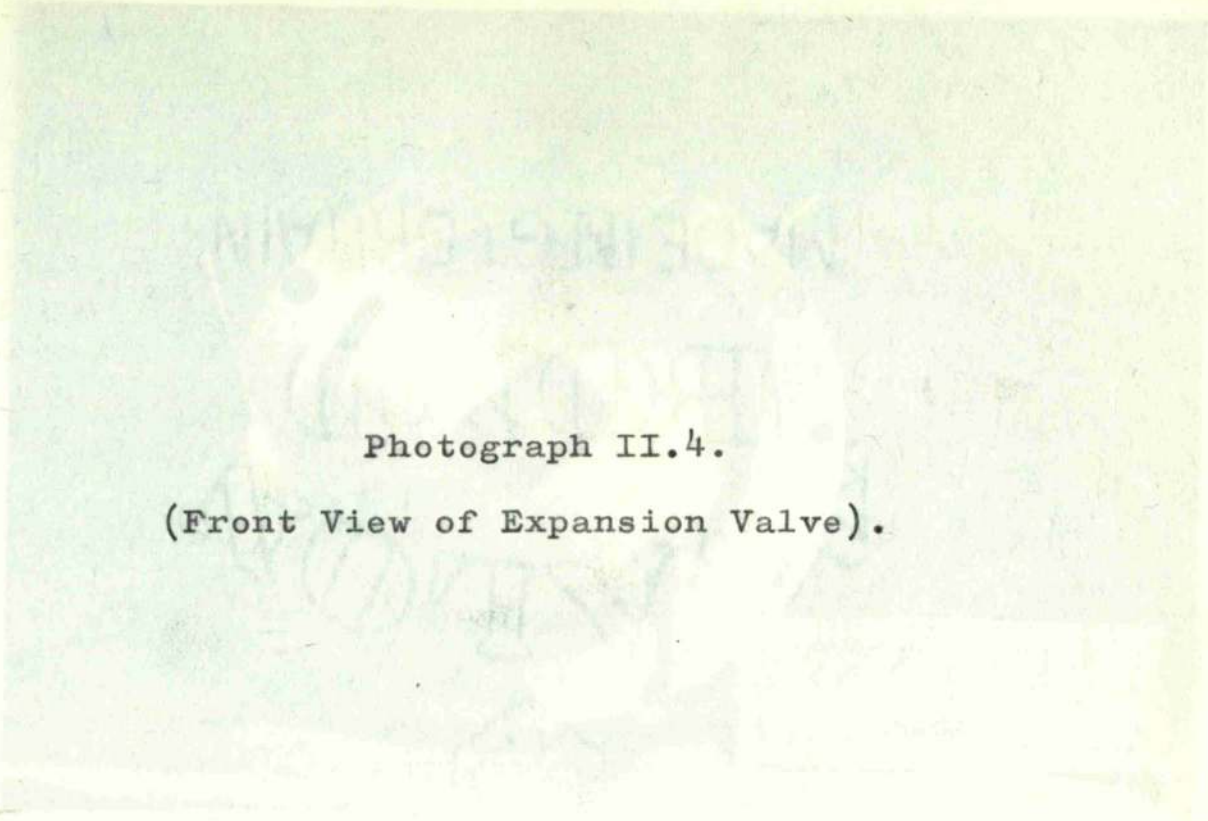
In the initial experiments a two-electrode spark system was used but its performance was unsatisfactory. This was mainly due to the fact that electrode erosion made the interelectrode spacing uncertain. Frequent adjustments were necessary and time consuming. The electrode erosion was caused by the large current which crossed the gap during a discharge produced when the trigger pulse from one of the counter telescopes was applied to the grid of a large thyratron. A 50  $\mu$ f condenser, charged to 3 kV, discharged across the gap when the thyratron conducted.

This system was replaced by a three-electrode spark gap. The new valve can be seen in photographs II.4 and II.5. and in figure II.2 where:-

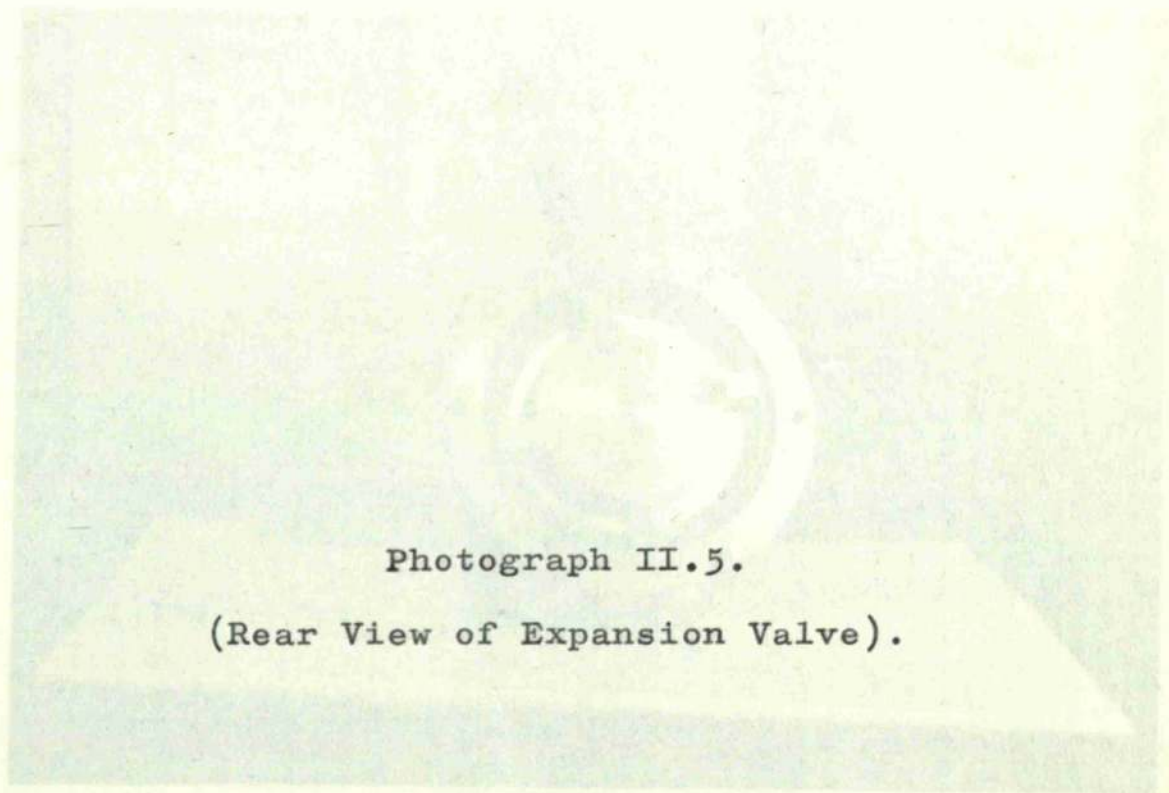
- A = earth electrode ; B = trigger electrode
- C = H.T. electrode ; D = orifice for escaping gas
- E = "O" rings ; F = "araldite" insulating block.

A steady voltage of 6 kV. is continuously applied between C and A by a voltage doubler unit seen in figure II.5.

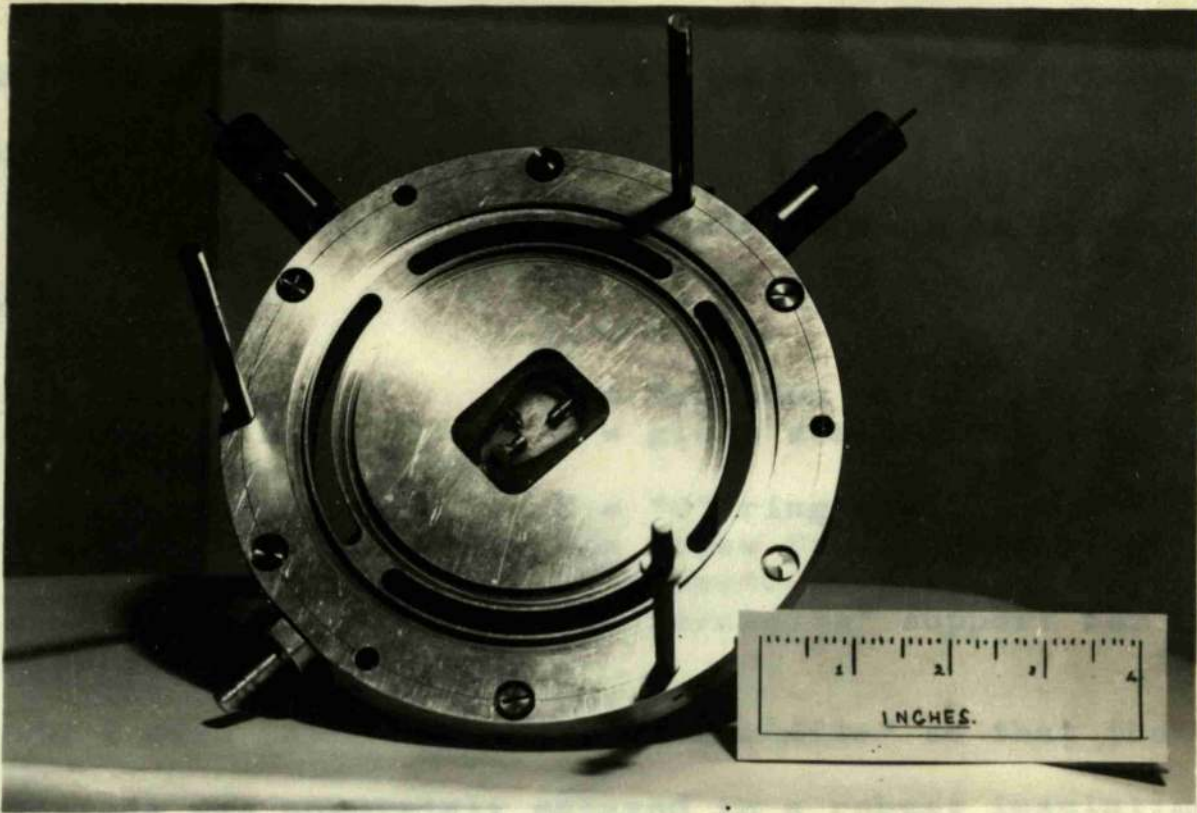
When a pulse is supplied from one of the counter telescopes to a trigger unit (figure II.4) a high voltage discharge is obtained from B. This produces ionisation in the gap and



Photograph II.4.  
(Front View of Expansion Valve).

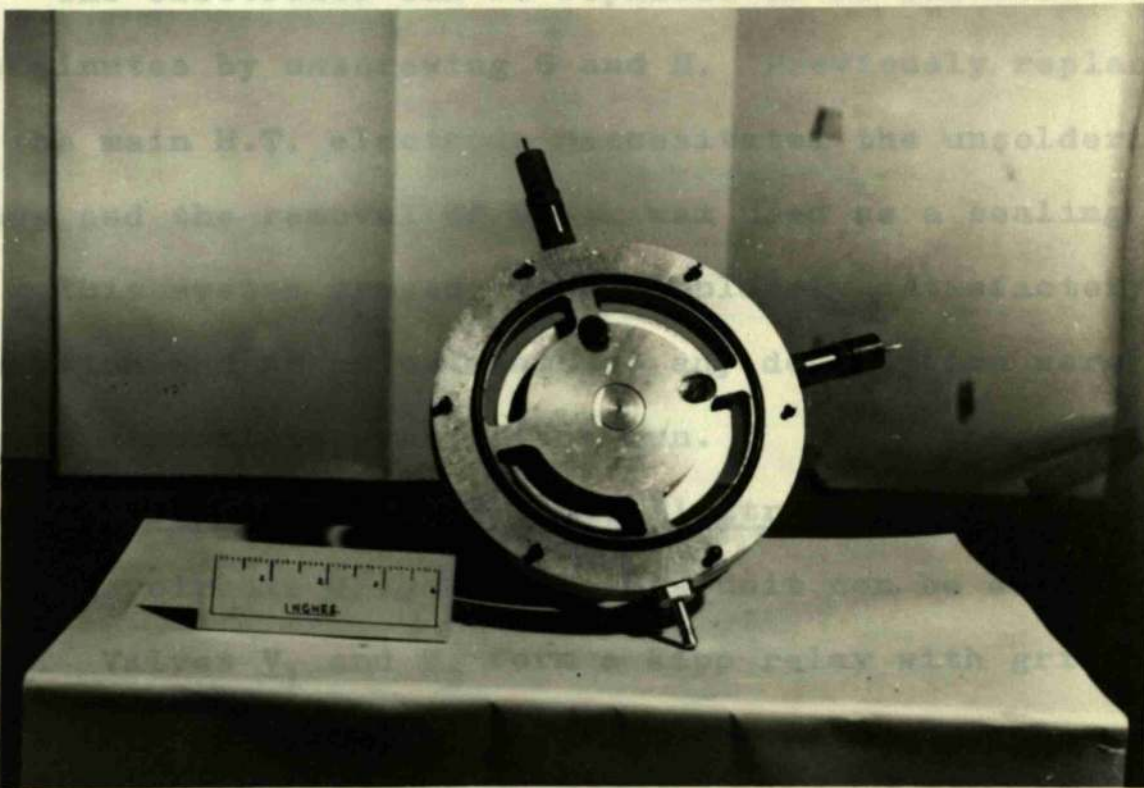


Photograph II.5.  
(Rear View of Expansion Valve).



material.

The electrodes can be replaced or re-adjusted in a



overswing on the positive input pulse to  $V_1$ . The positive pulse which results from the anode of  $V_2$  due to an input

the 6 kV discharge is obtained to blow off the expansion plate.

The electrode construction can be seen in figure II.3 where:-

A = pumping port	;	B = tungsten earth electrode
C = tungsten H.T. electrode	;	D = glass sealing and insulation
E = conducting wire	;	F = "O" ring seal
G = sealing screw	;	H = screw for adjustment of electrode position.
I = paxolin insulation	;	J = "araldite" support for glass.
K = tungsten contact.		

D and I were later replaced by "araldite" so that the electrode was completely encased in a robust insulating material.

The electrodes can be replaced or re-adjusted in a few minutes by unscrewing G and H. Previously replacement of the main H.T. electrode necessitated the unsoldering of leads and the removal of black wax used as a sealing agent.

This system proved to be completely satisfactory in operation and no adjustments of any description were made during a complete synchrotron run.

#### II.1.6. Trigger Unit for Three-Electrode Spark Gap.

The circuit diagram for this unit can be seen in figure II.4. Valves  $V_1$  and  $V_2$  form a Kipp relay with grids biased positively to overcome premature resetting by a negative overswing on the positive input pulse to  $V_1$ . The positive pulse which results from the anode of  $V_2$  due to an input

positive pulse on the grid of  $T_1$  is applied to the grid of the thyatron  $V_1$  in the spark gap. This pulse causes the 12  $\mu$ F capacitor, charged to 200v, and across the thyatron, is discharged through the primary of the ignition coil. The resulting high voltage output from the secondary is applied to the trigger electrode in this way thus producing ionization in this enclosed volume.

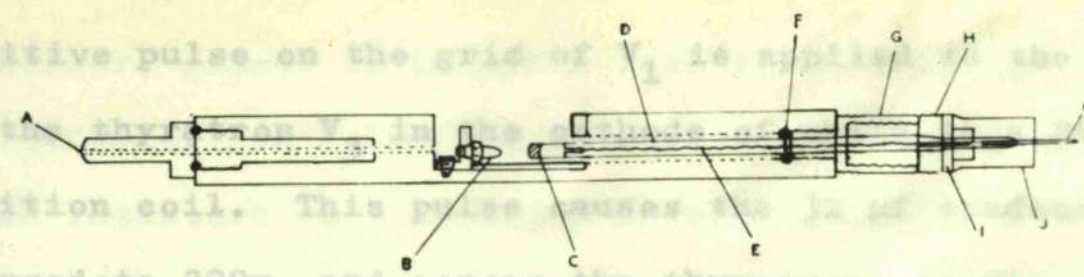


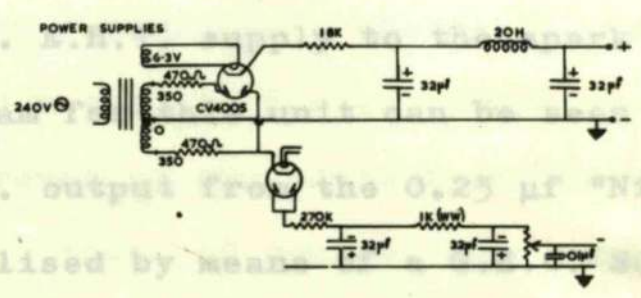
**FIG. II 3.**

A switch was incorporated to ground the grid of the thyatron and so enable the circuit to be expanded for testing purposes.

**II.1.7. High Voltage Unit for Three-Electrode Spark Gap.**

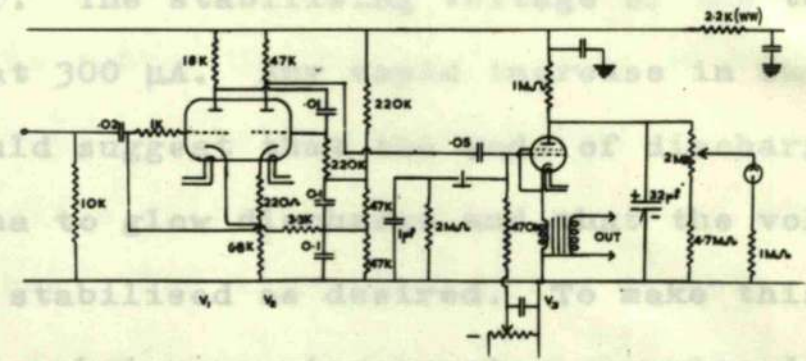
A full-wave voltage doubler unit was built to provide a steady 6 kV. This is applied to the spark valve. The circuit diagram of this unit is shown in figure II.5.

**SPARK TRIGGER UNIT**



The 6 kV. output from the 0.23  $\mu$ F "Nitrogel" capacitors was stabilised by means of a 300. Corona type stabiliser. The stabilising voltage of this

measured at 300  $\mu$ A. The voltage across the spark gap would change from corona to glow if the voltage was not being stabilised.



immediately obvious a microammeter was placed in series with the stabiliser to record the current being drawn.

**FIG. II. 4.**

The voltage across the spark gap was measured with a "Photo flash"

positive pulse on the grid of  $V_1$  is applied to the grid of the thyatron  $V_3$  in the cathode of which is a 24v. ignition coil. This pulse causes the 32  $\mu\text{f}$  condenser, charged to 200v. and across the thyatron, to discharge through the primary of the ignition coil. The resultant high voltage output from the secondary is applied to the trigger electrode in the spark gap thus producing ionisation in this enclosed volume.

A switch was incorporated to ground the grid of the thyatron and so enable the cloud chamber to be manually expanded for testing purposes.

#### II.1.7. High Voltage Unit for Three-Electrode Spark Gap.

A full-wave voltage doubler unit was built to provide a steady 6 kV. E.H.T. supply to the spark valve. The circuit diagram for this unit can be seen in figure II.5.

The 6 kV. output from the 0.25  $\mu\text{f}$  "Nitrogol" capacitors was stabilised by means of a G.E.C. SC4. Corona stabiliser. The stabilising voltage of the tube was measured at 300  $\mu\text{A}$ . Any rapid increase in current above 300  $\mu\text{A}$  would suggest that the mode of discharge had changed from corona to glow discharge and that the voltage was not being stabilised as desired. To make this situation immediately obvious a microammeter was placed in series with the stabiliser to record the current being drawn.

The voltage across a 1  $\mu\text{f}$  10 kV. "Photo flash"

condenser, placed in parallel with the stabiliser and microammeter, was continuously measured. The 1 K $\Omega$  anode resistors were included in case of rectifier flash-over.

Because the high voltages and capacities involved in the unit made it potentially lethal a safety switch was incorporated to short-circuit the output condenser when the E.H.T. was switched off. Indicator lamps showed that the switch was operating properly.

#### II.1.8. Speed of Expansion.

The speed of expansion of the cloud chamber was first measured by noting the time delay between the triggering pulse and the passage of the dural expansion plate through a beam of light falling on a photocell. Average times ranging from 3 m.sec. to 8 m.sec. were recorded as the distance of travel of the plate from the expansion valve was increased. This, of course, only determined the speed of the cover plate. A later method actually timed the speed of the rubber diaphragm. A beam of light was passed in turn through a series of small "mylar"-covered holes in the opposite walls of the high pressure region of the cloud chamber. The light from holes directly opposite each other was allowed to fall on a photomultiplier, since the light intensity was much smaller than in the previous instance. The time delay between the triggering particle and the motion of the diaphragm could then be readily

ascertained. The average speed of expansion was about 4 to 5 m.secs. although times as short as 3 m.secs. were recorded. In addition, measurement of the delay between the motion of the expansion plate and the rubber diaphragm was made by combining the two methods outlined above. This delay stayed fairly constant at about 2 m.secs.

With such a speed of expansion the width of fast proton tracks was about 0.5 mm. when the chamber was filled with oxygen at 1.5 atmos. and an alcohol-water vapour mixture was used.

#### II.1.9. Resetting of the Expansion Valve.

To reset the expansion valve the dural plate must be moved upwards for a distance of about 3 in. and pressed firmly on to the concentric "O" rings to allow evacuation of the spark gap. A pneumatic device was considered more suitable than a solenoid and piston for performing this function.

The operation of this resetting mechanism shown in figure II.6 (1-4) and photograph II.6. may be sufficiently clear from the diagrams. The piston rod has at its upper end a 1.5" diameter disc which lifts the expansion plate. A rotary valve (figures 2,3,4) controls the supply of compressed air to the cylinder. This valve has six holes two opposite pairs of which can be linked simultaneously by the motion of a cap having two grooves (shown as dotted lines in figure 3) cut in it. The position of the cap is



controlled by two electromagnets (figure 3 ). When current is passed through the left-hand magnet high pressure air flows into the bottom of the cylinder and the piston is forced upwards to seal the expansion valve. When the right-hand magnet is operated the valve cap changes over and the piston is forced down by the air passing into the upper half of the cylinder. Just before the piston rod reaches its lowest position two micro-switches, activated by a collar on the rod, cut off power to the electro-magnet and a trip on the rod serves to return the rotary valve to a neutral mid-way position when the lowest point of travel is reached.

The success of this mechanism allowed complete electrical link-up of the cloud chamber control system and enabled each operation in the recycling process to take place automatically.

#### II.1.10. Cameras and Photography.

The tracks in the cloud chamber gas were stereoscopically photographed by three cameras which were mounted so that their image planes all lay parallel to and 70 cm. above the chamber base. An 80 mm. f/4.5 "Ental" enlarging lens was mounted in each camera and apertures 1 to 16 were available. The lenses were laterally displaced to enable

use to be made of the full width of each film. Either Kodak R55 or Ilford 5G91 60 mm. unperforated recording film developed in I.D.33 was used in both experiments. The film passed through a gate and was held firmly in position between a glass pressure plate and the base of the camera. When reprojection of the photographs was desired the backs of the cameras were easily removed and a strong mercury vapour lamp placed above each film. In the oxygen experiment all films travelled perpendicular to the beam direction and similarly in the polarization experiment the direction of travel was at right angles to the incoming proton direction.

Photograph 11.7.

(See microscope records).

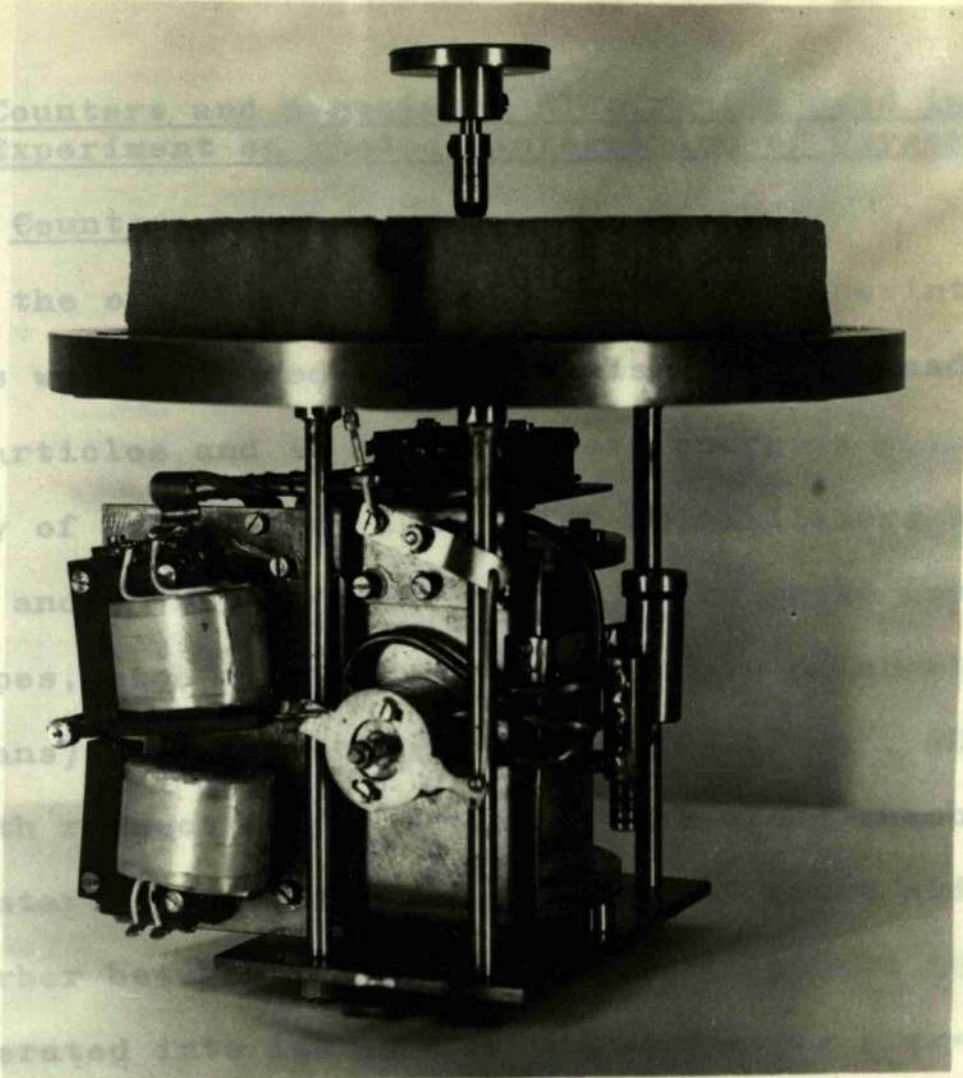
Photograph II.6.  
(Resetting Mechanism).

Photograph II.7.  
(Oscilloscope Traces).

II.2. Counters and Experiment

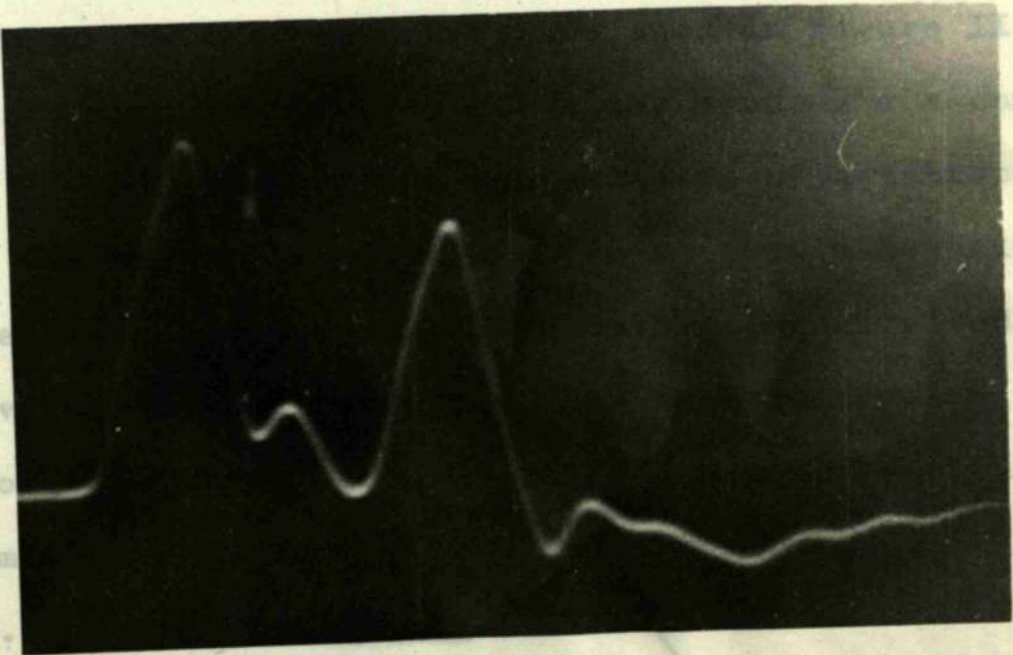
II.2.1. Counters

In the experiment of collimation  
counters were used to measure  
other particles and  
accuracy of  
elastic and  
telescopes,  
steradians,  
35° with  
two counter  
Cu absorber  
were operated  
of pulses.



II.2.2. Coincidence Circuits.

The screen  
grid.  
led to  
appeared  
positive  
used for  
diagram



II.2.3.

The operation of the counter electronics may be

## II.2. Counters and Associated Electronics Used in the Experiment on Photodisintegration of Oxygen.

### II.2.1. Counters.

In the oxygen experiment three pairs of scintillation counters were required to distinguish protons readily from other particles and to measure their energies with an accuracy of better than 10%. The scintillators were of plastic and 4" x 3" x 1/2" in size. The three counter telescopes, each subtending a solid angle of about  $1/14$  steradians), were placed at mean angles of  $45^\circ$ ,  $90^\circ$  and  $135^\circ$  with respect to the centre of the cloud chamber. The two counters of each telescope were 1/4" apart and had 1/16" Cu absorber between them. The photomultipliers (EMI 6262) were operated into low  $10\text{ k}\Omega$  impedances to prevent pile-up of pulses.

### II.2.2. Coincidence Circuits.

The coincidence Circuits are seen in figure II.7. The screen grid of the CV 2209 valve was used as a second control grid. The pulses from the two counters of a telescope were led to the two grids of this valve so that a negative pulse appeared at the anode only when both grids received a positive pulse simultaneously. An identical valve was used for the gating circuits which are also seen in the diagram.

### II.2.3. Counter Electronics.

The operation of the counter electronics may be



sufficiently clear from the block diagram for one telescope shown in figure II.8.

The discriminator bias voltage for the front counters was set above the value corresponding to mesons. That for the back counters was chosen so that only protons nearly stopping in the scintillator were accepted. The method for determining these bias voltages was similar to that described in (133).

Pulses from the amplifiers were delayed by passing through 1000  $\Omega$  cable and then displayed and photographed on a Tektronix 210 oscilloscope. These pulses enabled the energy of the triggering particle to be determined to within an accuracy of about 5%.

A pulse coincident with the synchrotron beam gated the output from the coincidence circuits and thus eliminated coincidence pulses produced by background radiation. The cloud chamber was expanded by a pulse from a Schmitt trigger. This pulse was also sent to the synchrotron control circuits to sweep the electron beam away from the synchrotron target thus reducing the background intensity in the cloud chamber.

Each cloud chamber photograph could be related to a particular telescope by consulting a record which was kept of the counts registered on four scalers.

Chapter III.

The Photodisintegration of Oxygen.

III.1. Experimental Arrangement.

The apparatus consisted of a square Wilson expansion cloud chamber along one side of which were arranged two pairs of scintillation counters set at mean angles of  $45^\circ$ ,  $90^\circ$  and  $135^\circ$ . The passage of a high energy neutron through the two counters of any pair, operated in coincidence, produced a single pulse which was used to trigger the chamber. Such a pulse resulted from a 150 MeV gamma ray

**Chapter III. The Photodisintegration of Oxygen.**

produced by the passage of the gamma-ray beam from the 150 MeV electron synchrotron. For technical reasons the peak gamma-ray energy was limited to 240 MeV during this experiment. The experimental arrangement can be seen in Figure III.1. Photograph III.1 shows a general view of the equipment and photograph III.2 displays the counter telescopes.

The chamber was attached to the synchrotron by a special port in the synchrotron collimating system in order to maintain the electron background within it at a minimum. Before reaching a 0.0005 in. thick "mylar" window covering the port, the beam passed through a vacuum chamber to ensure maximum cleanliness. This collimating system has been previously described (180) in detail.

## Chapter III.

### The Photodisintegration of Oxygen.

#### III.1. Experimental Arrangement.

The apparatus consisted of a square Wilson expansion cloud chamber along one side of which were arranged three pairs of scintillation counters set at mean angles of  $45^{\circ}$ ,  $90^{\circ}$  and  $135^{\circ}$ . The passage of a high energy proton through the two counters of any pair, operated in coincidence, produced a single pulse which was used to trigger the chamber. Such a pulse resulted from a 100 MeV proton produced by a photodisintegration in the cloud chamber gas by the passage of the gamma-ray beam from the 330 MeV electron synchrotron. For technical reasons the peak gamma-ray energy was limited to 240 MeV during this experiment. The experimental arrangement can be seen in figure III.1. Photograph III.1 shows a general view of the equipment and photograph III.2 displays the counter telescopes.

The chamber was attached to the synchrotron by a special port in the synchrotron collimating system in order to maintain the electron background within it at a minimum. Before reaching a 0.0005 in. thick "mylar" window covering the port, the beam passed through a vacuum chamber to ensure maximum cleanliness. This collimating system has been previously described (180) in detail.

### 3.2. Measurement of the Cloud Chamber Tracks

When analysing the cloud chamber photographs, we were able to use the conventional method of re-projection to measure and measure each nuclear event in three dimensions.

The developed films were replaced in the appropriate cameras which were positioned relative both to each other and to a flat table, substituted for the cloud chamber, as they had been during the experiment.

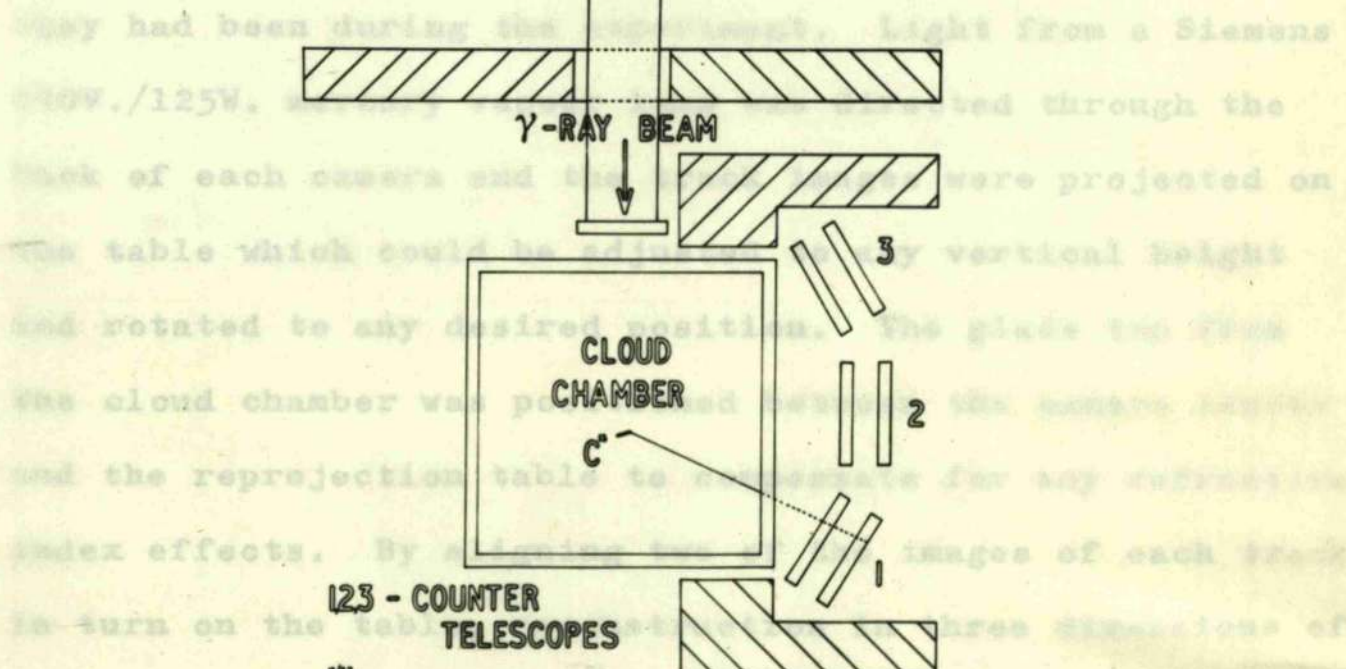


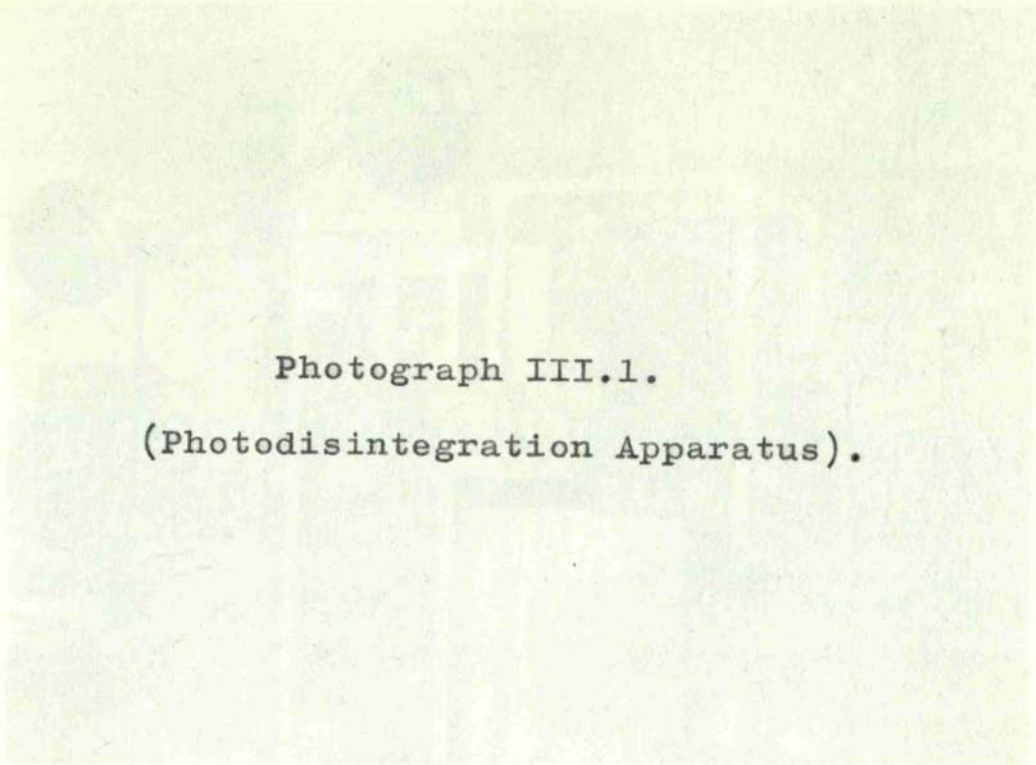
FIG. III 1.

Light from a Siemens 250V./125W. lamp was directed through the back of each camera and the tracks were projected on the table which could be adjusted by vertical height and rotated to any desired position. The glass top from the cloud chamber was positioned near the centre of the re-projection table to compensate for any refraction index effects. By using three counter telescopes, three images of each track in turn on the table were obtained. Three dimensions of each event was possible. This method compares very favourably with other systems for accuracy in measuring long tracks but is inherently incapable of making such measurements with the required degree of accuracy for tracks less than 1 cm. long. Since many of the recoil tracks in this experiment were below this value an additional method was employed. This involves using a microscope to measure the lengths of the images of each event, as shown on the three films, and relating these to the actual dimensions of the

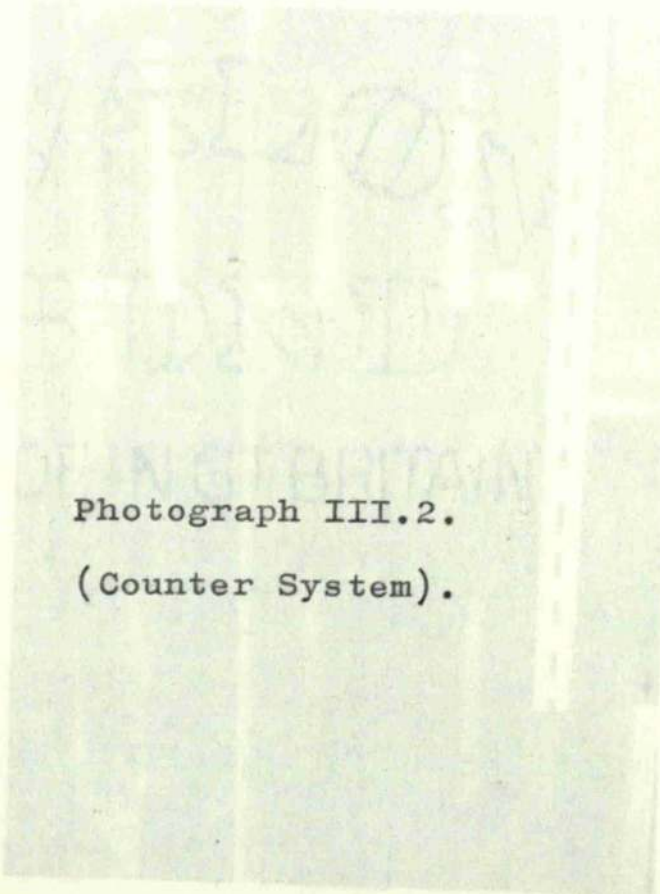
### III.2. Measurement of the Cloud Chamber Tracks.

When analysing the cloud chamber photographs, use was made of the conventional method of reprojection to reconstruct and measure each nuclear event in three dimensions.

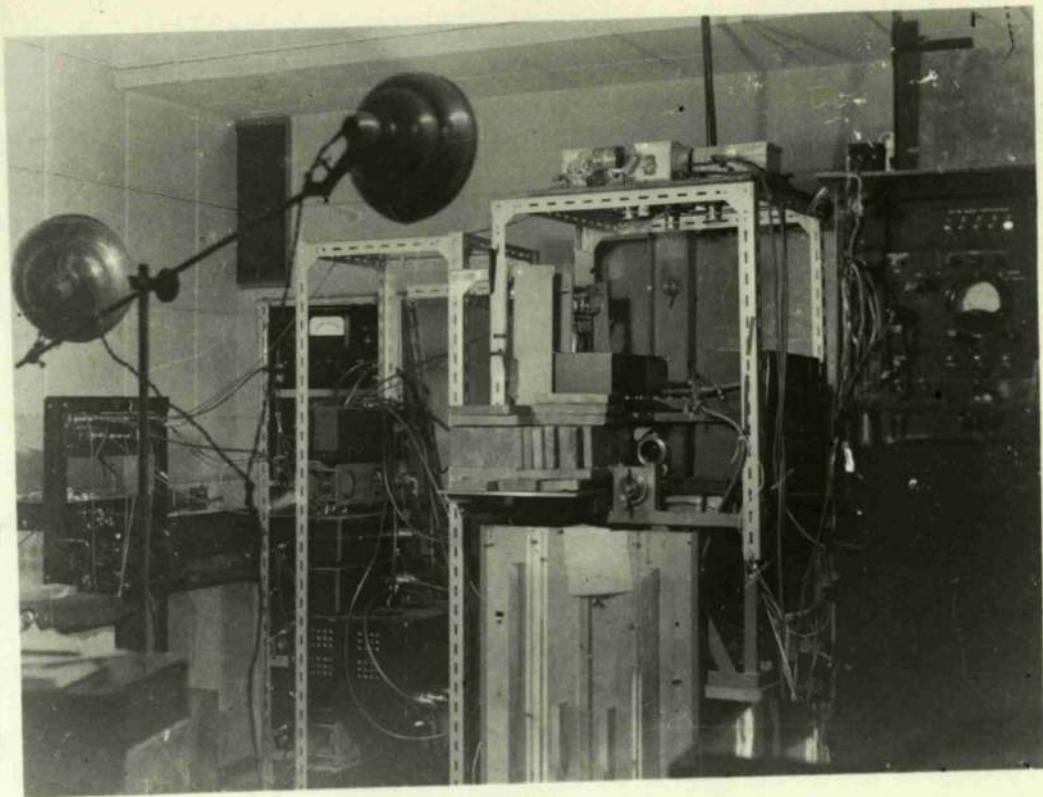
The developed films were replaced in the appropriate cameras which were positioned relative both to each other and to a flat table, substituted for the cloud chamber, as they had been during the experiment. Light from a Siemens 240V./125W. mercury vapour lamp was directed through the back of each camera and the track images were projected on the table which could be adjusted to any vertical height and rotated to any desired position. The glass top from the cloud chamber was positioned between the camera lenses and the reprojection table to compensate for any refractive index effects. By aligning two of the images of each track in turn on the table, reconstruction in three dimensions of each event was possible. This method compares very favourably with other systems for accuracy in measuring long tracks but is inherently incapable of making such measurements with the required degree of accuracy for tracks less than 1 cm. long. Since many of the recoil tracks in this experiment were below this value an additional method was employed. This involves using a microscope to measure the lengths of the images of each event, as shown on the three films, and relating those to the actual dimensions of the



Photograph III.1.  
(Photodisintegration Apparatus).



Photograph III.2.  
(Counter System).



tracks in space by means of a track simulator placed on the projection table, in the horizontal position, at the origin of the event. This system has been described in greater detail elsewhere (181).

### III.3. Beam Monitor.

The gamma-ray beam, after leaving the cloud chamber through a 0.0005 in. thick "mylar" window, passed into an ionisation chamber which was connected to an integrating circuit. The number of integrator units, corresponding to a given number of equivalent quanta, was recorded after each cloud chamber expansion.

### III.4. Calculation of Results.

Although the calculations involved in fitting a particular nuclear event to a specific nuclear reaction by momentum and energy balancing are not difficult, they are very tedious, as a single calculation involves more than two hundred separate steps.

In this particular experiment the cloud chamber was triggered by a high energy photoproton. Although from pulse height considerations it was believed that the proton energy,  $E_p$ , was always in the region of 100 MeV, the effect of varying the proton energy between 80 MeV and 120 MeV was regarded as valuable information. This meant repeating a large part of each calculation for each proton energy.

A programme was written to enable a DEUCE computer to do

this work hence eliminating much of the tedium. The information obtained from each event was limited only by the time taken by the machine to punch out the results and by the number of cards which could be conveniently handled.

The data selected for each event was:-

- a)  $\frac{E_{\gamma}}{c} - p_{nx}$ , the momentum of the  $\gamma$ -ray minus the component in the  $\gamma$ -ray direction of the momentum of the neutron required to give an energy and momentum balance.
- b)  $p_{ny}$ , the component in the y-direction of the momentum of the balancing neutron.
- c)  $p_{nz}$ , the component in the z-direction of the momentum of the balancing neutron.
- d)  $E_{\gamma}$ , the energy of the  $\gamma$ -ray.
- e)  $E_n$ , the neutron energy.
- f)  $p_n$ , the total neutron momentum.
- g)  $\alpha_n$ , the angle which the neutron direction makes with the horizontal.
- h)  $\beta_n$ , the angle which the projection of the neutron track on the horizontal makes with the  $\gamma$ -ray direction.

A source of error which arose in the calculations was the result of some of the tracks not stopping in the chamber in several of the multi-particle events. In these cases a minimum track length, which was always known, was used to obtain the energy of the particle i.e. the lower limit of the particle energy was used. This was borne in mind when

the final classification of events was made.

### III.5. Experimental Results.

#### III.5.1. Classification of Events.

In addition to the oxygen, the cloud chamber contained (a) helium, which was added to reduce the stopping power of the gas target and thus enable longer tracks to be obtained from the recoiling nuclei; (b) carbon, which was present in the alcohol-water vapour mixture; and (c) nitrogen, present as an impurity.

The various reactions for which an energy and momentum balance were attempted were therefore those in which the initial target nucleus was either oxygen, helium, carbon or nitrogen.

It is convenient in any experiment, in which a visual technique is used, to classify events according to the number of tracks (or charged particles) visible. This procedure is followed here.

One-Particle Events. Ten one-particle events were found. These were regarded as being ( $\gamma, pn$ ) events in which the recoil was too short to be observed. They were classified as the reaction  $O^{16}(\gamma, pn)N^{14}$ . The justification for this may become apparent later. No calculations could be attempted. In this case, of course, the "one-particle" is the triggering proton.

Two-Particle Events. A total of ninety-nine two-particle events were obtained.

Helium Disintegrations. Five of the two-particle events could be classified as being due only to helium because of the very long recoil obtained. In four cases the recoil did not stop in the cloud chamber.

Although none of the events had coplanar disintegration products an attempt was made to ascertain if they would satisfy the  $\text{He}^4(\gamma, p)T$  kinematics. For triggering proton energies of 80 MeV and 100 MeV all the  $E_\gamma$ 's obtained were possible, i.e. they lay between 80 MeV and 240 MeV which was the limit of the machine energy. For a proton energy of 120 MeV, only one event did not yield a feasible  $E_\gamma$ -value. In all cases, however, the value obtained for  $E_n$ , the "energy unbalance", was greater than 10 MeV hence none of the events satisfied this interpretation.

These five cases were then submitted to the test for the  $\text{He}^4(\gamma, pn)d$  reaction. For proton energies of 80 MeV and 100 MeV all the events fitted and for  $E_p = 120$  MeV only one did not give a reasonable value for  $E_\gamma$ . This particular event was the one producing a similar result for the  $\text{He}^4(\gamma, p)T$  reaction when  $E_p$  was 120 MeV. The five events were therefore attributed to the  $\text{He}^4(\gamma, pn)d$  reaction. A total of eight events were thus interpreted as  $\text{He}^4(\gamma, pn)d$

- 70 -

when the three discussed on page 71 were included.

Oxygen and Carbon Disintegrations.

Seven events were thought to be possible  $(\gamma, p)$  events because of their coplanarity. These events were tested for  $O^{16}(\gamma, p)N^{15}$  and subsequently for  $C^{12}(\gamma, p)B^{11}$ . In all cases, for  $E_p = 80, 100$  and  $120$  MeV, the values of  $E_\gamma$  obtained were within the limits of machine energy.

For the interpretation  $O^{16}(\gamma, p)N^{15}$  the residual energy,  $E_n$ , was below 5 MeV in five cases for  $E_p = 80$  MeV, in four cases for  $E_p = 100$  MeV and in only one case for  $E_p = 120$  MeV. In only one instance, for the interpretation  $C^{12}(\gamma, p)B^{11}$ , was the  $E_n$ -value less than 5 MeV, and this was for a triggering proton energy of 80 MeV. In this particular event the fit was better for  $O^{16}(\gamma, p)N^{15}$  than for  $C^{12}(\gamma, p)B^{11}$ .

Of these seven events, therefore, five were classified as  $O^{16}(\gamma, p)N^{15}$  and the other two as either  $O^{16}(\gamma, pn)N^{14}$  or  $C^{12}(\gamma, pn)B^{10}$ . The remaining two-particle events, eighty seven in number, were initially tested for the  $O^{16}(\gamma, pn)N^{14}$  and the  $C^{12}(\gamma, pn)B^{10}$  reactions.

	$E_p = 80$ MeV	$E_p = 100$ MeV	$E_p = 120$ MeV
No. of events unambiguously $O^{16}(\gamma, pn)N^{14}$	1	1	4
No. of events unambiguously $C^{12}(\gamma, pn)B^{10}$	2	0	0
No. of events fitting both $O^{16}(\gamma, pn)N^{14}$ and $C^{12}(\gamma, pn)B^{10}$	79	64	46
No. of events not fitting either $O^{16}(\gamma, pn)N^{14}$ or $C^{12}(\gamma, pn)B^{10}$	5	21	37

It was invariably found that an event not fitting for a proton energy of 80 MeV would not, in addition, give a reasonable  $E_\gamma$ -value for a proton energy of either 100 or 120 MeV.

Those five events which did not fit for  $E_p = 80$  MeV and the twenty-one which did not fit for  $E_p = 100$  MeV were tested for the  $He^4(\gamma, p)T$  and the  $He^4(\gamma, pn)d$  reactions. As might be expected, none of the events were found to fit  $He^4(\gamma, p)T$ . Of the five events which did not fit either  $O^{16}(\gamma, pn)N^{14}$  or  $C^{12}(\gamma, pn)B^{10}$  at all, three were found to fit  $He^4(\gamma, pn)d$  but only for a proton energy of 80 MeV.

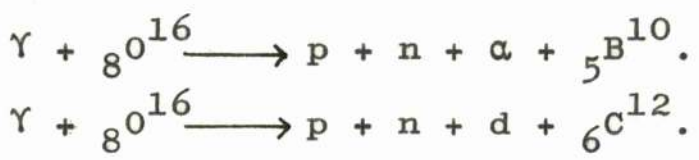
Thus, of the ninety-nine two-particle events, two do not fit at all.

Final Classification.

Target Element		$E_p = 80$ MeV	$E_p = 100$ MeV	$E_p = 120$ MeV
Two-prong non-coplanar i.e. ( $\gamma, pn$ )'s	( 0	1	1	4
	C	81	66	48
	(He	2	0	0
Two-prong coplanar i.e. ( $\gamma, p$ )'s	( 0	5	4	1
	C	0	0	0
	(He	0	0	0
Non-fits		2	23	42

Three-Particle Events.      Of the events displaying three charged fragments forty-seven examples were found. In twenty-one cases two of the tracks, including the triggering particle, did not stop.

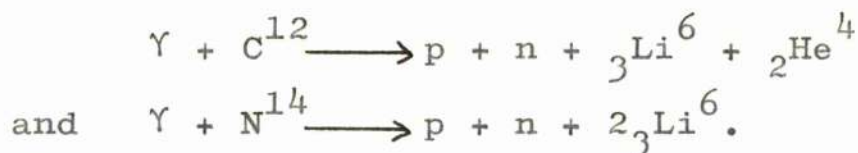
An attempt was made to fit each of these to two interpretations initially. The reactions were



Purely from computation, the following results were obtained.

	$E_p = 80$ MeV	$E_p = 100$ MeV	$E_p = 120$ MeV
No. of events unambiguously $O^{16}(\gamma, pna)B^{10}$	9	6	8
No. of events unambiguously $O^{16}(\gamma, pnd)C^{12}$	7	4	2
No. of events fitting both $O^{16}(\gamma, pna)B^{10}$ and $O^{16}(\gamma, pnd)C^{12}$	24	21	15
No. of events fitting neither $O^{16}(\gamma, pna)B^{10}$ nor $O^{16}(\gamma, pnd)C^{12}$	7	16	22

Those sixteen events which failed to fit for either  $E_p = 80$  MeV or  $E_p = 100$  MeV for either of the above two reactions were subsequently submitted to the test for the reactions



As stated previously these sixteen events necessarily included the seven cases which did not fit for a proton energy of 80 MeV. Again, entirely from computation, the following results were obtained.

	$E_p = 80$ MeV	$E_p = 100$ MeV	$E_p = 120$ MeV
No. of events unambiguously $C^{12}(\gamma, pn) {}_3Li^6, {}_2He^4$	2	1	0
No. of events unambiguously $N^{14}(\gamma, pn) 2{}_3Li^6$	1	1	1

	$E_p = 80$ MeV	$E_p = 100$ MeV	$E_p = 120$ MeV
No. of events fitting both $C^{12}(\gamma, pn)_3Li^6, {}_2He^4$ and $N^{14}(\gamma, pn)_2{}_3Li^6$ .	8	5	3
No. of events fitting neither $C^{12}(\gamma, pn)_3Li^6, {}_2He^4$ nor $N^{14}(\gamma, pn)_2{}_3Li^6$ .	5	9	12

In attempting to fit the forty-seven events to one or other of the above four reactions, success was achieved except in one case.

The above classification has referred only to computation; as yet, no detailed attention has been given to track density and length as seen in the cloud chamber photographs.

Bearing in mind the results of the computation, each event was now carefully observed and given a final assignment according to its appearance.

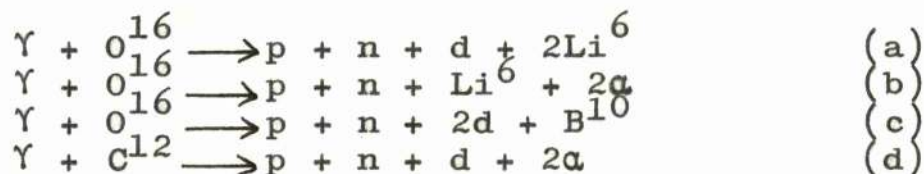
Those unambiguous events were used to provide standards of comparative track density. Final results for events having three charged particles were:

Event	No. of cases
$\gamma + O^{16} \longrightarrow p + n + \alpha + B^{10}$	25
$\gamma + O^{16} \longrightarrow p + n + d + C^{12}$	13
$\gamma + C^{12} \longrightarrow p + n + Li^6 + He^4$	4
$\gamma + N^{14} \longrightarrow p + n + 2Li^6$	2

One event which fitted both for  $O^{16} \longrightarrow p + n + \alpha + B^{10}$  and for  $O^{16} \longrightarrow p + n + d + C^{12}$  for all  $E_p$  had the appearance of the  $N^{14} \longrightarrow p + n + 2Li^6$  reaction. Another event which fitted  $O^{16} \longrightarrow p + n + \alpha + B^{10}$  and  $O^{16} \longrightarrow p + n + d + C^{12}$  for proton energies of 80 and 100 MeV could have been either interpretation and a single event did not fit any of the above four reactions for any of the three values of  $E_p$ .

Four-Particle Events. There were twenty-five cases in which the target nucleus split into four charged fragments and in fourteen of these, two of the fragments, including the high energy proton, failed to stop.

Four possible interpretations were tried:



From computation the following information was obtained.

	$E_p = 80$ MeV	$E_p = 100$ MeV	$E_p = 120$ MeV
No. of events unambiguously reaction (a)	0	0	0
No. of events unambiguously reaction (b)	0	1	1
No. of events unambiguously reaction (c)	1	1	0
No. of events unambiguously reaction (d)	2	1	1

	$E_p = 80$ MeV	$E_p = 100$ MeV	$E_p = 120$ MeV
No. of events fitting two or more of reactions (a)-(d)	20	19	13
No. of events not fitting any of reactions (a)-(d)	2	3	10

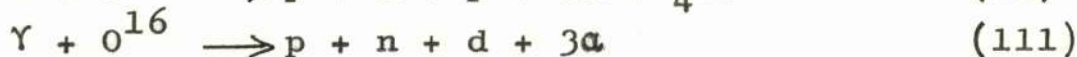
After re-examination of the film the following classification was arrived at:

Event	No. of cases obtained
$\gamma + O^{16} \rightarrow p + n + d + 2Li^6$	8
$\gamma + O^{16} \rightarrow p + n + Li^6 + 2\alpha$	6
$\gamma + O^{16} \rightarrow p + n + 2d + {}_5B^{10}$	5
$\gamma + C^{12} \rightarrow p + n + d + 2\alpha$	4

Two events do not fit any of the above four reactions.

Five-Particle Events. Nineteen events were found in which the target nucleus split into five charged particles. In twelve cases one of the fragments, other than the triggering particle, did not stop in the cloud chamber.

Attempts were made to obtain a fit for four possible reactions:



From computation alone the results obtained were:

	$E_p = 80$ MeV	$E_p = 100$ MeV	$E_p = 120$ MeV
No. of events unambiguously (1)	0	0	0
No. of events unambiguously (11)	0	0	0
No. of events unambiguously (111)	1	1	3
No. of events unambiguously (1V)	1	0	0
No. of events fitting two or more of (1)-(1V)	15	11	16
No. of events not fitting any of (1)-(1V)	2	7	10

The following conclusions were made after reconsidering the cloud chamber photographs:

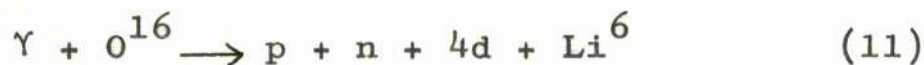
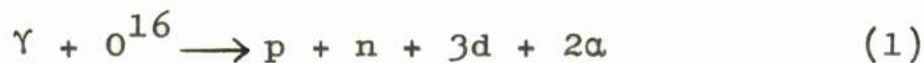
Event	No. of cases obtained
$\gamma + O^{16} \rightarrow p + n + d + 3\alpha$	7
$\gamma + O^{16} \rightarrow p + n + \alpha + 2d + Li^6$	6
$\gamma + O^{16} \rightarrow p + n + p + 2d + Be^9$	1
$\gamma + C^{12} \rightarrow p + n + \alpha + 3d$	2

One event could have been  $O^{16} \rightarrow p + n + p + 2d + Be^9$  or  $O^{16} \rightarrow p + n + d + 3\alpha$ .

Two events did not fit any of the above.

Six-Particle Events. Two cases of the target nucleus splitting into six charged fragments were obtained. In both cases one of the fragments, other than the triggering proton, did not stop.

Three reactions suggested themselves as possibilities:



One did not fit any of these reactions and the other fitted all three for a proton energy of 80 MeV. At a proton energy of 100 MeV, this event fitted only (1) and (111) and did not fit any when the value of  $E_p$  was raised to 120 MeV.

On examination of the film it was decided that the event which showed a fit was most aptly classified as



Final Classification.

The final assignment of events can be seen in table on page 78a. The line labelled "uncertain" refers only to those events mentioned in the previous discussion and is rather optimistic in that we cannot tell when two neutrons have been emitted in the disintegration. We can but assume that only one neutron is concerned. A further five events discussed in the section on neutron energy distributions, are also open to debate.

Final Classification.

	1 Prong	2 Prong		3 Prong	4 Prong	5 Prong	6 Prong	Total No. of events
		Coplanar	non-co planar					
Oxygen	10	5	79	38	19	14	1	166
Helium	0	0	8	0	0	0	0	8
Carbon	0	0	5	4	4	2	0	15
Nitrogen	0	0	0	2	0	0	0	2
Uncertain	0	0	0	2	0	1	0	3
Unidentified	0	0	2	1	2	2	1	8
<b>Total</b>	10	5	94	47	25	19	2	202

Histograms were plotted of proton angular, neutron angular and energy, and gamma-ray energy distributions. In all cases the same procedure was carried out: when all the events had been classified into particular reactions, the appropriate distributions were plotted for each reaction for proton energies of 80, 100 and 120 MeV. In many cases the statistics were very poor and hence none of these are shown. The histograms obtained were then summed to give the distributions for two, three, four and five charged particle groups and the latter were added to give the distributions for all events irrespective of classification.

In all previous work on the "quasi-deuteron" model of Levinger in the region beyond 100 MeV the energy of the neutron, detected in coincidence with a high energy proton, was not measured and was only known as being greater than a certain minimum energy. This minimum value was the threshold energy for the neutron detector and was usually about 20 MeV. The present work involving a cloud chamber technique enabled neutron energies of less than 1 MeV to be determined although any multi-particle event where the neutron energy was below 5 MeV might have been due to a pure ( $\gamma, p$ ) event in which inaccuracy of measurement produced an energy unbalance in the conservation calculations.

The proton and neutron angular distributions are already well known from counter work when they are detected

separately, and the angular distributions of neutrons emitted in coincidence with protons in a fixed direction are also fairly well known although few proton angles have been attempted.

### III.5.2. Proton Angular Distributions.

Figures III.2. to III.7 show histograms of the relationship between the number of protons and the laboratory proton angle with respect to the  $\gamma$ -ray beam. In this case " $\psi$ " is the angle which the proton forms with the beam in the plane of the proton and the beam. This angle cannot differ by more than two degrees from the angle " $\beta$ ", which the proton forms with the beam in the horizontal plane, as the counter geometry limited the angle of the proton with respect to the horizontal to a maximum of twelve degrees. This difference will not be significant in the angular distributions in which five degree intervals are taken.

The proton angular distributions do not, of course, vary with proton energy in our case as the protons were used to trigger the cloud chamber.

The distribution for all two particle events shows a distinct forward peak with most of the protons occurring in the  $60^\circ$  to  $80^\circ$  region. For all three particle events, the number of protons in the forward hemisphere is much greater than in the backward hemisphere but the peak has shifted back to the  $70^\circ$  to  $90^\circ$  region. The distributions for four and five particle events again show that the majority of the protons lie in the forward hemisphere. Unfortunately, no conclusions can be reached because of poor statistics, and to surmount this drawback we consider

the angular distribution for all events. The cloud chamber gas forms an extended target causing an apparently larger range of angles than is to be expected when using three fixed telescopes. The distribution is again markedly forward with peaks in the  $55^{\circ}$  to  $60^{\circ}$  and  $75^{\circ}$  to  $80^{\circ}$  regions. Considering  $10^{\circ}$  intervals most protons are found to occur in the  $70^{\circ}$  to  $80^{\circ}$  region.

The value obtained here for the angle at which the maximum in the angular distribution occurs is somewhat larger than from previous counter experiments. For 100 MeV photoprotons from carbon the maximum lies in the  $35^{\circ}$  to  $40^{\circ}$  interval. Levinger calculates that the peak should be slightly under  $60^{\circ}$  for 70 MeV protons (126, 131, 132, 133).

It would appear that we have obtained a final proton angular distribution which shows effects due to our fixed counter arrangement. The counter telescopes were placed at mean angles of  $45^{\circ}$ ,  $90^{\circ}$  and  $135^{\circ}$  with respect to the centre of the cloud chamber and at a distance of 30 cm. from this point in each case. Since the scintillators were 10 cm. and the target 30 cm. in length, the front, middle and back telescopes subtended the angular ranges  $25^{\circ}$  to  $88^{\circ}$ ,  $55^{\circ}$  to  $125^{\circ}$  and  $92^{\circ}$  to  $155^{\circ}$  respectively. Considering the angular distribution for carbon as given by Rosengren and Dudley and seen in figure III.8, it is seen that the overlap in angles given by the counter system between  $55^{\circ}$  and  $88^{\circ}$ , and

between  $92^{\circ}$  and  $125^{\circ}$  will give rise to maxima in these regions. This is more readily seen when we plot the distributions for the three telescopes separately as in figures III.9 to III.11.

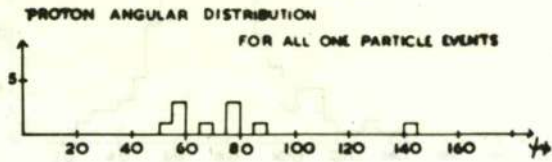


FIG. III 2.

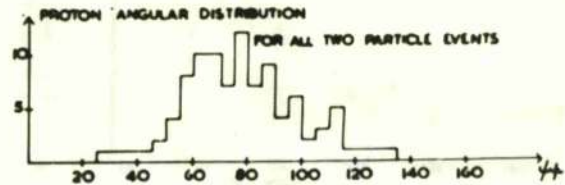


FIG. III 3.

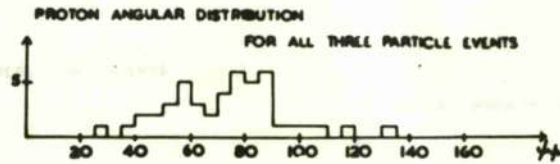


FIG. III 4.

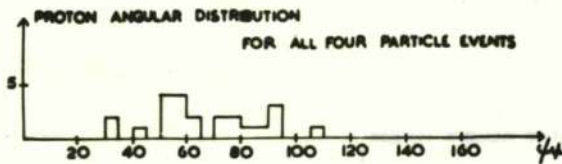


FIG. III 5.

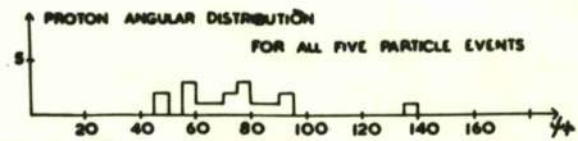


FIG. III 6.

FIG. III 11.

III.5.3. Neutron angular distribution

Because of the counter effect

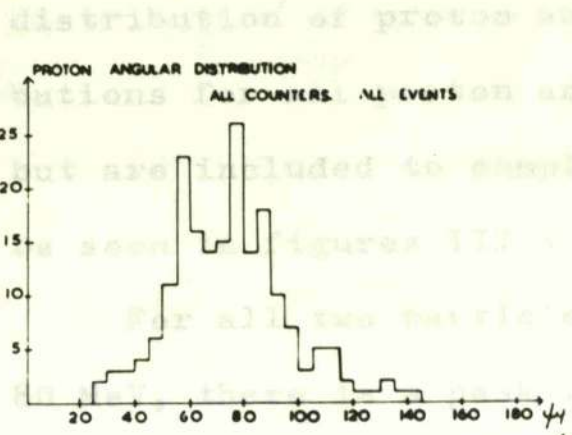
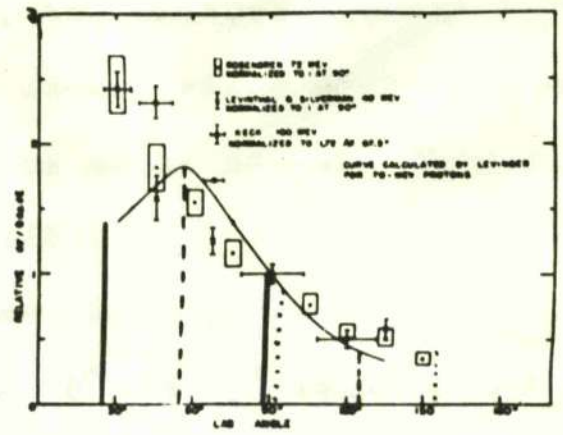


FIG. III. 7.



Angular distributions of photoprotons from carbon.  
FIG. III. 8

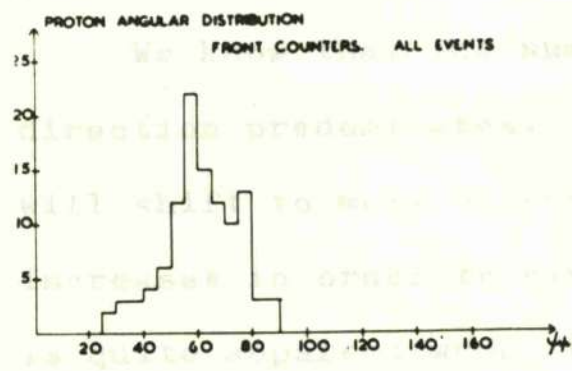


FIG. III. 9.

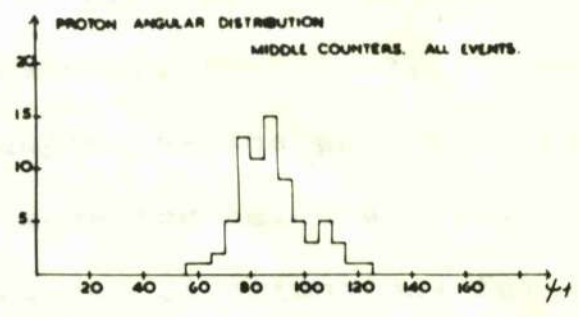


FIG. III. 10.

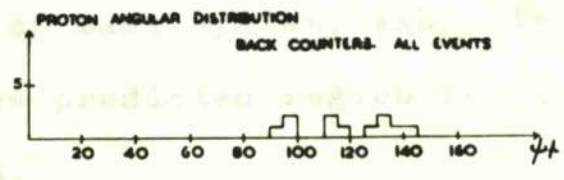


FIG. III. 11.

### III.5.3. Neutron Angular Distributions.

Because of the counter effect we experienced in the distribution of proton angles, the neutron angular distributions for all proton angles cannot yield much information but are included to complete the description. They can be seen in figures III.12 to III.17.

For all two particle events at a proton energy of 80 MeV, there is a peak in the  $70^{\circ}$  to  $75^{\circ}$  region, and an increase of proton energy results in the peak position moving to more backward angles. A similar effect can be seen for the three particle events. For the four and five particle events the statistics are poor.

We know that the number of protons in the forward direction predominates. In general, therefore, the neutron will shift to more backward angles as the proton energy increases in order to give a momentum balance. This shift is quite apparent when the neutron distributions for all events are considered.

The neutron angular distribution for 80 MeV protons in the region of  $70^{\circ}$  to  $80^{\circ}$ , corresponding roughly to  $90^{\circ}$  in the centre of mass system, exhibits a peak at  $75^{\circ}$  to  $80^{\circ}$  which is in the predicted region for "quasi-deuteron" disintegration.

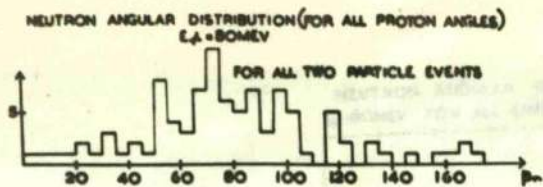


FIG III 12 a

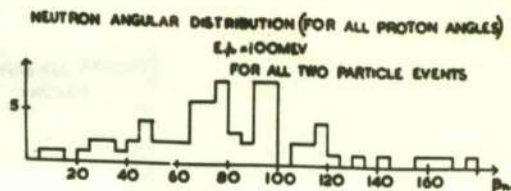


FIG III 12.b.

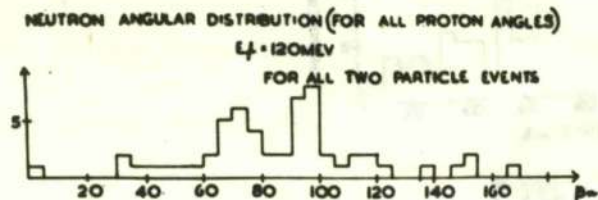


FIG III 12.c.

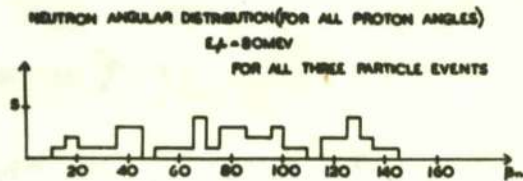


FIG III 13 a.

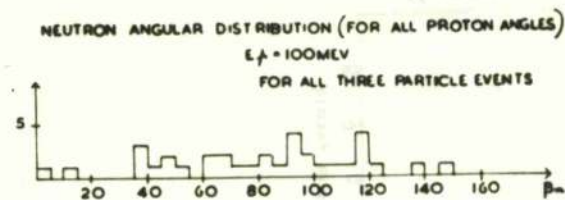


FIG III 13 b.

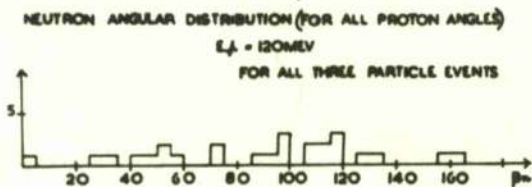


FIG III 13 c.

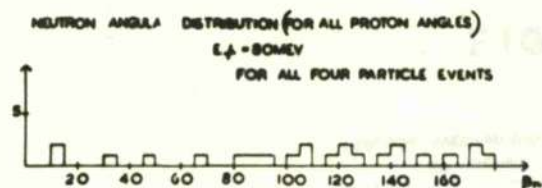


FIG III 14 a.

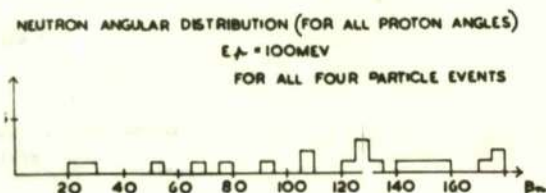


FIG III 14 b.

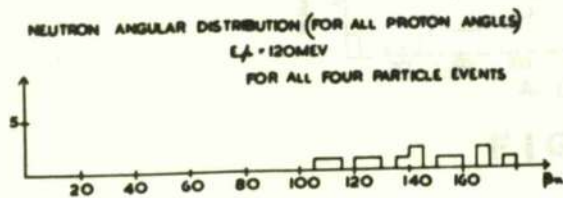


FIG III 14 c.

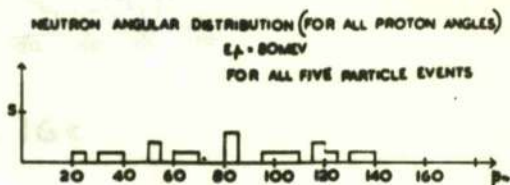


FIG III 15 a.

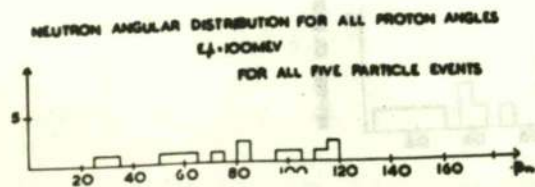


FIG III 15 b.

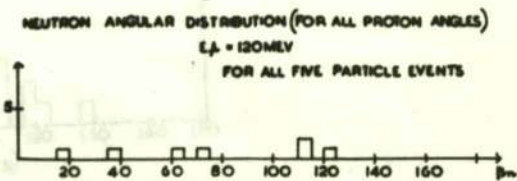


FIG III 15 c.

III.5.4. Gamma-Ray

NEUTRON ANGULAR DISTRIBUTION (FOR ALL PROTON ANGLES)  
 $E_p = 80\text{MEV}$  FOR ALL EVENTS

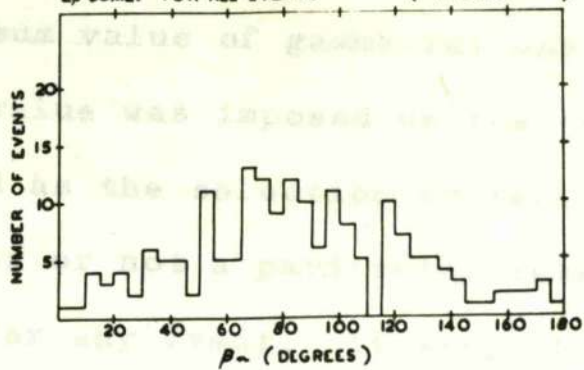


FIG. III 16a

NEUTRON ANGULAR DISTRIBUTION (FOR ALL PROTON ANGLES)  
 $E_p = 100\text{MEV}$  FOR ALL EVENTS

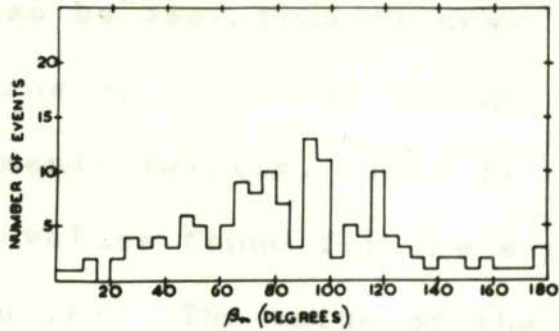


FIG. III 16b.

NEUTRON ANGULAR DISTRIBUTIONS (FOR ALL PROTON ANGLES)  
 $E_p = 120\text{MEV}$  FOR ALL EVENTS

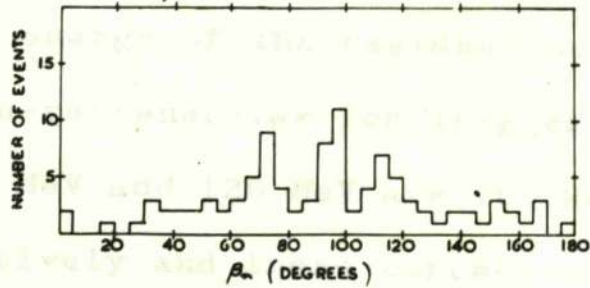


FIG. III 16c.

ANGULAR DISTRIBUTION OF NEUTRONS FOR  $70^\circ < \psi_p < 80^\circ$   
 $E_p = 80\text{MEV}$

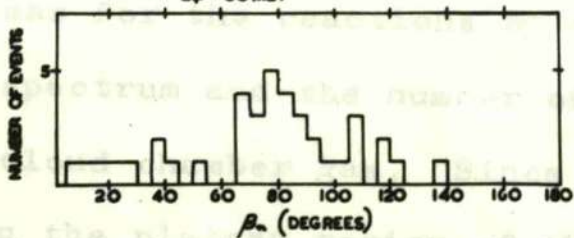


FIG. III 17.

### III.5.4. Gamma-Ray Energy Distributions.

The maximum value of gamma-ray energy is 240 MeV in all cases. This value was imposed on the results by the fact that it served as the selection criterion when it was decided whether or not a particular interpretation was satisfactory for any event. It was, of course, the maximum value of the bremsstrahlung spectrum produced by the synchrotron during the experiment.

It can also be seen from figures III.18 to III.22 that the minimum value of gamma-ray energy increases with the number of fragments emitted. This is not unexpected when we look at the values found for the excitation energies of the residual nuclei. The value of the gamma-ray energy for each reaction must include the triggering proton energy, the neutron energy, the threshold energy for the reaction, and the excitation energy of the residual nucleus. The minimum values of gamma-ray energies for triggering proton energies of 80 MeV, 100 MeV and 120 MeV are 100 MeV, 125 MeV and 140 MeV respectively and these correspond to two particle events.

The gamma-ray energy distributions can be used to derive the cross-sections for the reactions by considering the bremsstrahlung spectrum and the number of target nuclei present in the cloud chamber gas. Since all the values lie approximately in the plateau region of the spectrum the

cross-sections will be almost the same shape as the energy distributions.

The cross-section for production of photoprotons is defined by the following expression

$$n = K \int_0^{E_0} P(E, E_0) \sigma(E) dE$$

where:  $n$  is the number of photoprotons.

$K$  is the product of the number of reacting nuclei, the fractional solid angle in which the protons are observed and the number of roentgens delivered to the target.

$P(E, E_0) dE$  is the number of protons per square centimetre per roentgen with energies between  $E$  and  $E + dE$  in the spectrum of maximum energy  $E_0$ , and  $\sigma(E)$  is the cross-section for photo-production by photons of energy  $E$ .

If we consider only those photoprotons produced by photons in the energy interval between  $E$  and  $E + dE$ , then the number  $n_e$  of such protons is given by

$$n_e = KN_\gamma(E) \bar{\sigma}(E)$$

where  $N_\gamma(E)$  is the total number of photons per  $\text{cm}^2$  per roentgen in the energy interval  $\Delta E$ , and  $\bar{\sigma}(E)$  is the average cross-section over the energy interval  $\Delta E$ .

For 100 MeV ( $\pm 10$  MeV) protons at  $50^\circ$  ( $\pm 10^\circ$ ) to gamma-rays with energies between 140 MeV and 160 MeV it is found that  $\bar{\sigma}(E) = 0.3 \pm .03 \times 10^{-30} \text{cm}^2/\text{MeV} - Q - \text{steradian}$  where  $Q$  denotes the number of equivalent quanta.

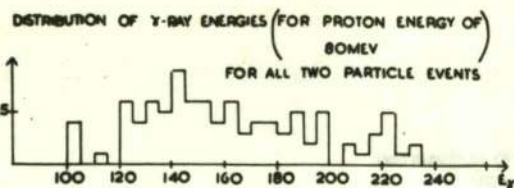


FIG. III 18a

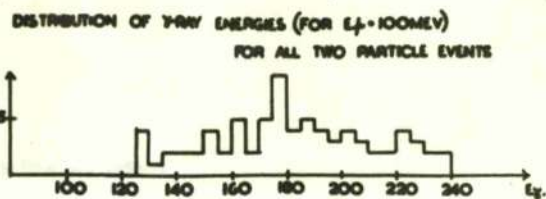


FIG. III 18b.

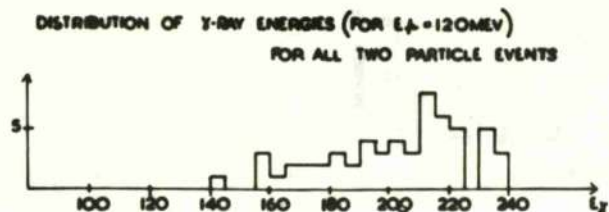


FIG. III 18c.

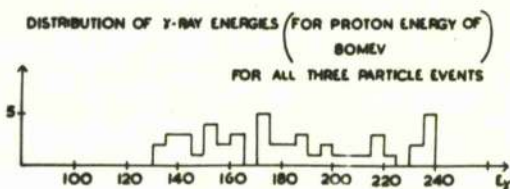


FIG III 19a

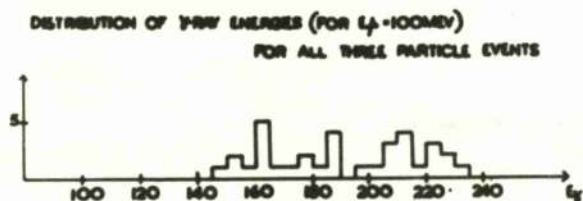


FIG III 19b.

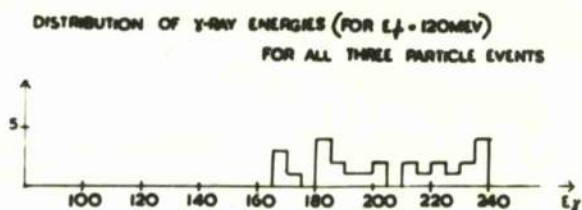


FIG III 19c.

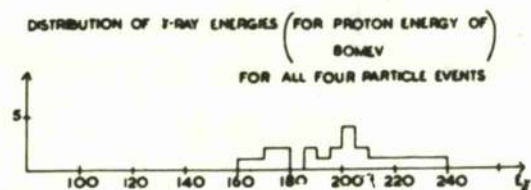


FIG III 20a

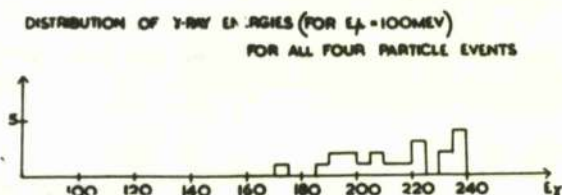


FIG III 20b

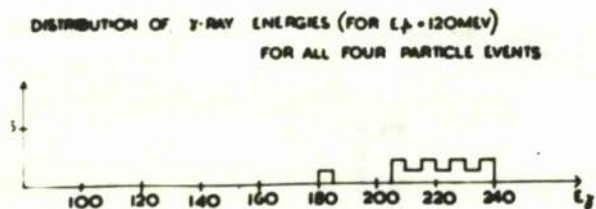


FIG. III 20c

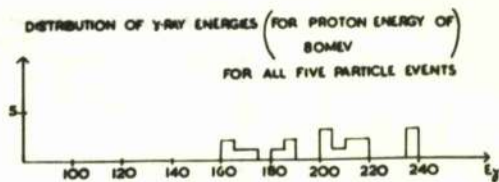


FIG III 21a

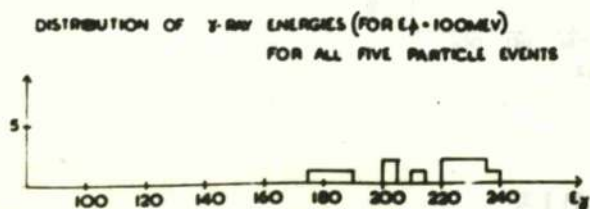


FIG III 21b.

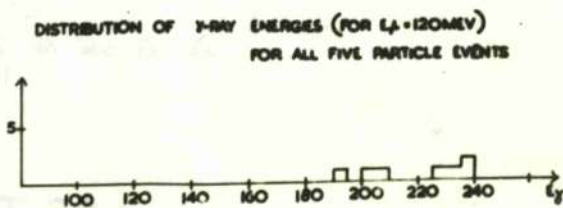


FIG III 21c.

DISTRIBUTION OF  $\gamma$ -RAY ENERGIES FOR ALL EVENTS  
(FOR  $E_A = 80$  MEV)

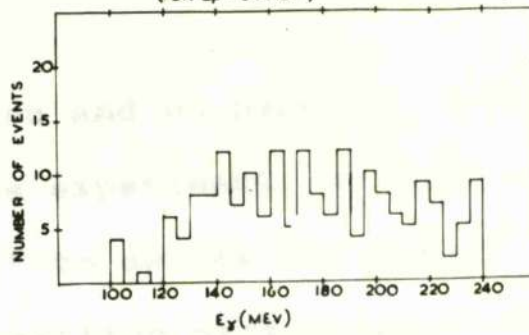


FIG III 22 a

DISTRIBUTION OF  $\gamma$ -RAY ENERGIES FOR ALL EVENTS  
(FOR  $E_A = 100$  MEV)

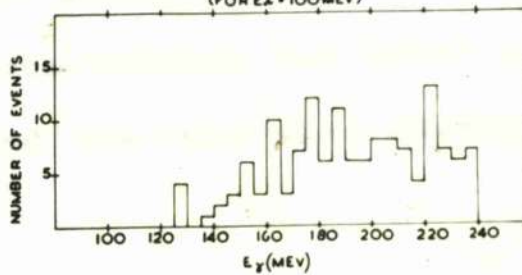


FIG III 22 b.

DISTRIBUTION OF  $\gamma$ -RAY ENERGIES FOR ALL EVENTS  
( $E_A = 120$  MEV)

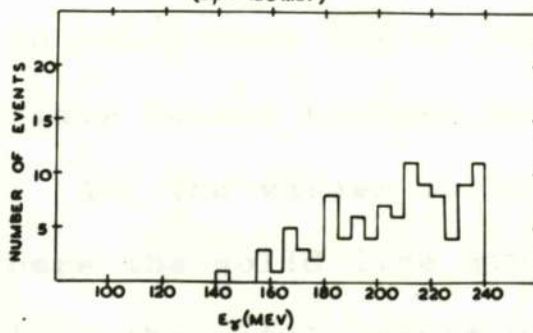


FIG III 22 c.

Addendum:

In this section and on page 98, when referring to the results of this experiment, we have used the term "excitation energy" to denote the sum of the kinetic energies of the recoiling particles, after emission of the proton-neutron pair, and the threshold energy for the reaction.

This differs from the usual use of the term "excitation energy" which is more commonly regarded as being the difference between the total energy of the excited nucleus and its rest mass energy in its ground state.

were available in which both the deuteron and  $C^{12}$  nucleus stopped. These gave values between 12 MeV and 20 MeV, which averaged 15 MeV. All the values obtained can be seen in Figure III.23 where the solid line gives the absolute values and the dotted line the total result when the minimum values are also considered.

### III.5.5. Excitation Energy Distributions.

The excitation energies of the residual  $N^{14}$  nucleus were calculated for all events. An absolute value could be obtained only when all the disintegration products stopped in the cloud chamber. When one or more particles passed through the chamber walls only a minimum value could be ascribed to the excitation energy.

Two-Particle Events. It was possible to assign a definite value to the excitation energy of the residual  $N^{14}$  nucleus in all of the seventy-nine two prong non-coplanar events originating from an oxygen target nucleus. Values ranging from 23 MeV to 36 MeV averaged 24 MeV.

Three-Particle Events. Fourteen cases were obtained of the reaction  $O^{16} \longrightarrow p + n + \alpha + B^{10}$  in which both the alpha particle and the  $B^{10}$  nucleus stopped in the cloud chamber. The excitation energies ranged from a minimum of 16 MeV to a maximum of 34 MeV, the average value being 25 MeV. For the reaction  $O^{16} \longrightarrow p + n + d + C^{12}$  only four examples were available in which both the deuteron and  $C^{12}$  nucleus stopped. These gave values between 12 MeV and 20 MeV, which averaged 15 MeV. All the values obtained can be seen in Figure III.23 where the solid line gives the absolute values and the dotted line the total result when the minimum values are also considered.

The average of the absolute values obtained for every three particle event was found to be 23 MeV.

Four-Particle Events. In only three examples of the reaction  $O^{16} \longrightarrow p + n + d + 2 Li^6$  did all the charged particles (except the triggering proton) stop. These gave absolute values ranging from 44 MeV up to 52 MeV, the average result being 49 MeV.

Four cases were obtained in which the residual  $N^{14}$  nucleus disintegrated into a  $Li^6$  nucleus and two alpha particles and in which all of these stopped. The excitation energies given by them lay between 25 MeV and 63 MeV and averaged 39 MeV.

Because of the energetic deuterons usually obtained in the reaction  $O^{16} \longrightarrow p + n + 2d + B^{10}$  only one example was available in which the two deuterons and the  $B^{10}$  nucleus stopped in the cloud chamber. The excitation energy of the residual  $N^{14}$  nucleus in this case was 47 MeV.

The above eight events gave an average value of 44 MeV. The distribution can be seen plotted in Figure III.24.

Five-Particle Events. Two examples were obtained for each of the reactions  $O^{16} \longrightarrow p + n + d + 3\alpha$  and  $O^{16} \longrightarrow p + n + \alpha + 2d + Li^6$  in which all the disintegration products of the residual  $N^{14}$  nucleus stopped. The values obtained for the

former reaction were 26 MeV and 29 MeV and for the latter they were 50 MeV and 67 MeV. No absolute values could be ascribed in the case of the  $O^{16} \rightarrow p + n + p + 2d + Be^9$  reaction. The average value for the above four events was 43 MeV.

When all events were considered the average value obtained was 26 MeV.

In the excitation energy distribution plotted for all the three, four and five charged particle events (Figure III.26) it can be seen that most of the values lie in the 20 MeV to 35 MeV region.



### III.5.6. Neutron Energy Distributions.

In all previous work on the "quasi-deuteron" model of Levinger, neutrons emitted in coincidence with protons were detected by means of a neutron counter, by observing the recoils from the neutrons scattering off nuclei of the scintillator. The detector usually had an efficiency of only approximately 10%. Applying this method Barton and Smith (159) obtained counts when the neutron energy was greater than 20 MeV, and Wattenberg et al. (156) observed neutrons with a minimum energy of 15 MeV. These energies were the threshold energies of the detectors and no information other than that the neutron energy was greater than these values was available.

Figures III.27 to III.31 show the energy distributions of the neutrons, emitted in coincidence with the high energy protons, obtained from the present experiment.

Two-Particle Events. For a triggering proton energy of 80 MeV the energies of the neutron vary from 5 MeV to 135 MeV. A large number of neutrons have energies below 40 MeV with a maximum appearing in the 20 MeV to 40 MeV region. Of the total of ninety-two events twelve have energies below 20 MeV. One event with a neutron energy below 5 MeV is obtained for a proton energy of 100 MeV. The maximum observed in the previous case appears to have moved to the

40 MeV to 60 MeV region. The total number of events has dropped to eighty-two of which eight have energies below 20 MeV. When the proton energy is increased to 120 MeV, two events with neutron energies less than 5 MeV are obtained. A large number appear in the 60 MeV to 80 MeV region and the maximum energy obtained is 90 MeV. Seven events out of a total of fifty-six have energies below 20 MeV.

In the case of only one event was the interpretation  $O^{16}(\gamma,p)N^{15}$  suggested by the low value of neutron momentum but, even in this case, the coplanarity criterion for the ejected proton and the  $N^{15}$  recoil was unsatisfied. The event must therefore be regarded as a  $(\gamma,pn)$  in which the neutron has low momentum.

Similar trends are seen in the distributions for three, four and five particle events.

Three-Particle Events. For each of the three proton energies considered, three events appear with neutron energies of less than 5 MeV. These events were all listed in the general classification as the reaction  $O^{16}(\gamma p n \alpha)B^{10}$ . They may perhaps be  $O^{16}(\gamma, p \alpha)B^{11}$ . The neutron energies obtained for these events were 0.85 MeV, 3.37 MeV and 4.02 MeV for a proton energy of 80 MeV.

For proton energies of 80 MeV, 100 MeV and 120 MeV the proportion of events with neutron energy less than 20 MeV

were 22%, 28% and 35% respectively of the total number.

Four-Particle Events. No events in this group have a neutron energy less than 5 MeV for any of the proton energies considered.

Thirteen, twenty and twenty-five per cent of the total number of events for proton energies of 80, 100 and 120 MeV respectively have neutron energies below 20 MeV.

Five-Particle Events. One event, for proton energies of 80 MeV and 100 MeV, has a neutron energy less than 5 MeV. For a proton energy of 120 MeV this neutron energy has to rise above 5 MeV to attain a momentum and energy balance. This event was classified as  $O^{16} \rightarrow p + n + d + 3\alpha$ , the neutron energy being 4.3 MeV for an 80 MeV proton. A small probability therefore exists that the reaction may be  $O^{16} \rightarrow p + t + 3\alpha$ .

All Events. For proton energies of 80 MeV, 100 MeV and 120 MeV the percentages of the total number of events with neutron energy less than 20 MeV are 15%, 17% and 22% respectively. At most, five events which have already been discussed, out of a total of more than one hundred and eighty events are in doubt with regard to classification.

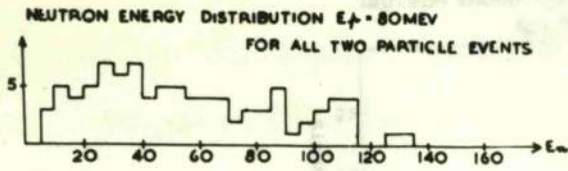


FIG III 27a

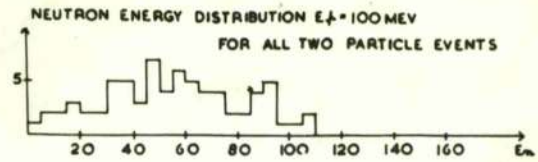


FIG III 27b.

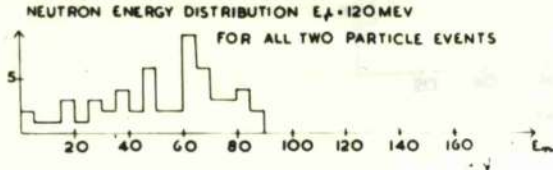


FIG III 27c

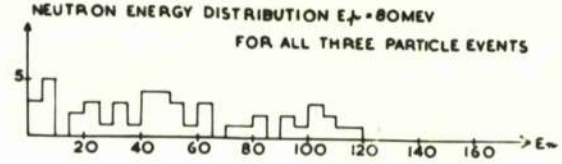


FIG III 28a

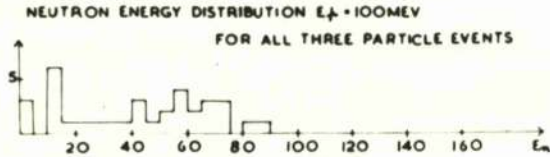


FIG III 28b.

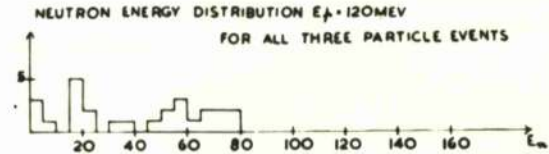


FIG III 28c.

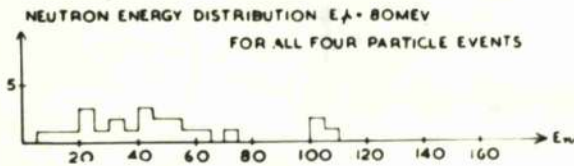


FIG III 29a

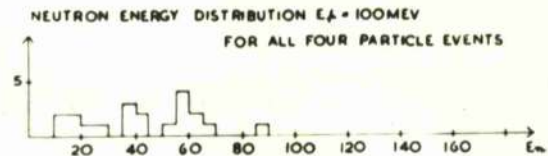


FIG III 29b.

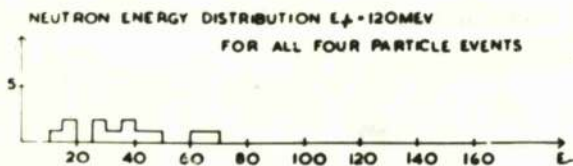


FIG III 29c

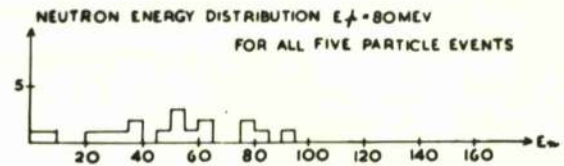


FIG III 30a

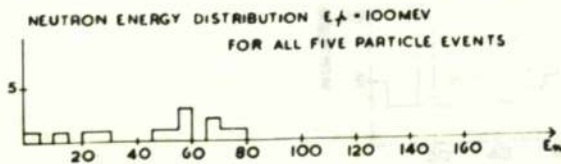


FIG III 30b

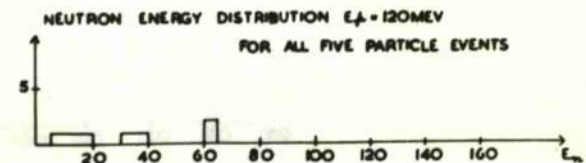


FIG III 30c.

NEUTRON ENERGY DISTRIBUTION FOR ALL EVENTS

$E_f = 80 \text{ MEV}$

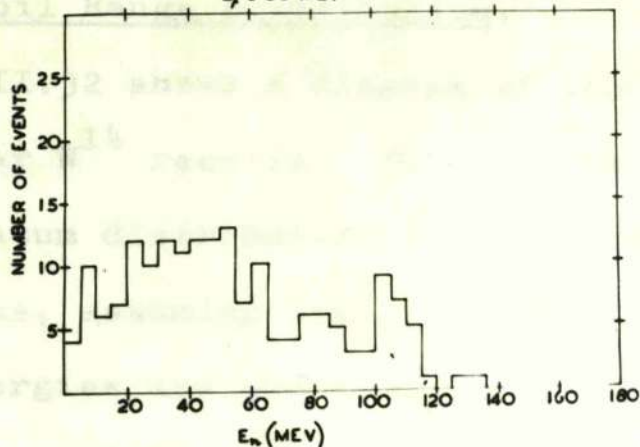


FIG. III 31a.

NEUTRON ENERGY DISTRIBUTION FOR ALL EVENTS

$E_f = 100 \text{ MEV}$

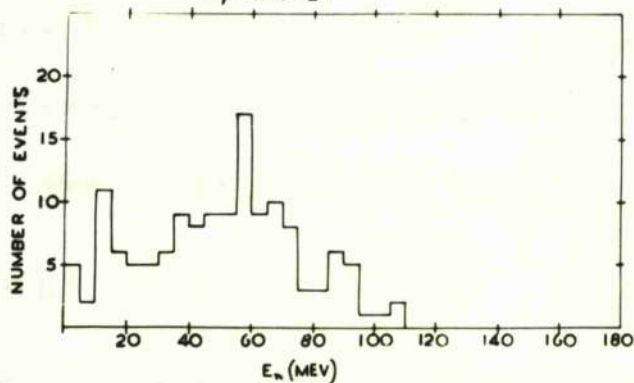


FIG. III 31b.

NEUTRON ENERGY DISTRIBUTION FOR ALL EVENTS

$E_f = 120 \text{ MEV}$

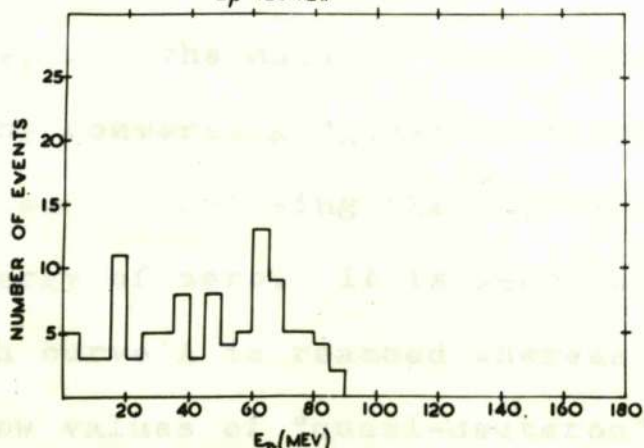


FIG. III 31c

### III.5.7. Recoil Range Distribution.

Figure III.32 shows a diagram of the range distribution of non-coplanar  $N^{14}$  recoils. This diagram represents the internal momentum distribution of the "quasi-deuterons" in the  $O^{16}$  nucleus, assuming the Levinger model to be correct. The recoil energies are shown on the bottom scale and on the assumption that this energy is arising from internal momentum equal and opposite to that of the "quasi-deuteron", the corresponding "quasi-deuteron" energies will be obtained by multiplying by seven.

The results have been fitted to two momentum distributions taken from previous experiments: the distribution, A, which is of the form

$$P(D) = 0.13e^{-P_D^2/4ME_1} \quad E_1 = 20 \text{ MeV}$$

was taken from the experiment of Wattenberg et al. (157) and the curve designated "B" which represents the distribution

$$P(D) = 0.36e^{-P_D^2/4ME_2} + 0.07e^{-P_D^2/4ME_3} \quad \begin{array}{l} E_2 = 1.6 \text{ MeV,} \\ E_3 = 30 \text{ MeV.} \end{array}$$

was able to explain the data of Cence (182). A comparison was obtained by converting "quasi-deuteron" momenta to  $N^{14}$  recoil energy and normalising the curves to the data at a  $N^{14}$  recoil energy of zero. It is seen that very good agreement with curve A is reached whereas curve B is not a good fit at low values of "quasi-deuteron" momenta. The implications of these results will be discussed in greater detail in the next chapter.

III. 3. Possible Recoil Range

Fourteen of the ...  
 which was very ...  
 travelling with about ...  
 proton. Because to ...  
 chamber no ...  
 In all cases ...

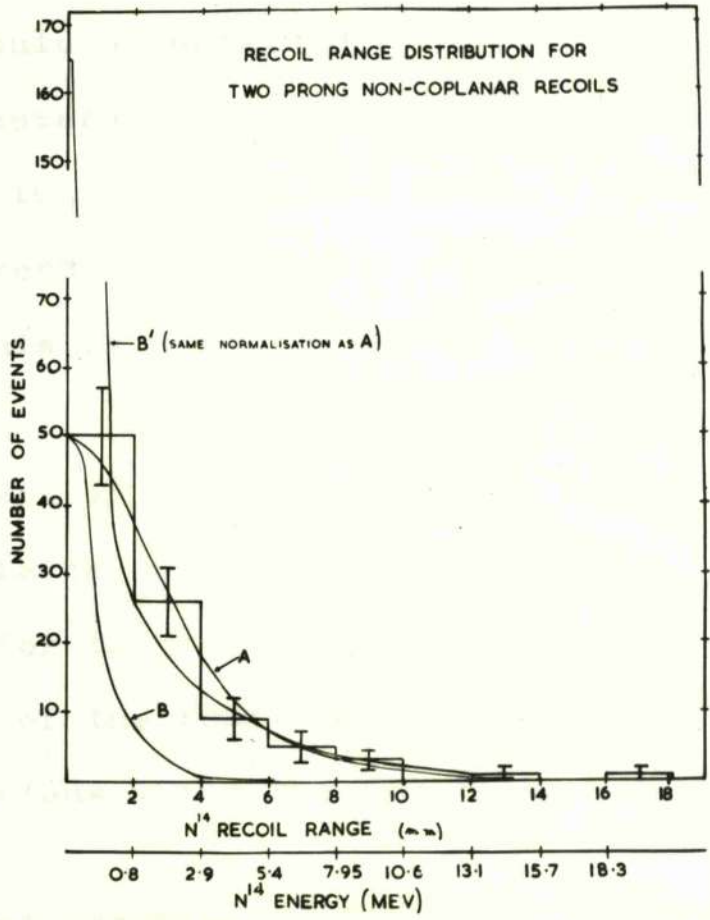
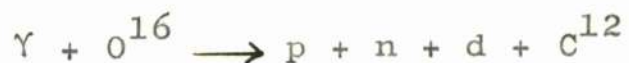


FIG III 32

### III.5.8. Possible Proton-Proton Coincidences.

Fourteen of the events incorporated a fast particle which was very similar in appearance to, and which was travelling with about the same speed as the triggering proton. Because these tracks did not stop in the cloud chamber no positive identification was possible.

In all cases a satisfactory momentum and energy balance could be obtained by assuming the fast particle to be a deuteron. As has already been stated, we cannot tell when two neutrons have been emitted. The possibility of the second fast particle being a proton does therefore exist. This is illustrated by considering the reaction



to which six of the events were ascribed. A momentum and energy balance could probably have been attained in addition for the  $\gamma + O^{16} \longrightarrow p + p + 2n + C^{12}$  reaction.

Three of the fourteen events arose from a carbon target nucleus while the remaining eleven were from oxygen nuclei.

Several examples of this type of event can be seen in the cloud chamber photographs in Appendix 2. The significance of the occurrence of such possible proton-proton coincidences will be discussed in the next chapter.

Concluding Remarks.

The neutron angular distributions, together with the momentum and energy balance calculations, and counter pulse height considerations strongly indicate that the proton energies detected were predominantly in the 80 MeV to 100 MeV region.

The author is of the opinion that the most important topics in this chapter are presented in sections III.5.4 to III.5.8. The results summarised in figures III.22a and III.22b (gamma-ray energy distributions), III.23 to III.26 (excitation energy distributions), III.31a and III.31b (neutron energy distributions), and III.32 (Recoil range distribution) are regarded as being most significant.

Discussion

Chapter IV. Discussion of Photodisintegration Results.

Chapter IV.

Discussion of Photodisintegration Results.

The experiment described in the preceding chapter is complementary to that performed at Glasgow by Reid and Lalovic (183). The programming of the conservation of energy and momentum calculations for the DEUCE computer enabled the author to derive the distributions shown in Chapter III, hitherto mostly unknown, and thus extend previous work. Section III.5.4 on gamma-ray energy distributions which enable one, in principle, to determine cross-sections for individual nuclear reactions in the high energy region is one example of this.

Some of the more important aspects of the results given in Chapter III will now be discussed.

IV.1. The Impulse and Closure Approximations.

In Gottfried's work (166) both the impulse and closure approximations were assumed to be valid for the high energy photoeffect. From the results gained in the present experiment it would appear that these approximations are not completely permissible.

(a) The Impulse Approximation. Application of the impulse approximation assumes that the interaction between the incoming particle and a single nucleon occurs in a time that is short compared to the period of the nucleons in the nucleus. For the high energy photoeffect the name

cannot be used in its strictest sense. One can only assume that it is possible to ignore the influence of the remaining nucleons during the absorption act.

If the impulse approximation were to be valid the emission of very few low energy neutrons in coincidence with 100 MeV protons would be expected. On the contrary, the present results show that, although a large number of neutrons have energies in the 40 MeV to 70 MeV range, a considerable fraction of the total number lie below 20 MeV. There exists the possibility that many of the low energy neutrons are evaporated neutrons or alternatively that they are higher energy neutrons which have lost energy on the way out of the nucleus due to scattering. It does, however, seem to be the case that the influence of the remaining nucleons cannot be ignored completely during the absorption act.

(b) The Closure Approximation. In the impulse approximation, the presence of the other nucleons provide the initial momentum distribution. Although conservation of energy is omitted in the individual interactions it must be considered after the process is complete. This is done by use of the closure approximation.

In the formalism of the "quasi-deuteron" model the gamma-ray transfers all its momentum and energy to a single neutron-proton pair. Any excitation energy received by

the residual nucleus arises because the final neutron and proton undergo nuclear collisions before leaving the nucleus. After emission of any proton-neutron pair the residual nucleus will therefore be left in a variety of quantum states. In order to calculate the cross-section the sum over final states must be carried out. Before this can be done the excitation energy of the residual nucleus must be very small compared with the gamma-ray energy.

It has been shown in the present work that the excitation energy is in the region of 30 MeV for a large number of the events and in one case is as high as 80 MeV. Furthermore, Barton and Smith (159) showed that the effective binding energy for the ejection of a proton-neutron pair,  $E_b$ , 'which includes the excitation of the residual nucleus and the kinetic energy of any other particles which may escape as well as the actual binding energy of the neutron and proton' had values of  $25 \pm 5$  MeV for Li and  $45 \pm 5$  MeV for He. The application of the closure approximation therefore hardly seems permissible.

#### IV.2. ( $\gamma$ ,p) Events.

The only events which are not predicted by the "quasi-deuteron" model of Levinger are the five ( $\gamma$ ,p) events and possibly some of the five events, previously discussed in

the section on neutron energy distributions, where the existence of a neutron is in doubt. If the "quasi-deuteron" model is assumed to be true for all events then a  $(\gamma, p)$  event involving the emission of a 100 MeV proton must be regarded as one in which the disintegration of an  $(n, p)$  pair with momentum of about  $400 \frac{\text{MeV}}{c}$  in the direction of the emitted proton takes place. The neutron would then acquire very little energy and might fail to escape from the residual nucleus.

Assuming a Gaussian momentum distribution with a  $\frac{1}{e}$  value of 15 MeV, about 1% of the events would be expected to be of this type. Experiment has shown that about 2.5% of the events are of this nature.

The  $(\gamma, p)$  events could either have been produced by the neutron absorption process described above or by direct photoproton production in the manner proposed by Courant (65). The photon is assumed to interact directly with one of the protons in the nucleus and gives it enough energy to overcome the potential barrier without the formation of an intermediate "compound nucleus" state. Using a square well potential Courant derived the following expression for the cross-section for photo-ejection of one proton from a complex nucleus:

$$\sigma = \frac{16\pi e^2}{3hc} \left(1 - \frac{Z}{A}\right)^2 \frac{TW}{(\hbar\omega)^3 \left\{ (\hbar\omega + T)^{1/2} + (\hbar\omega + T - W)^{1/2} \right\}} \left( \frac{\hbar^2}{2MR^2} \right)^{3/2} R^2$$

where  $T$  is the kinetic energy of the proton in the nucleus and  $W$  is the depth of the potential well;  $M$  is the proton mass and  $R$  is the nuclear radius. Assuming a Fermi distribution for the nucleon internal momentum distribution with  $T_{\text{max}} = 20$  MeV, and  $W = 30$  MeV the cross-section is approximately  $1.10^{-30}$  cm<sup>2</sup> which is an order of magnitude smaller than is obtained in the present experiment. This estimate has assumed that Courant's formula can be extended to the higher energies. Although the statistics in this experiment are not sufficient to state any certain conclusions it does appear that the  $(\gamma, p)$  cross-section at these energies is higher than theoretically expected.

#### IV.3. Emission of Two Fast Particles.

The emission of two fast protons in coincidence has already been discussed in section I.4.B.6. where it was seen that the results of Weinstein et al. (161) at M.I.T. could be explained by the scattering of the neutrons with resultant production of recoil protons following "quasi-deuteron" absorption. The value of  $(2.2 \pm 2.0 - 1.2)\%$  obtained for oxygen is considerably smaller than the 7% contribution seen in the present experiment. This is perhaps not surprising since the range of proton energies accepted by both counter telescopes in the M.I.T. experiment was somewhat limited.

Smith and Larson (184) have recently performed a similar experiment to that of Weinstein et al. with the

exception that a very wide range of proton energies is accepted by each telescope. Approximately 10% as many proton-proton coincidences as neutron-proton coincidences have been observed. Each high energy proton is found to coincide with a low energy proton. By keeping the angle of one counter telescope fixed with respect to the gamma-ray direction and varying the angle of the other, in identical fashion to the neutron-proton coincidence experiments, a proton angular distribution can be obtained. This distribution is almost identical to the neutron angular distribution observed in the proton-neutron coincidence experiments and the peak value occurs at the same angle. This would suggest that direct gamma-ray interaction with proton-proton subunits is taking place. On the other hand, the anti-correlation in proton energy does not agree with this explanation. It is possible that the low energy protons are produced by a process in which photodisintegration of a proton-neutron pair is followed by scattering of the neutron with resultant production of a recoil proton which is then emitted in approximately the same direction as the neutron was originally travelling. Correct interpretation of the data is, however, in doubt.

The present results have shown that emission of two fast particles does occur (Appendix A.2.) but the statistics are too poor to draw any conclusions about their angular

correlation.

It is possible that they have been produced by electric quadrupole absorption of a gamma-ray by a proton-proton pair or by the collision process already mentioned. These events could also arise from a process in which a  $\pi^+$  meson was re-absorbed by a proton-neutron pair. An alternative explanation would be that in which photons interact with subunits of the nucleus consisting of two protons and a neutron or two neutrons and a proton. This would lead one to expect both proton-deuteron and neutron-deuteron coincidences with emission occurring at kinematically predictable angles. In this experiment only proton-deuteron coincidences would be detected. It does seem possible that some of the events detected are of this nature. Some evidence for such a three-body interaction has also been found in the experiment of Cence which is discussed in section IV.5. A slight discontinuity was observed in the proton energy spectrum at approximately  $2/3$  of the gamma-ray energy. The effect could, however, have been a statistical fluctuation.

#### IV.4. Internal Nucleon Scattering.

By comparing the numbers of neutron-proton coincidences from ten different elements including deuterium Stein et al. (185) have recently investigated the scattering and absorption of photonucleons on their way out of nuclei.

The cross-section per nucleon pair in the nucleus relative to that for deuterium decreased with increasing atomic weight. This decrease can be qualitatively explained by the Serber (186) semi-classical picture of high energy reactions. In this representation the probability that both nucleons escape without scattering decreases as the size of the nucleus increases. The data for medium weight elements could be fitted to the relation

$$\sigma_{(Z,A)}(\text{neutron-proton coincidences}) = 3.0 \frac{NZ}{A} \sigma_{\text{deuterium}} P\left(\frac{2R}{\lambda}\right).$$

where  $P\left(\frac{2R}{\lambda}\right)$  is a probability of escape factor. It is the probability that both nucleons escape without either one undergoing interaction. Assuming the mean free path,  $\lambda$ , to be the same for both neutrons and protons, the density of nuclear matter to be uniform, and the nucleons to be emitted at  $180^\circ$  to each other, the escape probability was found to be 0.36 for lithium and 0.27 for oxygen.

Barton and Smith (159) define a function  $\alpha$  to be the probability for a nucleon making a collision. The ratio of the number of neutron-proton coincidences to the single proton counting rate is then  $(1-\alpha)$ . Values for  $\alpha$  of  $0.15 \pm 0.05$  for He and  $0.28 \pm 0.05$  for Li are thereby obtained. In this derivation the neutron and proton scattering probabilities were, however, assumed to be independent of each other. This cannot be true since the smaller the

distance travelled by one nucleon, the larger the distance travelled by the other. Furthermore, accurate determination of  $(1-\alpha)$  depends on accurate knowledge of the neutron counter efficiency. In addition a considerable source of error arises in that correction must be made for the fact that a proton observed at one energy may have been created at a greater energy and scattered into a lower energy region. This was estimated to amount to a 50% correction to  $\alpha$ . Moreover, the method assumes that there is no source of protons other than the "quasi-deuteron" mechanism.

Weil and McDaniel (130) also attempted an estimation of the internal scattering of photonucleons. The fraction of protons, initially produced by the "quasi-deuteron" process, which escaped from carbon without scattering was estimated to be 55% i.e.  $\alpha_p = 0.45$ .

Scattering of fast neutrons and protons on their way out of the nucleus will give rise to events more complicated than  $(\gamma, pn)$ . Following Reid and Lalovic, the probability that a proton will suffer a collision on its way out of the nucleus can be written  $\alpha_p = 1 - f_1 - f_2$  and similarly for the neutron we can write  $\alpha_n = \frac{f_2}{f_1 + f_2}$  where  $f_1$  is the probability that the proton will escape and the neutron be scattered. In the present work  $f_1$  is related to all two prong non-coplanar events and  $f_2$  is related to all multiprong

*neutron and proton will escape and  $f_2$  is the probability that both*

events assuming only "quasi-deuteron" absorption to be taking place. Reid and Lalovic calculated  $f_1$  and  $f_2$  for several specific cases and obtained values for  $\alpha_n$  in nitrogen which ranged from 0.60 for a 72 MeV neutron to 0.47 for a 110 MeV neutron both results being for a 330 MeV bremsstrahlung spectrum. Gamma-rays with maximum energy of 240 MeV were considered in the case of neon and the  $\alpha_n$  values ranged from 0.65 MeV for a 60 MeV neutron to 0.53 for a 100 MeV neutron.

For oxygen the experimental values are found to be

$$\frac{f_2}{f_1} = 0.89; \quad \alpha_n = 0.47.$$

A certain proportion of the two prong non-coplanar events must be multiprong stars involving a neutron as the evaporated particle. A correction can be applied by assuming that there will be the same number of neutron three prong events as there are proton events of this type. In addition it is probable that, while the basic process is "quasi-deuteron" absorption, in many instances the rest of the nucleus is at the instant of photon absorption in an excited configuration. In these cases a multiprong event occurs although the photonucleons may be unscattered.

Although the uncorrected value of 0.47 for  $\alpha_n$  is not greatly at variance with those obtained less directly from counter experiments (Stein et al. found P for oxygen to be 0.27 i.e.  $\alpha = 1 - \sqrt{P} = 0.48$ ), the necessity for applying

the two corrections mentioned above does prevent us from equating multiprong stars with "scattering" events and the agreement may be somewhat fortuitous.

#### IV.5. Momentum of "Quasi-Deuterons".

Barton and Smith (159) and Wattenberg et al. (157) estimated the momentum of the "quasi-deuterons" in nuclei by considering the spread in the neutron angular distributions for a fixed proton energy and angle and fitting these distributions to a function of the form

$$P(D) = Ke^{-D^2/4ME_0}$$

where  $P(D)$  is the probability that a particular neutron-proton pair is moving with a momentum between  $D$  and  $D + dD$ ,  $M$  is the mass of a single nucleon, and  $E_0$  is the Gaussian parameter. This method obviously has the great disadvantage that only average values are measured and, in addition, the large background counting rates experienced at small angles make it difficult to judge the position at which the half-height of the Gaussian peak occurs. The Barton and Smith estimation that the background provided 66% of the "neutron"-proton coincidences from Li at  $40^\circ$  serves to illustrate this point. It is perhaps not surprising that a large discrepancy exists in the M.I.T. and Illinois  $E_0$  values for lithium. Barton and Smith find  $E_0$  for Li to be  $5.0 \pm 1.0$  whereas Wattenberg et al. find the value to be  $9.0 \pm 1.0$ . The method employed by these two groups is probably most

useful in obtaining relative values for different nuclei as is strikingly evident from the fact that both agree that the angular spread for Li is considerably smaller than that for other nuclei.

Cence (182) has recently performed an experiment, using the method of Weil and McDaniel (130), in which interactions produced by  $245 \pm 15$  MeV gamma-rays were selected from all those arising from a 340 MeV bremsstrahlung spectrum.

The energy spectrum of protons between 105 MeV and 250 MeV emitted from a carbon target at  $60^\circ$  to these gamma-rays was measured. To keep the accidental counting rate to a minimum the gamma-ray intensity had to be limited. This meant that only two protons per hour were obtained from the selected gamma-quanta and of the total of 694 protons recorded, 248 were accidentals. The total number of protons accepted was thus 446.

A large high energy tail was found in the proton energy spectrum up to the maximum value allowed by conservation of energy. The spectrum also showed a sharp maximum at 119 MeV whereas that derived with a bremsstrahlung spectrum showed no such maximum. The evidence for this peak rests primarily on a point at 105 MeV where the cross-section was found to be considerably lower than that at 119 MeV.

It is to be noted that the maximum occurs at that proton energy which would be obtained by bombarding free

deuterium with selected photons of the same energy.

The M.I.T. momentum distribution, a Gaussian with a  $1/e$  value of 20 MeV, gave a reasonable fit to the data except in the region of 120 MeV where it did not give the sharp maximum exhibited by experiment.

A momentum distribution given by the sum of two Gaussians with  $1/e$  values of 1.6 MeV and 30 MeV gave a fairly sharp maximum at the correct energy. To obtain agreement the low momenta had to be enhanced by a very large amount.

The M.I.T. and Illinois results were analysed by assuming the internal momentum distribution of nucleons in the nucleus to be of the form  $D^2 e^{-\alpha D^2}$ . This distribution leads one to expect a neutron angular distribution of the form  $K e^{-\alpha D^2}$ .

At first sight it might seem that the results found from the present experiment would have to be fitted to the former distribution since the recoil ranges are measured in a cloud chamber and would appear to have a completely random angular dependence. This would certainly be true if the cloud chamber were expanded randomly and the recoil ranges then measured. In this experiment, however, the fact that counter telescopes selected protons with an energy of 100 MeV will mean that selection of "quasi-deuterons" with high momenta in the same direction as the proton will be favoured. This means that the average neutron energy will be less than

100 MeV. This has been seen to be true. Because of the  $1/E$  nature of the bremsstrahlung spectrum high momentum "quasi-deuterons" will be over-emphasised. It might also be stated that a less important error will arise from the probability of the residual nucleus evaporating neutrons.

In the M.I.T. and Illinois experiments,  $E_\gamma$ ,  $E_n$ ,  $E_R$ ,  $\alpha_R$  and  $\beta_R$  were unknown (see section III.4 for notation). The system could therefore be described in terms of one independent variable. In Cence's experiment at Berkeley  $E_n$ ,  $\alpha_n$ ,  $\beta_n$ ,  $E_R$ ,  $\alpha_R$  and  $\beta_R$  were unknown which meant that the system had two independent variables. Although all data could be calculated in the present experiment the statistics were too poor to obtain significant recoil range distributions which were completely defined. The distribution was drawn for all recoil angles and gamma-ray energies. The final system is therefore described by two independent variables.

Attempts were made to fit the data to the probability distributions satisfying both the M.I.T. and Berkeley results. It has already been seen in section III.5.7 that good agreement in shape is obtained with the M.I.T. momentum distribution. If the area under the curves is successively integrated from a  $N^{14}$  recoil energy of zero to 0.8 MeV and from zero to 23 MeV respectively, the latter being the maximum permissible range for 240 MeV gamma-rays producing

100 MeV protons, it is possible to find the percentage of "quasi-deuterons" with momenta below  $145 \frac{\text{MeV}}{c}$ . The non-linear energy scale resulting from the range-energy relations is rather misleading and the rather surprising result is obtained that the present experiment finds 52% of the total to be below this momentum value while the M.I.T. and Berkeley experiments find 25% and 34% respectively. On the other hand the peak at very low values of momentum (below  $100 \frac{\text{MeV}}{c}$ ) is neither visible in the present results nor in the M.I.T. values. This is certainly not surprising in the M.I.T. case where the use of a bremsstrahlung spectrum of gamma-rays has the effect of smoothing out the proton energy spectrum and hiding details of the interaction. The present results could have been given in 1 mm. intervals of recoil range but an appreciable uncertainty occurs for the lowest momentum range where the accuracy of recoil measurement becomes poor. It must also be remembered that ten events (approximately 10% of the total) which had no visible recoil were included in the lowest momentum range. These events must be regarded as resulting from the disintegration of a "quasi-deuteron" with essentially zero internal momentum. Cence's observation that there are "quasi-deuterons" with energy greater than 80 MeV is corroborated by the results found in the present experiment. While the present experiment and that of Cence at Berkeley agree that a very large

contribution from the low momentum components does occur, they are both statistically poor and further experiments are required to resolve the ambiguities occurring at the present time.

There are two observations which can be made about the large contribution from the low momentum components: Firstly, a proton-neutron pair obeys Bose-Einstein statistics. This means that there is no Pauli Principle to prevent a large number of "quasi-deuterons" from being put in the same state. It is therefore possible for them to assemble in the low momentum states. Secondly, it is possible that the large momenta observed for single nucleons in the nucleus may be due to two-body correlations. This would mean that the momentum distribution of pairs of nucleons should be narrower than would be predicted from a random distribution of nucleons in the nucleus.

#### IV.6. Future Experiments.

The most important experiment which should be attempted is a counter telescope investigation of proton-neutron coincidences in which both the proton and neutron energies are measured. The neutron energy could be determined by a time-of-flight method. Further measurements on the momentum distributions of "quasi-deuterons" in the nucleus are also required. These are probably best obtained by using

essentially monochromatic gamma-rays, following the method of Weil and McDaniel, with a counter telescope to detect protons or by further experiments with the triggered cloud chamber. In addition, counter telescope investigations of proton-proton and proton-deuteron coincidences would prove most interesting.

Finally, experiments to investigate gamma-ray absorption in the 30 MeV to 100 MeV region, which is relatively unexplored at the present time, would help to distinguish between the Levinger and Courant models of the nucleus at these energies.

Section B.

The Polarization of Photonucleons.

Introduction.

Chapter V. Introduction.

## Chapter V.

### Introduction.

Spatial orientation may be introduced into any nuclear system in which the direction of the beam of incident radiation is defined. The combination of the angular momentum properties of the nuclear system and directional effects in the absorption of radiation by the system may give rise to anisotropic effects in the emission of the reaction products. By studying these effects we can gain much information about many aspects of the interaction. It is found that ambiguities which occur in measurements of the angular distributions are frequently eliminated when a study is made of the spin orientations of the initial and final systems.

### V.1. Polarization Effects in Nucleon-Nucleus Scattering.

If spin-selective nuclear forces exist in the scattering of an unpolarized beam of particles then the coupling of the spins of the incident particles with their orbital angular momenta about the scattering nuclei will result in the production of a beam of nucleons with spins pointing preferentially in one direction.

Suppose we have a beam of unpolarized protons passing to left and right of target nuclei then those passing to the left will have their orbital angular momenta pointing downwards while those to the right will be upwards. Those

protons with spin up and passing to the right of the scattering centre will have their spin and angular momentum vectors parallel while those with spin down will have these vectors anti-parallel. For protons passing to the left the opposite situation will arise.

We can represent the force acting on the incident particle by a potential:

$$U(r) = U_{\text{spin-orbit}}(r) \quad \underline{L.S.}$$

For a nucleon pointing in a given direction the force will have opposite sign on opposite sides of the nucleus. Thus one group of particles will be scattered preferentially to the left and the other group to the right. A polarized beam is therefore obtainable at almost any angle although the absolute value of the polarization will vary with angle. Here we may emphasise that there is no asymmetry in the scattered intensity as a function of azimuthal angle,  $\phi$ , after single scattering from an unpolarized target.

To measure the polarization of any scattered beam produced in this way an analyser is required. By the preceding argument we see that such a polarized beam if passed into another solid target will result in more protons being scattered to one side than to the other. By measuring this asymmetry in scattering we can gain a measure of the polarization of the incoming beam. The asymmetry in such a double scattering experiment is defined as

$$\mathcal{E} = \frac{L - R}{L + R} = P_1(\theta_1) \cdot P_2(\theta_2)$$

where  $L$ ,  $R$  are the numbers scattered to left and right respectively,  $P_1$  is the polarization produced at an angle  $\theta_1$  from the first target, and  $P_2$  is the polarization produced at an angle  $\theta_2$  from the second target.

If the two targets are identical and if  $\theta_1 = \theta_2$  then  $P = \pm \sqrt{\mathcal{E}}$ . The sign of the polarization is defined by

$$\underline{P} = P(\theta) [\underline{k} \times \underline{k}']$$

where  $\underline{k}$  and  $\underline{k}'$  are the wave numbers of the incident and scattered particles respectively. This means that a scatter left corresponds to a spin upwards.

We see from the preceding arguments that the polarization of the outgoing nucleons is perpendicular to the plane of the reaction. In addition if the initial or final states of the system are described only by S-waves then the polarization of the emitted particles must be zero and similarly if there is no spin-orbit coupling there can be no polarization.

Considerable effort has been expended in the investigation of polarization effects occurring in nucleon-nucleus scattering since the first double scattering experiment performed by Oxley et al. (187) in 1953. An excellent review on the subject of the polarization of fast nucleons has been given by Wolfenstein (188).

The information gained from polarization experiments is very valuable as can be seen from the fact that the first

evidence for the proton-proton force possessing non-central components came from such an investigation; the strength of the spin-orbit force being found to be only about 2% of the central force.

V.2. The Polarization of Photonucleons Emitted in Non-Mesonic Processes - Theoretical Investigations.

Theoretical work on the polarization of photonucleons is rather limited. One of the first calculations was made by Rosentsveig (189) who assumed central neutron-proton forces and zero range approximation to estimate the polarization of the neutrons from photodisintegration of deuterium for gamma-ray energies below 10 MeV. The polarization was seen to be caused by electric dipole (E1) - magnetic dipole (M1) interference.

Czyz and Sawicki approached the problem by considering a model for the  $\text{Be}^9$  nucleus which had been formulated by Guth and Mullin (190). In this model the odd neutron was assumed to move in a potential well provided by the remaining nucleons. This is not an unreasonable assumption when we consider that the binding energy of the neutron is only 1.63 MeV compared with the usual 8 MeV to 10 MeV for a nucleon in the nucleus. Furthermore, although we see that the  $\text{Be}^8$  nucleus is unstable the instability is only 116 KeV and the lifetime of  $\text{Be}^8$  is long compared with the time required for ejection of a neutron from  $\text{Be}^9$ . Guth and Mullin based their calculations on the assumption of a  $P_{3/2}$

ground state for the  $\text{Be}^9$  nucleus. For the  $\text{Be}^8$ -neutron interaction a spherical potential well, giving rise to a non-tensor interaction, was taken.

Czyz and Sawicki (191) used the Guth and Mullin model together with time-dependent perturbation theory to calculate the polarization of the outgoing neutron from  $\text{Be}^9$ . These workers further assumed the interaction potential to contain a spin-orbit coupling term. The maximum predicted polarization was about 45%. This was the value for emission of the neutron at  $45^\circ$  to 2 MeV gamma-rays (figure V.1). This polarization decreases to about 25% for 3 MeV gamma-rays and for larger energies rapidly becomes negligible. It is suggested that measurements of the polarization might give information concerning interactions between the outgoing nucleons and the residual nucleus in the  ${}^1_1\text{D}^2$ ,  ${}^3_3\text{Li}^6$ ,  ${}^3_3\text{Li}^7$  and  ${}^4_4\text{Be}^9$  nuclei for which their approach would be applicable.

Most of the theoretical work has, of course, been done on the polarization of photonucleons from deuterium where it is hoped that measurements may give information on the neutron-proton interaction. In the photodisintegration of the deuteron the possible transitions are:

$$\text{Electric dipole E1: } {}^3\text{S}_1 + {}^3\text{D}_1 \rightarrow {}^3\text{P}_{0,1,2} + {}^3\text{F}_2.$$

$$\text{Magnetic dipole M1: } {}^3\text{S}_1 \rightarrow {}^1\text{S}_0 \text{ and } {}^3\text{D}_1 \rightarrow {}^1\text{D}_2.$$

$$\text{Electric quadrupole E2: } {}^3\text{S}_1 + {}^3\text{D}_1 \rightarrow {}^3\text{S}_1 + {}^3\text{D}_{1,2,3} + {}^3\text{G}_3.$$

In the medium energy range the E1 transitions are more important than both M1 and E2. The M1 contribution is especially important at energies below 10 MeV.

Initially Czyz and Sawicki (192) considered only E1 and M1 transitions from the  $^3S_1 + ^3D_1$  ground state of the deuteron and in addition neglected the presence of the  $^3F_2$  state. Furthermore, only the M1 transition to the  $^1S_0$  state was taken into account. Corrections were later made for E2 transitions. The angular dependence of the polarization was found to be given by

$$P = \frac{a \sin 2\Theta + b \sin\Theta}{c + d \sin^2\Theta} \quad \text{V.2.1}$$

The "a sin 2 $\Theta$ " term is due to E1 transitions while the "b sin $\Theta$ " term is caused by E1-M1 interference. The former is small and the latter causes the larger contribution for low values of gamma-ray energy. As the gamma energy increases the E1 term may have a greater effect. The "c" term is produced by E1 and M1 transitions while the "d sin<sup>2</sup> $\Theta$ " term is from pure E1 transitions. Since the nucleon-nucleon interaction was not well-known they assumed various forms of neutron-proton interaction. In particular the phase shifts of Clementel and Villi (193) derived from nucleon-nucleon scattering were applied in the manner of Hsieh (194,195) and Austern (196). Tensor coupling was also assumed in the neutron-proton interaction potential. A

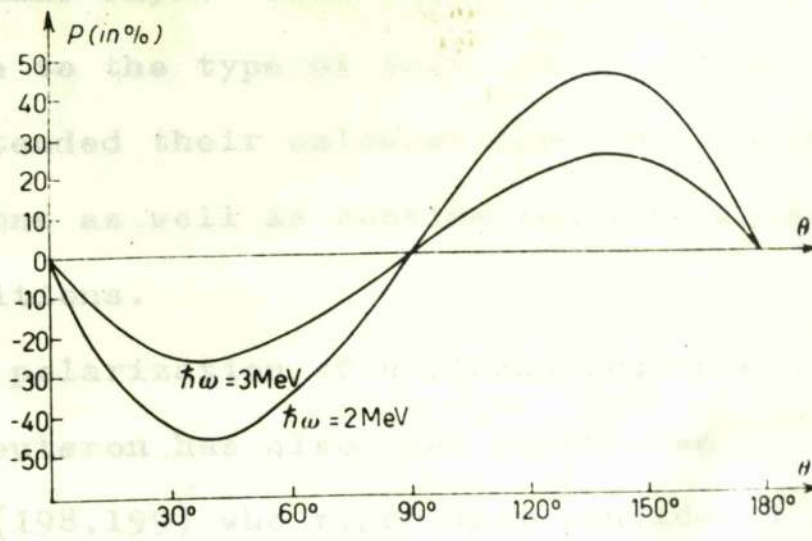


FIG. V I.

Table I. Summary of results.  $a$ ,  $b$ , and the  $\gamma_i$ 's are in  $\mu\text{b sterad}$ .

$E_\gamma$ lab (MeV)	9.3	11.3	22.5	40.6	53.7	80.4
$a$	4.45	4.22	4.46	4.89	4.87	4.54
$b$	171.5	135.7	49.3	16.7	9.39	4.35
$\rho_1$	0.04	0.05	0.10	0.13	0.13	0.14
$\rho_2$	0.18	0.20	0.32	0.47	0.57	0.70
$\gamma_0(p)$	-15.4	-11.6	-4.46	-2.18	-1.62	-1.02
$\gamma_0(n)$	-15.2	-11.5	-4.42	-1.87	-1.27	-0.58
$\gamma_1(p)$	2.16	2.6	3.87	3.38	2.84	1.97
$\gamma_1(n)$	4.61	4.9	4.68	3.48	2.65	1.84
$\gamma_2(p)$	0.43	0.43	0.86	0.79	0.66	0.80
$\gamma_2(n)$	-0.43	-0.43	-0.86	-0.79	-0.66	-0.80

TABLE VI.

$$\left(\frac{d\sigma}{d\Omega}\right)_{\theta=0}(\theta) = \sin^2 \theta \dots$$

value of -41% was found for nucleons emitted at  $149^\circ$  to 45 MeV gamma-rays. This value however was shown to be very sensitive to the type of interaction chosen. These workers later extended their calculations (197) to include M2 transitions as well as considering the  ${}^3F_2$  state in the E1 transitions.

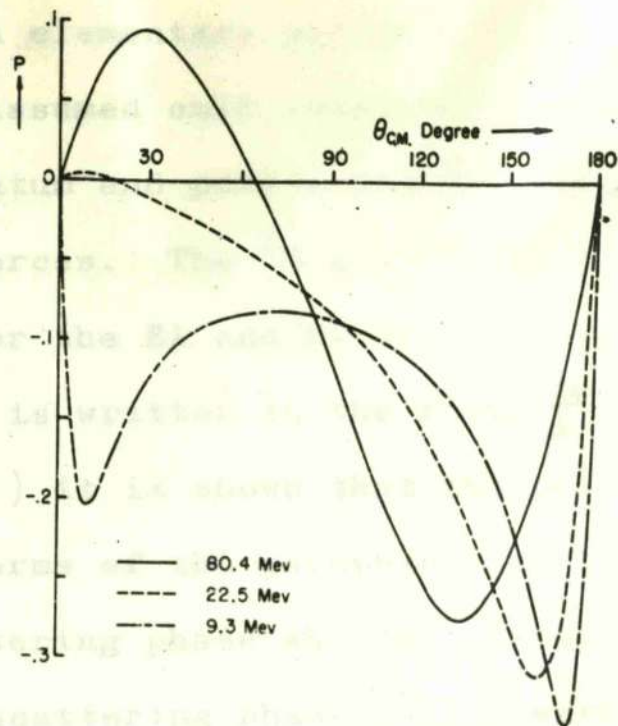
The polarization of nucleons from photodisintegration of the deuteron has also been calculated by De Swart and Marshak (198,199) who rigorously considered the final state interactions and assumed a 6.7% D-state contribution to the ground state of the deuteron. This high percentage of D-state does not contradict the observed values of magnetic moment and quadrupole moment of the deuteron. They also used the Signell-Marshak nuclear force potential (200). The polarization was calculated for gamma-ray energies ranging from 9.23 MeV to 152.4 MeV. More confidence is felt for the results in the region up to 77.3 MeV than in the energy range above this value. This opinion is held because gamma-ray energies between 9.23 MeV and 77.3 MeV correspond to nucleon-nucleon scattering between 14 MeV and 150 MeV where the phase shifts are known rather better.

The polarization of the outgoing nucleon for unpolarized gamma-rays is found to be given by

$$\left(\frac{d\sigma}{d\Omega}\right)_0 P_0(\theta) = \sin \theta (\gamma_0 + \gamma_1 \cos \theta + \gamma_2 \cos^2 \theta) \quad \text{v.2.2}$$

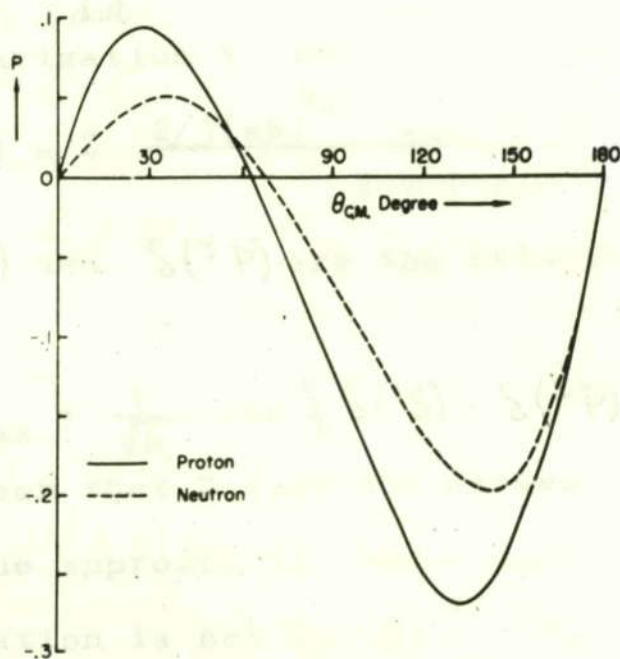
where the angular distribution  $\left(\frac{d\sigma}{d\Omega}\right)_0 = a(1 \pm \beta_1 \cos \theta) + b \times \sin^2 \theta (1 \pm \beta_2 \cos \theta)$ . This equation is a more elaborate form of equation V.2.1. Here the plus and minus signs refer to protons and neutrons respectively. The  $\gamma$ 's can be directly expressed in terms of the phase shifts and transition amplitudes. The a's, b's,  $\beta$ 's and  $\gamma$ 's were calculated numerically. The E1-E1, E1-E2, E1-M1 spin flip, and E2-M1 spin flip interferences were calculated taking final state tensor coupling into account. The results obtained by De Swart, Czyz and Sawicki (201) for gamma-ray energies up to 80 MeV when making the same assumptions as De Swart and Marshak are summarised in Table V.1 and figures V.2 and V.3. At low energies P is determined mainly by large  $\gamma_0$  and large b. As the energy increases the others begin to exercise more effect. The difference between the neutron and proton polarizations is chiefly due to the M1-E2 interference at the lower energies and to the E1-E2 interference at higher energies. They state that the maximum difference occurs near the peak of the polarization curve and is 2% at 9.3 MeV, 5% at 22.5 MeV and 7% at 80.4 MeV.

Kawaguchi (202) has also computed the polarization of the proton from photodisintegration of the deuteron by a phenomenological approach. No detailed interaction between the neutron and proton was assumed. The deuteron was



Polarization of the protons for  $\gamma$ -ray energies in the lab of 9.3 Mev, 22.5 Mev, and 80.4 Mev.

FIG V 2.



Neutron and proton polarization at  $\gamma$ -ray energy in the lab of 80.4 Mev.

FIG V 3.

treated as an elementary particle of spin 1. The calculation assumed only conservation of energy, momentum, angular momentum and parity and the charge independence of nuclear forces. The  $^1S$  and  $^3P$  final states only are considered for the E1 and M1 transitions. If the angular distribution is written in the form  $\frac{d\sigma}{d\Omega} = a + b \sin^2 \theta (1 + 2c \cos \theta)$  it is shown that the polarization can be written in terms of the parameters a, b, c and the nucleon-nucleon scattering phase shifts. Experimental values of a, b, c and scattering phase shifts were substituted when possible.

At low gamma-ray energies the cross-section can be written:

$$\frac{d\sigma}{d\Omega} = a + b \sin^2 \theta$$

and the polarization is then given by:

$$P(\theta) = \pm \frac{2/3(ab)^{1/2} \sin \theta \sin \{ \delta(^1S) - \delta(^3P) \}}{a + b \sin^2 \theta}$$

where  $\delta(^1S)$  and  $\delta(^3P)$  are the relevant scattering phase shifts.

$$P_{\max} = \frac{1}{\sqrt{6}} \sin \{ \delta(^1S) - \delta(^3P) \}$$

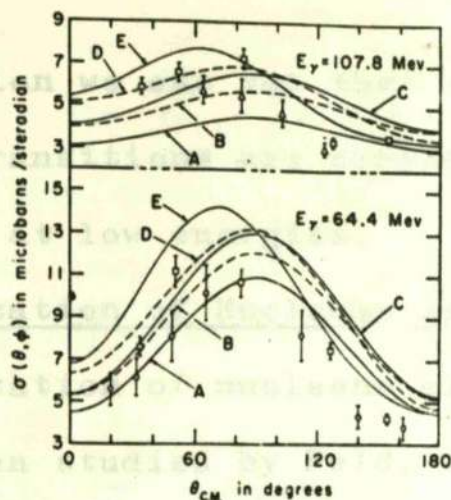
It can be seen that P does not exceed  $1/\sqrt{6}$  i.e. 41%. A defect in the approach is that a derivation of the sign of the polarization is not possible. For gamma-ray energies up to 40 MeV, 20% to 30% polarization is expected. This value decreases to 10%-20% for an energy of 140 MeV over a large range of angles in the centre of mass system.

Zernik, Rustgi and Breit (203) have calculated the polarization of the photoprotons from photodisintegration of the deuteron for six gamma-ray energies between 22.2 MeV and 177.2 MeV (corrected values). These workers used a modified form of the Signell-Marshak nuclear force potential (200) and successively introduced different transitions. The effects of adding the different forms of absorption could then be readily ascertained. The cross-sections and polarizations were calculated numerically and some of the results can be seen in figures V.4 and V.5.

Curve A was obtained when only E1 transitions were considered. The coupling between the  $^3F_2$  and  $^3P_2$  states was neglected at this point. Curve B arose when tensor coupling was taken into account. The consequence of the introduction of M1 transitions to the  $^1S_0$  state which results in curve C is seen to be quite marked. When the M1 transitions to triplet states are included, in addition, the effect is also appreciable as seen in curve D. Finally, insertion of the E2 transitions to the S, D and G states gives rise to curve E.

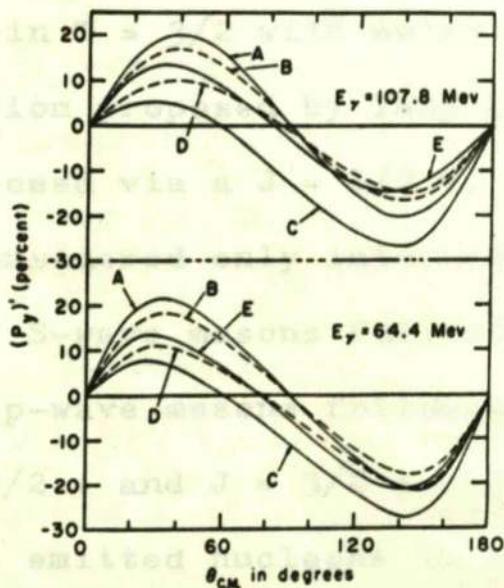
The results obtained for  $\sigma$  as given in curve A are fairly consistent with the results of De Swart and Marshak (103) who used a slightly different potential.

The calculation of Czyz and Sawicki (197) although somewhat less accurate, yielded results in qualitative



Differential cross section for the  $D(\gamma, n)p$  reaction with unpolarized gamma rays of energy 64.4 Mev and 107.8 Mev in the laboratory system. The experimental points of various investigators are represented as follows: circles for those of L. Allen, Jr., at 66 Mev [Phys. Rev. 98, 705 (1955)]; squares for those of Whalin, Schriever, and Hanson at 65 and 105 Mev [Phys. Rev. 101, 377 (1956)]; triangles for those of J. C. Keck and A. V. Tollestrup at 105 Mev [Phys. Rev. 101, 360 (1956)].

**FIG. V. 4.**



Percentage polarization of protons from the  $D(\gamma, n)p$  reaction with unpolarized gamma rays of energy 64.4 Mev and 107.8 Mev in the laboratory system.

**FIG. V. 5.**

agreement with the values for P for a gamma-ray energy of 64 MeV.

In conclusion we can see that the effects of introducing the M1 and E2 transitions are considerable and this is especially true at low energies.

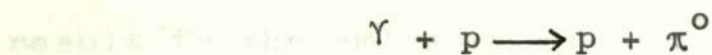
### V.3. The Polarization of Nucleons Emitted in Meson Production.

The polarization of nucleons emitted in production of  $\pi$ -mesons has been studied by Feld, Watson et al. and Sakurai.

#### (a) The Fermi and Yang Solutions.

Feld (204) considered not only the photoproduction of mesons but also meson-nucleon scattering. The angular distribution of the emitted nucleons was seen to be fitted by two solutions. One solution given by Fermi (205) assumed the most important intermediate state in the meson-nucleon interaction to be that with angular momentum  $J = 3/2 +$ , and isotopic spin  $T = 3/2$  with emission of p-wave mesons. The other solution proposed by Yang (206) considered the reaction to proceed via a  $J = 1/2 +$ ,  $T = 3/2$  intermediate state. Feld considered only intermediate states which led to the emission of S-wave mesons following E1 absorption to  $J = 1/2 -$ , and p-wave mesons following M1 and E2 absorption to  $J = 1/2 +$ ,  $3/2 +$  and  $J = 3/2 +$  respectively. The polarizations of the emitted nucleons in the various reactions, however, showed appreciable differences for the two solutions. The greatest difference appeared in the photoproduction of

neutral mesons on hydrogen.



For this reaction the Yang solution predicts appreciable polarization of the outgoing nucleons whereas the Fermi solution predicts essentially zero polarization. There is a strong theoretical argument, based on the dispersion relations, against the Yang solution.

Watson et al. (207) used the "(3,3) enhancement" model which assumes that the state of the pion-nucleon system having  $\ell = 1$ ,  $J = 3/2$ ,  $T = 3/2$  is one of strong interaction and managed to qualitatively explain the principal experimental results. These workers state that a detailed test of the model is possible if the polarization of the recoil nucleon is measured. At 300 MeV a polarization of less than 2% is predicted for the recoil proton in  $\pi^0$  production.

(b) The Wilson-Peierls Ambiguity.

At higher gamma-ray energies a second resonance appears in the cross-section for photoproduction of a single pion. Wilson (208) and Peierls (209) have attempted to explain this resonance. Wilson assumed the reaction to take place via a  $T = 1/2$ ,  $J = 3/2$  state with even parity which must result in the emission of a p-wave pion and a nucleon. Peierls on the other hand showed that  $\pi^+$  production is more readily understood if the reaction is regarded as proceeding

via a  $T = 1/2$ ,  $J = 3/2$  state with odd parity. This must result in the emission of a nucleon plus a d-wave pion. The two models cannot be distinguished by examination of the  $\pi^0$  angular distribution.

The ambiguity has been discussed by Sakurai (210) who showed that the situation can be resolved by measurement of the polarization of the recoil nucleon. Wilson's model is seen to predict no polarization while Peierls' model predicts a polarization of about 80% over a range of angles between  $40^\circ$  and  $140^\circ$  at a gamma-ray energy of about 550 MeV.

#### V.4. Experimental Investigations.

Although considerable work has been done on the polarization of the emitted gamma-rays from radioactive sources (211-218), there has been only one experiment to determine the polarization of nucleons resulting from bombardment of nuclei by gamma-rays. This experiment performed by Stein (219) measured the polarization of the recoil proton from photoproduction of  $\pi^0$ -mesons on hydrogen. A liquid hydrogen target was bombarded by 550 MeV and 700 MeV bremsstrahlung beams. The proton recoils from  $\pi^0$  production were scattered in a carbon analyser and detected by two pairs of scintillation counters to left and right of the scatterer, looking along the direction of the incident proton. A coincidence was demanded between each proton and one of the photons produced by a  $\pi^0$  - meson decay in a Cerenkov counter on the

opposite side of the gamma-ray beam from the proton detectors. The proton telescopes subtended a very small solid angle at the carbon analyser. This enabled the polarization to be derived from the left-right asymmetry in scattering.

At 550 MeV a total of 116 left scatters and 90 right scatters was obtained. This resulted in a value of  $30\% \pm 12\%$  for the polarization. When a peak gamma-ray energy of 700 MeV was used a total of 530 left scatters and 280 right scatters gave a value of  $59\% \pm 6\%$  for the polarization.

The value at the higher energy indicates that the parity of the second resonance is negative. It is possible that neither the Wilson nor the Peierls models give the correct interpretation. From the experimental result we can certainly say that the Wilson model is unsuccessful.

This experiment is remarkably good in that the polarization can be calculated simply from measurement of a left-right asymmetry. The experimenter must have had a very intense gamma-ray beam at his disposal.

Stein also refers to preliminary results of Connolly and Weill (220) who performed the same experiment at 550 MeV with emulsions and found a value of  $+30\%$  for the polarization of the recoil proton.

### V.5. Information Obtainable from Polarization Measurements.

The polarization of the outgoing photonucleons from deuterium is theoretically found to be much more sensitive to the neutron-proton interaction assumed than is the angular distribution. Thus ambiguities which arise from the various assumptions may be settled by measurements of this polarization. In addition, it has been seen (Section I.4A.2) that E1-M1 interference is destructive in the forward hemisphere and constructive in the backward hemisphere for neutron emission so that a measure of the relative E1 and M1 transitions as well as the spin dependence of the neutron-proton forces can be gained by examination of the deviation from symmetry of the polarization about  $\theta = 90^\circ$ . Furthermore we see that at  $\theta = 90^\circ$  the polarization is due only to E1-M1 interference. Polarization measurements might also yield information on the nuclear forces as well as the electromagnetic properties of the nucleon. They would give an estimate of the contributions from E1, M1 and E2 transitions and would also indicate the effect of tensor forces and of the magnitude of the D-state of the deuteron. Information might also be gained about the types of interaction for some simple nuclei for which a two body model might be applied

Solution of the Fermi-Yang and the Wilson-Peierls Ambiguities can also be obtained by measurement of the polarization of the recoil proton in  $\pi^0$  meson production as discussed in section V.3.

Chapter VI. The Polarization of Photoprotons from Carbon.

Chapter VI.

The Polarization of Photoprotons from Carbon.

An experimental determination of the polarization of photoprotons from deuterium would be very desirable since it could possibly answer many of the questions previously discussed in section V.5. However, as will be seen, the apparatus required for this experiment is very extensive since it not only includes a considerable amount of cloud chamber control equipment but also a complicated counter system with elaborate electronics. Although a liquid deuterium target was available in the laboratory its introduction would have proved an additional complication to an untried experimental arrangement. It was therefore decided to use a carbon target for a preliminary experiment in spite of the fact that no theoretical work had been performed on the polarization of photoprotons from this nucleus.

VI.1. The Measurement of Polarization.

The polarization of a beam of nucleons can be determined by a scattering experiment from a material of known analysing power such as carbon or helium. By measuring the asymmetry in the scattering the polarization of the beam can be calculated. In the experiment about to be described measurement of the polarization of protons with energies of about 100 MeV was desired and carbon is the most suitable analysing material since it has a good analysing efficiency

for these proton energies and is also easy to handle.

The conservation of parity in strong interactions demands that the direction of polarization be at right angles to the plane of the reaction. In the present experiment the photoprotons were selected in the horizontal plane thus requiring the polarization of the proton beam to be in the vertical direction. Furthermore, the analysing power of the carbon depends on the azimuthal angle,  $\phi$ , of the scatter. Thus the simplest method of performing the experiment would be to have two counters set to left and right of the carbon analyser looking along the direction of the incident proton at equal polar angles to it in the horizontal plane and at azimuthal angles  $\phi = \pm 90^\circ$  only. The left-right asymmetry would then give a measure of the polarization. However the counting rate in such an experiment would be very small because of the very small solid angle of acceptance and background troubles would be very serious if one did not have a very intense  $\gamma$ -ray beam. A better method would use a much larger range of angles and by measuring both the azimuthal and polar angles of scatter still have the necessary information to work out the polarization accurately.

The triggered cloud chamber which has been described previously provides an ideal arrangement for such a measurement. By choosing an appropriate array of counters one can select only those particles which scatter in a carbon block

in the cloud chamber and can measure the angles of scatter very accurately.

### V1.2. Experimental Arrangement.

In the experiment to be described in this chapter the cloud chamber was used to analyse the spin orientations of photoprotons from an external solid target. Protons produced from a carbon target by the 330 MeV gamma-ray beam from the synchrotron were detected by two proton telescopes arranged around the cloud chamber as shown in figure V1.1. A carbon block inside the chamber produced scattering of the protons and the counters were accurately positioned so that no proton from the target could pass straight through the carbon into the back telescopes. The azimuthal and polar angles of scatter could be readily and accurately measured from the cloud chamber photographs which were taken when expansion of the chamber was produced by a pulse from the counters. Counters 2 and 4 were operated in coincidence with counter 1 while 3 and 5 were anti-coincidence counters.

### V1.3. Cloud Chamber Modifications and Operation.

This experiment required the mounting of a solid carbon scatterer inside the cloud chamber. To act both as a support for the carbon and as shielding for the counters a brass block with dimensions 4 in. x 11 in. x 1/2 in. was positioned between the clearing field wires and firmly attached to the cloud chamber by pillars through the perforated brass plate.

carbon in the form of a ...  
of this brass block. The  
in photographs A.2.7 & ...  
One of the walls which ...  
"mylar" window for ...  
by a flat wall ...  
essentially uniform ...

**PROTON POLARISATION  
EXPERIMENT**

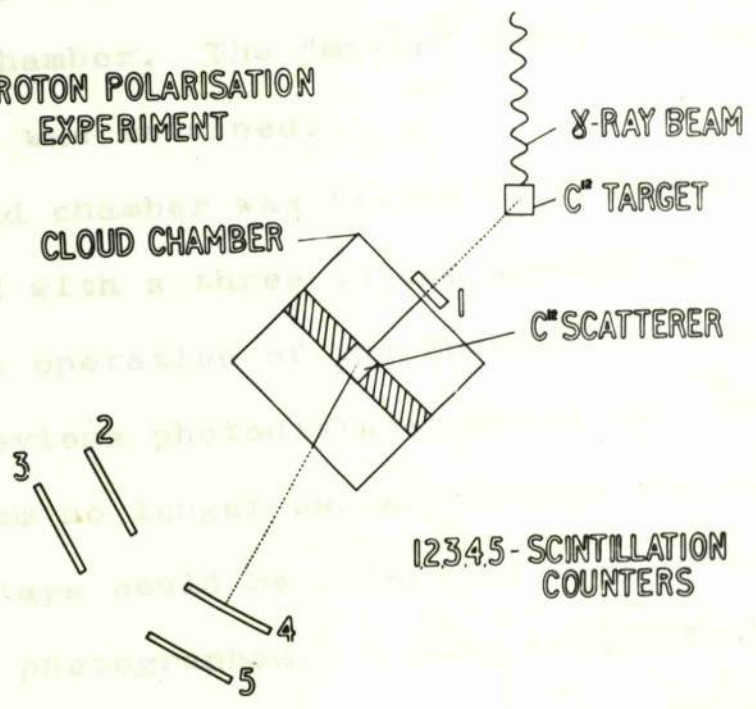


**FIG. VI 1.**

difference between the ...  
and pressure recorded ...  
the 1.5° and 0.5° ...  
unattended for some ...  
and the tracks suffered no ...

The carbon in the form of a 2 in. cube was fitted into the middle of this brass block. The arrangement can be clearly seen in photographs A.2.7 to A.2.11.

One of the walls which had previously carried a 2 in. diameter "mylar" window for beam exit was removed and replaced by a flat wall composed entirely of dural. Thus an essentially uniform path was provided for the protons leaving the chamber. The "mylar" entry window in the opposite wall was retained.

The cloud chamber was filled to 1.5 atmos. with Argon gas saturated with a three to one alcohol-water vapour mixture. The operation of the chamber was not so critical as in the previous photodisintegration experiment since the gamma-ray beam no longer passed through the chamber gas. Long lamp delays could be tolerated thus allowing fully grown tracks to be photographed. A lamp delay of 80 m.secs. was found to give satisfactory results. A continuous record was kept of the temperature and pressure in the beam room. The difference between the maximum and minimum values of temperature and pressure recorded throughout the entire experiment was  $1.5^{\circ}$  and 0.5 cm. respectively. The cloud chamber was left unattended for more than an hour on numerous occasions and the tracks suffered no degeneration.

#### V1.4. Counters.

Plastic scintillation counters were used entirely in this experiment.

The author built counters 2, 3, 4 and 5 which were of basically the same design as those used in the previous photodisintegration experiment but were larger and had slight modifications in constructional details. The scintillator size of 7 in. x 4 in. x 1/2 in. subtended a solid angle of 1/14 steradians at the centre of the carbon block. Both the crystal and the light guide to the photomultiplier were covered with a layer of 0.0002 in. thick "mirralon" film and then with 0.0002 in. thick aluminium to make the system light-tight. All of these counters had EMI 6262 photomultipliers.

Counter 1 with a circular crystal 2 in. in diameter and 3/4 in. thick had an RCA 6810 photomultiplier.

#### V1.5. Counter Electronics.

Figure V1.2 shows the block diagram of the counter electronics for the proton polarization experiment.

The operation may be sufficiently clear from this diagram. Counter 1 was only 8 in. from the carbon target and was therefore detecting numerous electron pulses. An RCA 6810 photomultiplier together with a coincidence - anti-coincidence circuit with a resolving time of 40 millimicroseconds was therefore employed. Counters 2, 3,



4 and 5 although not requiring to be exceptionally fast had to be carefully balanced to prevent any counter asymmetry in the detection of protons. All used EMI 6262 photo-multipliers.

A measurement of  $\frac{dE}{dx}$  in counter 1 and of E in counters 2 and 4 were displayed on the X and Y plates respectively of two cathode-ray tubes. The double discriminator circuit selected only those pulses with a  $dE/dx$  and E corresponding to a proton in the required energy range. Such a response was displayed on the cathode-ray tube as an extra bright spot and in addition produced expansion of the cloud chamber.

#### VI.6. Counter Alignment.

Rapid and accurate alignment of the equipment in the synchrotron beam was desirable. Any misalignment of the counters could lead to unwanted photographs and a loss of synchrotron running time. This was always an important consideration. A system of sights was designed to facilitate this alignment.

The carbon block was first positioned accurately in the middle of the cloud chamber so that a perpendicular through the centre of the exit wall passed through the centre of the block and also through 1/32 in. holes in two metal discs 2 in. apart and fitted outside the chamber to the supporting frame.

The four back counters had to be accurately placed on either side of the carbon block at equal polar and azimuthal angles and held firmly in position. A T-shaped table, with four metal stands to support the counters, was designed for this purpose. Fitted on the line midway between the two pairs of stands were two sights similar to those on the cloud chamber. This counter table was sitting in grooves on a pneumatic metal table and could be accurately levelled by three adjustable screws. The two sights on the table were lined up with those on the cloud chamber by adjusting the heights until the light from a mercury vapour lamp formed a small spot on the centre of the cloud chamber wall. The counters were attached to the supports by clamps which had three degrees of freedom. They were positioned at the appropriate angles by means of a theodolite. The theodolite was placed at the same distance from the sights on the table as the carbon block and was lined up with them. Counters 3 and 5 were then aligned with the theodolite cross-wires set in turn at equal angles on either side of the straight through position. Counters 2 and 4 were then similarly positioned. By this procedure counters 2, 3, 4 and 5 were empirically found to be positioned with respect to the carbon to within an accuracy of  $\pm 1/2^\circ$ .

The complete experimental arrangement could then be quickly set up beside the synchrotron beam: The carbon

target was first lined up in the beam by means of sights permanently in the beam room. The front counter and cloud chamber were then set at  $45^\circ$  to the beam direction and the back counters were wheeled into place behind the cloud chamber and quickly positioned by means of the sights and mercury vapour lamp. The arrangement can be seen in photographs V1.1 and V1.2.

The complete experimental arrangement was lined up to an accuracy of better than  $1^\circ$ .

#### V1.7. Mathematical Analysis of Results.

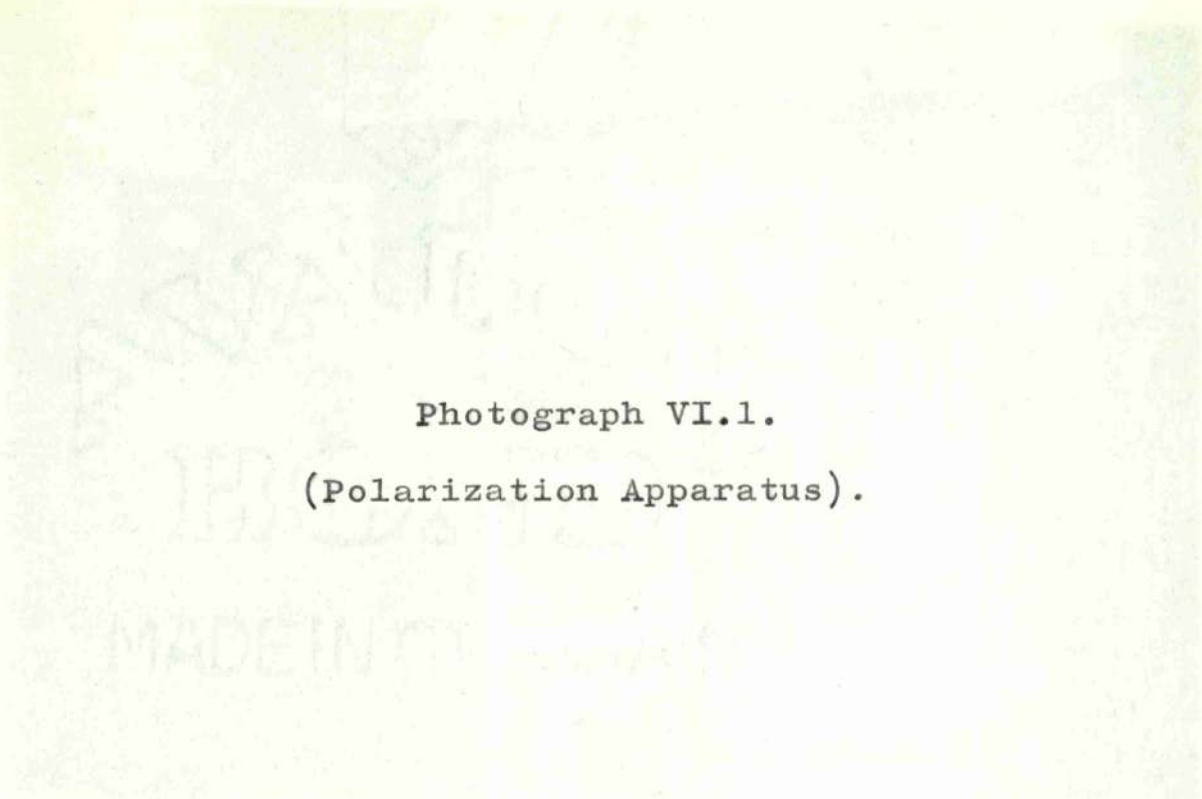
(a) Maximum Likelihood Calculations. To make greatest possible use of all the data available the maximum likelihood method of calculating the polarization was employed.

If a distribution function can be found to give the probability of any event scattering into a given solid angle we can use the whole range of solid angle,  $\mathcal{N}$ , rather than accurately measure the probability of scattering into a small angle  $d\mathcal{N}$ .

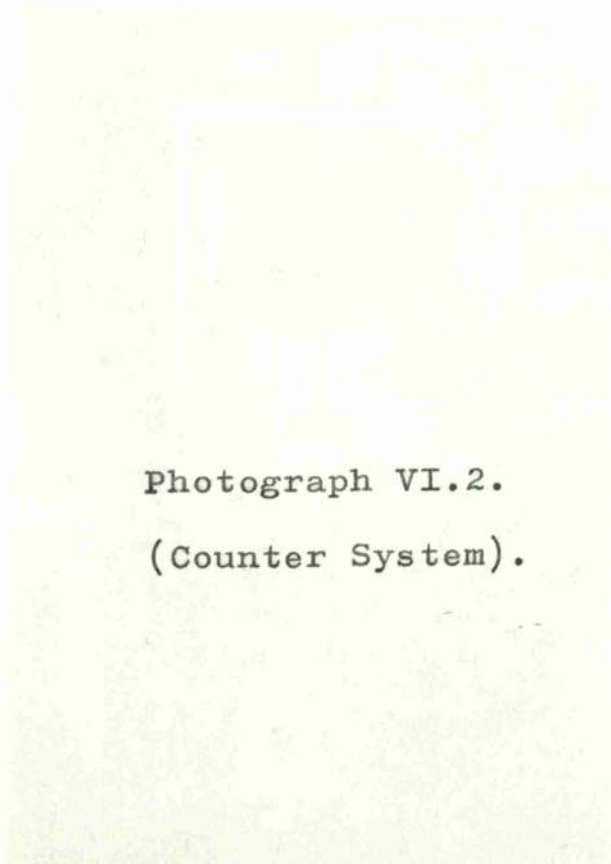
Several hundred events would then be sufficient to give a good measurement of the polarization if a distribution function could be found to satisfy all the events.

We can write

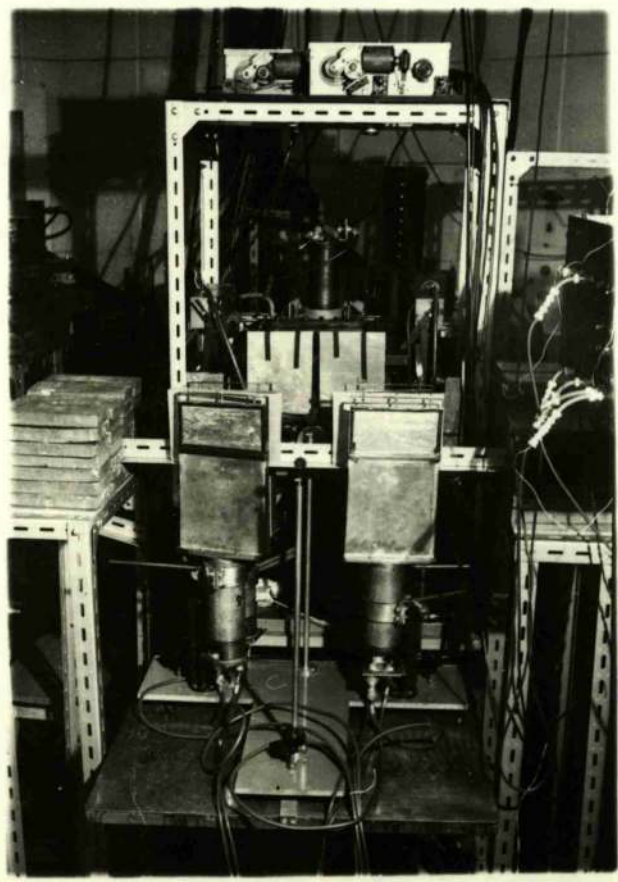
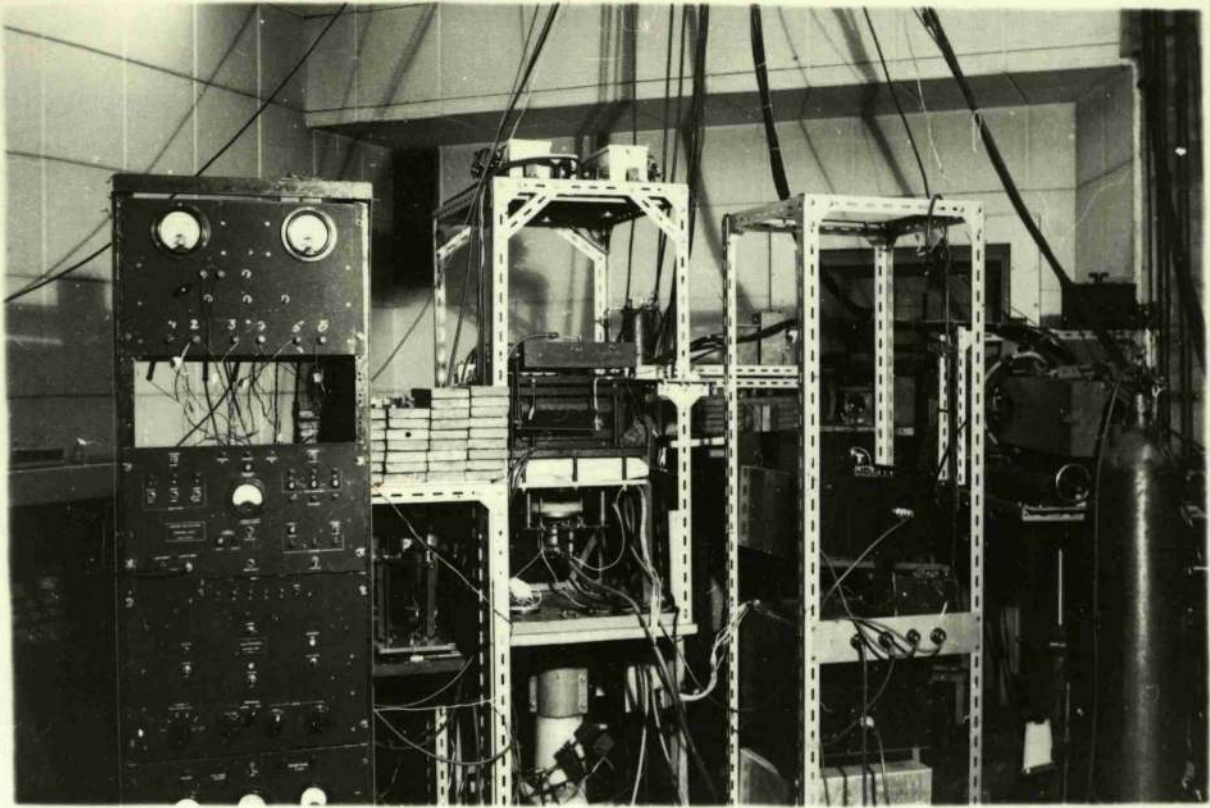
$$\omega(\theta, \phi, E) = K \frac{d\sigma(\theta, E)}{d\mathcal{N}} \left\{ 1 + P P_c(\theta, E) \sin \phi \right\} d\mathcal{N}.$$



Photograph VI.1.  
(Polarization Apparatus).



Photograph VI.2.  
(Counter System).



as the distribution function for the probability of a proton being scattered at a polar angle  $\Theta$  and azimuthal angle  $\phi$ . where

$K$  = a normalisation factor

$\frac{d\sigma}{d\Omega}$  = differential cross-section for proton production.

$P_c$  = polarization produced in a proton beam of energy  $E$  by scattering from carbon at angle  $\Theta$ .

$P_{c \sin \phi}$  = effective analysing power of carbon

$P$  = assumed polarization of the investigated beam.

Any value of  $P$  will give a value for the probability,  $\omega$ , for each event. Multiplying all these probabilities together will give a probability  $L$  for the function  $\omega$  representing all the events. By repeating the process for numerous values of  $P$  we can derive a curve the peak of which will give the maximum  $L$  or likelihood.

This likelihood curve is almost a Gaussian and the standard deviation can be found by taking the width at  $0.6 L_{\max}$ . This width gives only the statistical error of the calculation.

(b) Carbon Polarization Data. The values of  $P_c(\Theta, E)$  for a proton of energy  $E$  scattered at an angle  $\Theta$  from carbon were taken from the Harwell data (221, 222). The value of  $\Theta$  was obtained from the reprojection measurement and  $E$  was gained from the cathode-ray tube photographs.  $P_c$  is taken to be positive if the spin is regarded as being downwards for a scatter to the right. No corrections were made for inelastic scattering of protons from the 4.43 MeV, 7.65 MeV,

or 9.61 MeV excited levels of the  $C^{12}$  nucleus since this only becomes appreciable for angles greater than  $30^\circ$  and none of the finally selected events had values of  $\theta$  greater than this.

#### VI.8. Experimental Analysis of Events.

(a) Measurement System. All of the film was first scanned on a viewer before reprojection commenced. Thus the possibility of tracks being overlooked was small.

Essentially the same reprojection system as used in the photodisintegration experiment, and described in section III. 2, was again employed. An accurate reconstruction of the experimental arrangement was made so that the observer could readily see which tracks originated in the target and passed through the counter system. The polar angle,  $\theta$ , and the azimuthal angle,  $\phi$ , of scatter and the horizontal and vertical positions on the carbon block of the incoming proton were directly measured on the reprojection table. By extrapolating the incoming and outgoing proton tracks the position of scatter in the block could also be readily ascertained.

(b) Reflection Criterion. In the present experiment a measurement of an asymmetry in the scattering of protons was being performed. It was therefore important to eliminate any possible asymmetry which might have been created by the experimental arrangement.

Suppose we consider identical scatterings for protons

with opposite spin directions. We see that they will differ only in the sign of azimuthal angle  $\phi$ . For every event accepted we therefore have to observe whether the event reflected in  $\phi$  would have been recorded and accepted with the same absolute value of  $P_c(\theta, E) \sin \phi$ , the effective analysing power of the carbon.

The reconstruction of the counter system made this procedure comparatively easy. Each scattered track was first extrapolated on to the appropriate counter telescope and then reflected in  $\phi$  to see if it passed through the opposite telescope.

(c) Track Displacement. Corrections were made for the vertical displacement of all tracks caused by the downward motion of the cloud chamber diaphragm. The real inclination of any track to the horizontal was increased by this motion. A simple calculation assuming downward displacement of the gas to be a linear function of height showed that the maximum change in azimuthal angle would be less than  $2^\circ$ . For horizontal tracks the correction was zero.

(d) Track Distortion. Slight distortion appeared in a small fraction of the tracks in the region near the carbon block. This was probably caused by adhesion of the gas to the solid material and resulted in slight track curvature. An example of this can be seen in photograph A.2.7. No error arose from this distortion since that part of the track near

the carbon was not used in the measurements.

#### V1.9. Testing of the Experimental Equipment.

A total of fifteen days running time was available in the synchrotron beam. Extensive tests were made during the first ten days to ensure that the counters and cloud chamber were functioning properly and were not liable to produce any experimental asymmetry in the proposed measurement.

Counters 2, 3, 4 and 5 were first balanced by setting them, in line, to detect unscattered photoprotons from the carbon target. Adjustment of the counter electronics could thus be achieved.

The cloud chamber was then interposed and photographs were taken of protons passing straight through the carbon scatterer. Carbon and polythene absorbers, each 0.5 in. thick, were placed between the target and counter 1 to reduce the number of low energy electrons being detected. Aluminium absorber 0.25 in. thick was placed between the cloud chamber and counters 2 and 4 and a 0.5 in. thick block of the same material was inserted between the coincidence and anti-coincidence counters. Under these conditions protons with energies between 80 MeV and 130 MeV were detected. Additional absorber was later inserted to increase the accepted energies to the range between 120 MeV and 160 MeV.

More than five hundred test photographs were taken in this way. The cloud chamber was able to detect protons at

all energies attempted.

Counters 2, 3, 4 and 5 were then arranged, as in figure V1.1, to left and right of the carbon scatterer, looking along the direction of the incident proton, at equal minimum angles of  $8.5^{\circ}$  and maximum angles of  $28.5^{\circ}$  in relation to the centre of the carbon scatterer.

Test photographs of scattered protons were then taken with this arrangement.

During the full experimental run, for which five days of synchrotron time were available, protons with energies between 80 MeV and 130 MeV were selected.

#### V1.10. Results.

Although the counters were positioned so that no proton could pass straight through the carbon scatterer and enter either back telescope it was possible for a proton to do so when scattered by only a few degrees. Early in the experimental run it was apparent that many of the photographs were being triggered by events of this type. This difficulty could easily have been overcome by moving the back telescopes outwards from the "straight through" position to larger angles. It was also apparent that exposures were being taken of events in which the triggering particle passed through the brass shielding. These particles corresponded to protons with a minimum energy of 120 MeV and could have been eliminated by the insertion of further brass shielding inside

the cloud chamber. This modification would, however, have consumed considerable time. In the interests of a proposed succeeding experiment with a deuterium target it was decided to continue with an unchanged experimental arrangement to ascertain the fraction of events which could be accepted.

A total of one hundred and ninety triggering protons was obtained.

During a short period of time, owing to a camera fault, the counter responses were not recorded from the cathode-ray tubes. For this reason thirty-four of the photographs had to be discarded. An arbitrary value chosen to be  $6^\circ$ , below which all scatters would be rejected, had to be taken for the polar scattering angle,  $\theta$ . This criterion resulted in elimination of all events which could possibly have been produced by multiple Coulomb scattering in the carbon. A total of sixty-six events were discarded for this reason. The distributions of polar and azimuthal scattering angles  $\theta$  and  $\phi$  seen in figures V1.3 and V1.4, help to clarify the situation. Elimination of a further twenty-five events resulted from the proton paths being at least partly through the brass shielding. Six scatters, which were presumably further scattered in the back wall of the cloud chamber, did not appear to enter either of the back telescopes and were rejected. The double discriminator bias settings in the counter display unit were then chosen so that no electronic

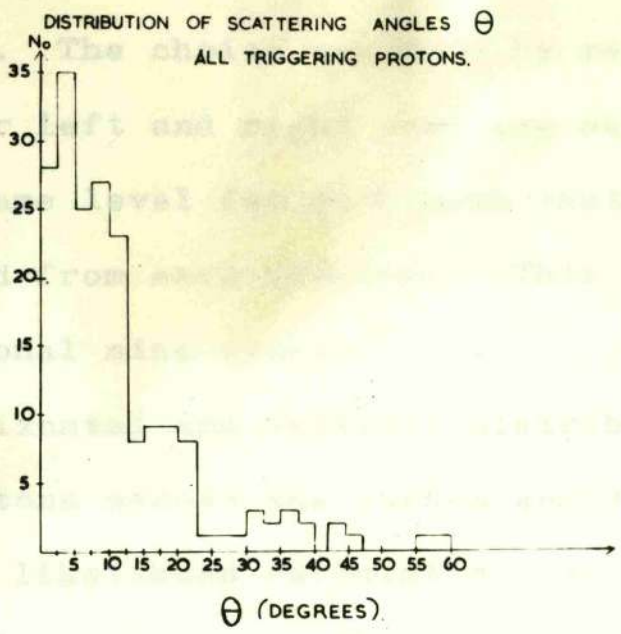


FIG. VI.3.

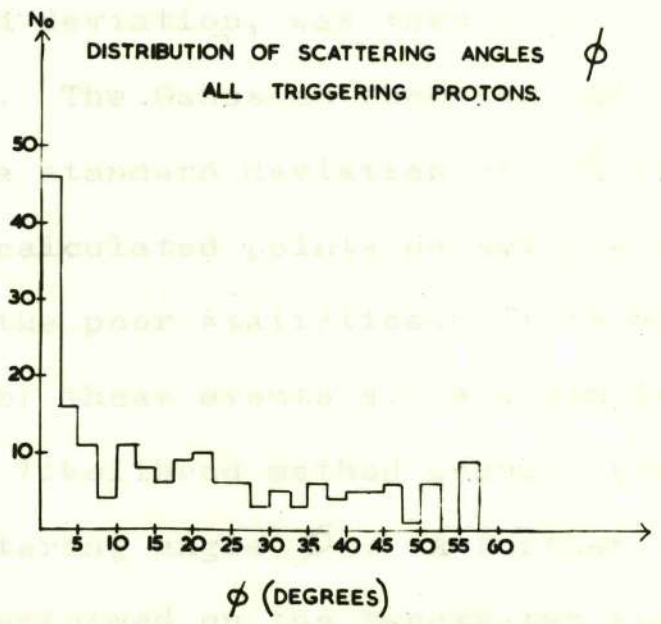
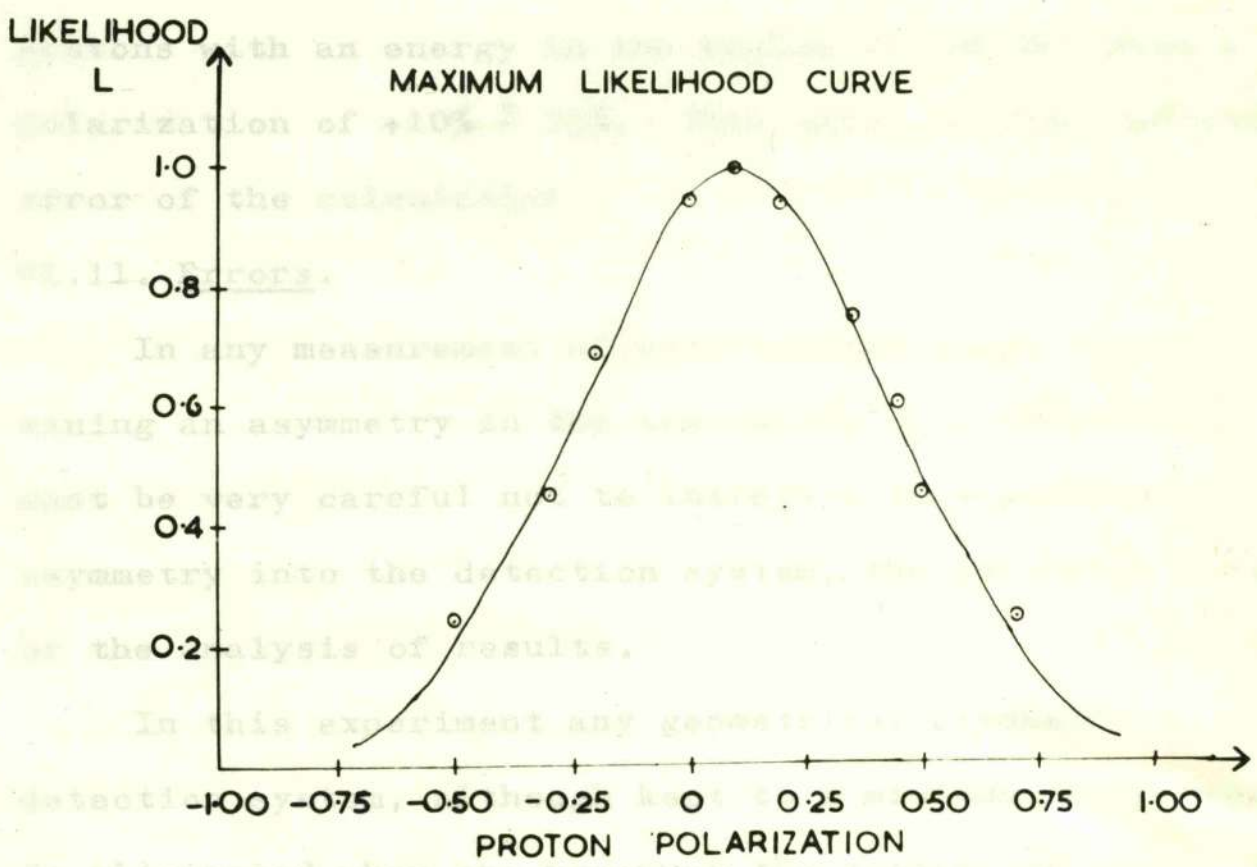


FIG. VI.4.

asymmetry in the selection of the counter responses could have existed. The choice was made by replotting the counter responses for left and right scatters separately and then taking the same level for each such that a few responses were rejected from each telescope. This caused elimination of an additional nine events.

The horizontal and vertical distributions of all the incoming protons across the carbon analyser were isotropic so a maximum likelihood calculation was performed for the fifty remaining scatters. The points calculated for ten different assumed polarizations can be seen in figure V1.5. A curve of the function  $L = L_{\max} e^{-(P-P_0)^2/2\sigma^2}$ , where  $P_0$  is the polarization at the maximum of the curve and  $\sigma$  is the standard deviation, was then drawn through these calculated points. The Gaussian function having a value of +10% for  $P_0$  and a standard deviation of 33% is seen to fit quite well. The calculated points do not lie exactly on the curve because of the poor statistics. It is not completely valid to use all of these events since a simple interpretation of the maximum likelihood method assumes symmetry in the azimuthal scattering angle  $\phi$ . A further calculation was therefore performed on the twenty-two events which also satisfied the reflection criterion. An almost identical curve with the same maximum value of polarization and same standard deviation resulted. The calculations were performed

hand. If the statistics had been better, a computer programme could have been written to give the maximum likelihood for a large number of assumed values of polarization. The attempt was made to separate the results into two groups because of the small number of events in each group. From the maximum likelihood curve...



**FIG. VI. 5.**

the cloud chamber photographs... minimum and maximum values of... direction. In addition, examination of... photographs eliminates the possibility... which scatter is material other than... The biggest argument against... in the present form lies in the...

by hand. If the statistics had been better a computer programme could have been written to perform the calculation for a large number of assumed values of polarization. No attempt was made to separate the events into separate energy bins because of the small number of events available.

From the maximum likelihood curve we see that photo-protons with an energy in the region of 100 MeV have a polarization of  $+10\% \pm 33\%$ . This error is the statistical error of the calculation.

#### V1.11. Errors.

In any measurement of polarization where one is determining an asymmetry in the scattering of a proton beam one must be very careful not to introduce an experimental asymmetry into the detection system, the recording system or the analysis of results.

In this experiment any geometrical asymmetry in the detection system, although kept to a minimum for convenience, is eliminated when one measures the scattering angles from the cloud chamber photographs and then selects the same minimum and maximum values of acceptance for each spin direction. In addition, examination of the cloud chamber photographs eliminates the possibility of neglecting protons which scatter in material other than the carbon analyser.

The biggest argument against performing the experiment in the present form lies in the fact that two telescopes are

used to detect the scattered protons. An electronic asymmetry in the detection efficiency is thus possible. However, every effort was made to ensure that this did not occur and the use of identical bias levels for the counter responses from the two telescopes must largely eliminate any such asymmetry. Removal of electronic asymmetry will be discussed in more detail later.

Most errors in the measurement of the cloud chamber tracks such as an observer consistently measuring angles too large or too small would be expected to be symmetrical. Such an error would not make an appreciable difference to the final value of polarization as it would appear on both sides of the scattering asymmetry.

#### V1.12. Discussion.

The technique described in this chapter, with a few minor modifications, is capable of performing any experiment to measure the polarization of high energy protons. The present experiment, of course, suffers from a lack of statistics. This is primarily due to insufficient synchrotron running time and to defects in the experimental apparatus which resulted in many wasted photographs. These defects can be readily overcome.

(a) The biggest loss of photographs was seen to be due to small angle scatters. This can be overcome by reducing the width of the carbon scatterer and by moving the counter

telescopes to larger angles from the incoming proton direction. This will result in a reduced counting rate but the optimum situation can be found by a suitable choice of parameters.

(b) The second largest loss of photographs was due to insufficient brass shielding of the counters from direct photoproton emission. This can be easily overcome by increasing the thickness of the shielding or, alternatively, by placing a thin scintillation counter adjacent to that side of the carbon analyser nearest the back telescopes and of the same dimensions as the carbon. If this counter is designated "counter 1'" then a coincidence between counters 1,1' and 2 or 1,1' and 4 would be demanded. A disadvantage of such an arrangement would be that a few scatters might occur in the scintillator rather than in the carbon analyser. One could, however, allow for such scatters.

(c) An additional loss was due to scattering in the back wall of the cloud chamber. By reducing the thickness of this wall from 1/2 in. to 1/16 in. of dural such a loss could be considerably cut down.

(d) Better counter resolution could be achieved by the introduction of another counter into each of the back telescopes. Counter 1 would then be used only as a coincidence counter and could be placed nearer to the gamma-ray beam without much difficulty. This would increase the

solid angle of acceptance and the counting rate. The first two counters of each back telescope (now consisting of three counters) would then be used to provide a  $\frac{dE}{dx}$  and E measurement.

(e) A certain method for ensuring that no electronic asymmetry occurs would be to replace the two back telescopes by a single anti-coincidence in the "straight through" position so that all scatters of greater than a certain minimum angle are accepted. While such a procedure is desirable it is not possible in this particular experiment because a large range of proton energies is present and no means of measuring this range would then be available. An alternative method would involve combination of the coincidence and anti-coincidence methods and replacement of the proposed six back counters by three counters with very long scintillators so that all angles out to the maximum of  $28.5^{\circ}$  are subtended. A single anti-coincidence counter could then be inserted between these counters and the cloud chamber to cut out all angles between  $-8.5^{\circ}$  and  $+8.5^{\circ}$ . This method while the most desirable is not easy to put into practice because of the very large scintillators required (approximately 20 in. long) with resultant light collection difficulties.

(f) There are no theoretical predictions or previous experimental determinations with which the value obtained for the polarization of photoprotons from carbon can be compared.

Although the error is large the result is encouraging for such a short experiment. Elimination of the difficulties experienced in the above experiment could lead to the acquisition of a much larger number of acceptable events in a short time. It is estimated that a total of fifteen hundred useful events could be obtained in an experiment of about four weeks duration. Such a number would probably be sufficient to give a value for the polarization to an accuracy of better than 5%.

PROGRAMS FOR SCIENTISTS  
CALCULATORS

Appendices.

Appendix 1.Programme for Conservation of Energy and Momentum  
Calculations in the Oxygen Experiment.

The Tabular Interpretive Programme was found to be the most useful scheme for performing the conservation of energy and momentum calculations on the DEUCE computer.

The calculations could have been carried out manually using a sheet of paper ruled into rows and columns so that the numbers in any column are mathematical functions of the numbers in the corresponding rows of any other column. The computer performed the calculations in an identical manner when the instructions were presented in the Tabular Interpretive scheme.

For T.I.P. the computer is regarded as having its storage space divided into 128 columns numbered 0 to 127 and each having 30 rows numbered 0 to 29. These quantities are rather inadequate if each column can only be used once. However, any instruction which requires DEUCE to write in a particular column will obliterate anything previously stored there. A total of 128 positions is also reserved for constants which are referred to as  $N_0, N_1, \dots, N_{127}$ . These may be used if we wish to operate on all rows of a column with the same number.

Each codeword is written in the form  $r \quad a \quad b \quad c$  where  $a$ ,  $b$  and  $c$  refer to column numbers or constants and  $r$  denotes a function which is the code number of the operation.

Note: It is very often convenient, when writing a programme of appreciable length, to introduce irrelevant instructions which may be deleted at will when additional codewords require to be inserted.

Constants.

N0 to N31 are preset values.

$$N32 = 2m_p, N33 = m_n, N34 = c, N35 = c^2, N36 = c^4$$

N37 = 1,2,3,4,5 depending on whether 2,3,4,5,6 particles

$$N38 = 1,2,3,4,5,6 \quad " \quad " \quad " \quad 1,2,3,4,5,6 \quad "$$

$$N39 = 4,8,12,16,20,24, \quad " \quad " \quad " \quad 1,2,3,4,5,6 \quad "$$

$$N40 = 2,4,6,8,10,12, \quad " \quad " \quad " \quad 1,2,3,4,5,6 \quad "$$

$$N41 = 3,6,9,12,15,18 \quad " \quad " \quad " \quad " \quad "$$

$$*N42 = 0,1,2,3,4 \quad " \quad " \quad " \quad 2,3,4,5,6 \quad "$$

$$N43 = Q$$

$$N44 = \sqrt{2m_p E'_p}, N45 = \sqrt{2m_p E''_p}, N46 = \sqrt{2m_p E'''_p}$$

$$N47 = 2m_n$$

$$N48 = \pi/2 = 1.570796.$$

$$N49 = 7, \text{ say. Used as a "filler".}$$

\*For two particle events certain instructions deleted.

	<u>Codeword</u>				<u>Meaning.</u>
	a	b	c	r	
0	NO	29	0*	13	{ Fills 1st 30 rows of 1st 100 cols. with zeros.
1	0	100	0	16	
2	0	0	0	18	Reset asterisked codes in loop.
3	18	0	N32	4	Reads 18 constants.
4	N49	N49	N100	0	Irrelevant instruction.
5	0	0	0*	4	Reads $m_2, \dots, m_6$ .
6	0	0	5*	4	Reads $E_2, \dots, E_6$ .
7	0	N37	5	16	Jump to 5 until instructions from 5 have been obeyed N37 times Reset.
8	0	0	0	18	
9	0	0	10*	4	Reads $\theta_p, \dots, \theta_6$
10	0	0	16*	4	Reads $\psi_p, \dots, \psi_6$
11	0	0	22*	4	Reads $\alpha_p, \dots, \alpha_6$
12	0	0	28*	4	Reads $\beta_p, \dots, \beta_6$
13	0	N38	9	16	
14	0	0	0	18	
15	10*	N8	10*	1	Converts <b>L</b> 's to radians.
16	0	24	15	16	Jump to 15 until instructions from 15 have been obeyed 24 times
17	0	0	0	18	
18	10*	0	34*	12	cos $\theta$ 's
19	16*	0	40*	12	cos $\psi$ 's
20	16*	0	16*	11	sin $\psi$ 's
21	10*	0	10*	11	sin $\theta$ 's
22	10*	16*	10*	0	sin $\theta$ sin $\psi$ 's

23	10*	N6	10*	0	To make two systems identical:
24	16*	34*	16*	0	$\sin \psi \sin \theta$ $\sin \psi \cos \theta$ 's.
25	10*	10*	34*	0	$(\sin \psi \sin \theta)^2$
26	N1	34*	34*	3	$1 - (\sin \psi \sin \theta)^2$
27	34*	0	34*	6	$+\sqrt{1 - (\sin \theta \sin \psi)^2}$
28	16*	34*	16*	1	$\sin \beta$
29	40*	34*	40*	1	$\cos \beta$ 's & 1's
30	0	N38	18	16	
31	0	0	0	18	
32	28*	0	46*	12	$\cos \beta$ 's & 1's
33	40*	N6	40*	2	$(\cos \beta - 1)$ 's & zeros.
34	46*	N6	46*	2	$(\cos \beta - 1)$ 's & zeros.
35	40*	46*	40*	2	$(\cos \beta - 1)$ 's
36	N1	40*	40*	2	$\cos \beta$ 's.
37	0	6	32	16	
38	0	0	0	18	
39	10*	0	10*	23	$\sin^{-1}, \alpha_p, \dots, \beta_6.$
40	10*	22*	10*	2	$\alpha_p, \dots, \beta_6.$
41	10*	0	22*	11	$\sin \alpha_p, \dots, \sin \beta_6.$
42	10*	0	10*	12	$\cos \alpha_p, \dots, \cos \beta_6.$
43	0	12	39	16	
44	0	0	0	18	
45	N49	N49	N100	0	
46	N49	N49	N100	0	
47	N49	N49	N100	0	

48	N49	N49	N100	0	
49	N49	N49	N100	0	
50	N49	N49	N100	0	
51	N49	N49	N100	0	
52	N49	N49	N100	0	
53	10*	28*	28*	0	$\cos \alpha \sin \beta.$
54	10*	40*	10*	0	$\cos \alpha \cos \beta.$
55	N1	28*	16*	0	$\cos \alpha \sin \beta.$
56	0	N38	53	16	
57	0	0	0	18	
58	0*	5*	5*	0	$m_2 E_2$
59	N2	5*	5*	0	$2m_2 E_2$
60	5*	0	5*	6	$\sqrt{2m_2 E_2}$
61	0	N37	58	16	
62	0	0	0	18	
63	N1	N44*	N44	0	Introduces new $E_p$ 's.
64	N44	10	52	0	$p_1^x$
65	N44	16	58	0	$p_1^y$
66	N44	22	64	0	$p_1^z$
67	5*	11*	53*	0	$p_2^x \dots \dots p_6^x$
68	5*	17*	59*	0	$p_2^y \dots$
69	5*	23*	65*	0	$p_2^z \dots$
70	0	N37	67	16	
71	0	0	0	18	

72	52*	0	0	5	Punches px's
73	58*	0	0	5	Punches py's
74	64*	0	0	5	Punches pz's
75	0	N38	72	16	
76	0	0	0	18	
77	52	53	28	2	
78	58	59	29	2	
79	64	65	30	2	
80	N49	N49	N100	0	{ 80 28 54* 28 2 { 81 29 60* 29 2 { 82 30 66* 30 2 { 83 0 N42 80 16 { 84 0 0 0 18
81	N49	N49	N100	0	
82	N49	N49	N100	0	
83	N49	N49	N100	0	
84	N49	N49	N100	0	

Insert for events of greater than two particles.

85	N6	29	29	0
86	N6	30	30	0
87	28	0	0	5
88	29	0	0	5
89	30	0	0	5
90	52*	52*	52*	0
91	58*	58*	58*	0
92	64*	64*	64*	0
93	0	N38	90	16

Punches  $c_3, c_1, c_2$  where  $c_1 = p_{ny}, c_2 = p_{nz}, c_3 = \frac{E\gamma}{c} - p_{nx}$

$p_x^2$

$p_y^2$

$p_z^2$

94	0	0	0	18	
95	52*	58*	52*	2	
96	52*	64*	52*	2	$p_1^2, \dots, p_6^2$
97	0	N38	95	16	
98	0	0	0	18	
99	52	N32	52	1	$p_1^2/2m_p$
100	N2	0*	0*	0	$2m_2 \dots \dots \dots 2m_6$
101	53*	0*	53*	1	$p_2^2/2m_2 \dots \dots$
102	0	N37	100	16	
103	0	0	0	18	
104	52	53	31	2	
105	N49	N49	N100	0	105 31 54* 31 2
106	N49	N49	N100	0	106 0 N42 105 16
107	N49	N49	N100	0	107 0 0 0 18
108	31	N43	31	2	than two particles.
109	31	0	0	5	Punches $c_4 = E_\gamma - \frac{pn^2}{2m_n}$
110	28	N34	32	1	$c_3/c$
111	N33	32	32	2	$m_n + c_3/c$
112	32	32	33	0	$(m_n + c_3/c)^2$
113	N36	33	34	0	$(m_n + c_3/c)^2 c^4$
114	N49	N49	N100	0	
115	N47	31	36	0	$2m_n c_4$
116	28	28	37	0	$c_3^2$
117	29	29	38	0	$c_1^2$
118	30	30	39	0	$c_2^2$

} Insert  
for  
events  
of  
greater

119	36	37	36	2	
120	36	38	36	2	
121	36	39	36	2	$(2m_n c_4 + c_1^2 + c_2^2 + c_3^2)$
122	36	N35	36	0	$(2m_n c_4 + c_1^2 + c_2^2 + c_3^2) c^2$
123	34	36	37	3	$(m_n + c_3/c)^2 c^4 - (2m_n c_4 + c_1^2 + c_2^2 + c_3^2) c^2$
124	37	37	38	25	Branch
125	38	90	38	26	Mix
126	38	0	38	6	$\sqrt{\{(m_n + c_3/c)^2 c^4 - (2m_n c_4 + c_1^2 + c_2^2 + c_3^2) c^2\}}$
127	32	N35	39	0	$(m_n + c_3/c) c^2$
128	39	38	40	2	$(m_n + c_3/c) c^2 + \sqrt{\{(m_n + c_3/c)^2 c^4 - (2m_n c_4 + c_1^2 + c_2^2 + c_3^2) c^2\}}$
129	39	38	41	3	$(m_n + c_3/c) c^2 - \sqrt{\{(m_n + c_3/c)^2 c^4 - (2m_n c_4 + c_1^2 + c_2^2 + c_3^2) c^2\}}$
130	40	0	0	5	$E_{\gamma+}$ (Physically non-real value)
131	41	0	0	5	$E_{\gamma-}$
132	40	31	42	3	$E_{\gamma+} - c_4 = E_{n+}$
133	41	31	43	3	$E_{\gamma-} - c_4 = E_{n-}$
134	42	N47	44	0	$2m_n (E_{\gamma+} - c_4)$
135	44	44	46	25	Branch
136	46	90	46	26	Mix
137	46	0	44	6	$P_{n+}$
138	43	N47	45	0	$2m_n (E_{\gamma-} - c_4)$
139	45	45	47	25	Branch

140	47	90	47	26	Mix
141	47	0	45	6	$P_{n-}$
142	42	0	0	5	Punches } $E_n$ 's (Physically non-real)
143	43	0	0	5	
144	44	0	0	5	Punches } $P_n$ 's (Physically non-real)
145	45	0	0	5	
146	30	45	46	1	$\sin \alpha_n$
147	29	45	47	1	$\cos \alpha_n \sin \beta_n$
148	46	0	48	23	$\alpha_n$ ( $\alpha$ always $< 90^\circ$ ).
149	48	0	49	12	$\cos \alpha_n$ .
150	47	49	50	1	$\sin \beta_n$ .
151	50	0	51	23	$\beta_n$ ( $\beta < 90^\circ$ ). Can tell by inspection of events whether $\beta >$ or $< 90^\circ$ .
152	48	N8	48	0	
153	51	N8	51	0	
154	48	0	0	5	Punches $\alpha_n$ 's.
155	51	0	0	5	Punches $\beta_n$ 's.
156	0	3	63	16	
157	0	0	0	31	End of programme. Clears 0 to 127, and constants N32 to N127, resets constants N0 to N31.

Appendix 2.

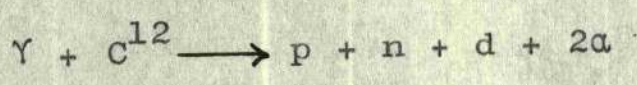
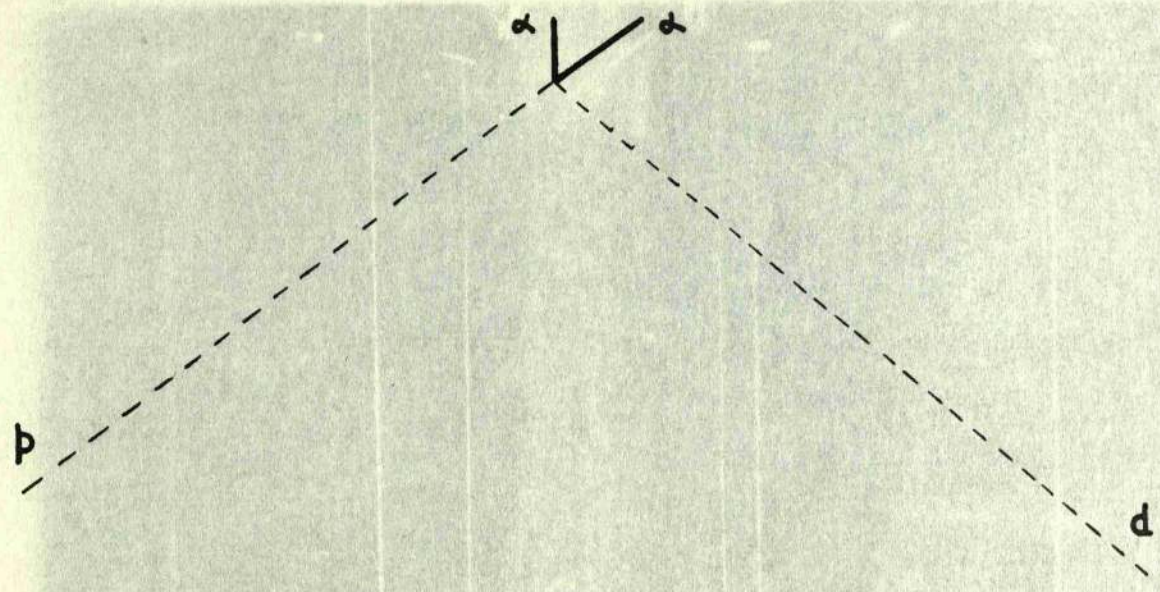
Cloud Chamber Photographs.

In this appendix are shown some examples of the cloud chamber photographs obtained in the experiments previously described.

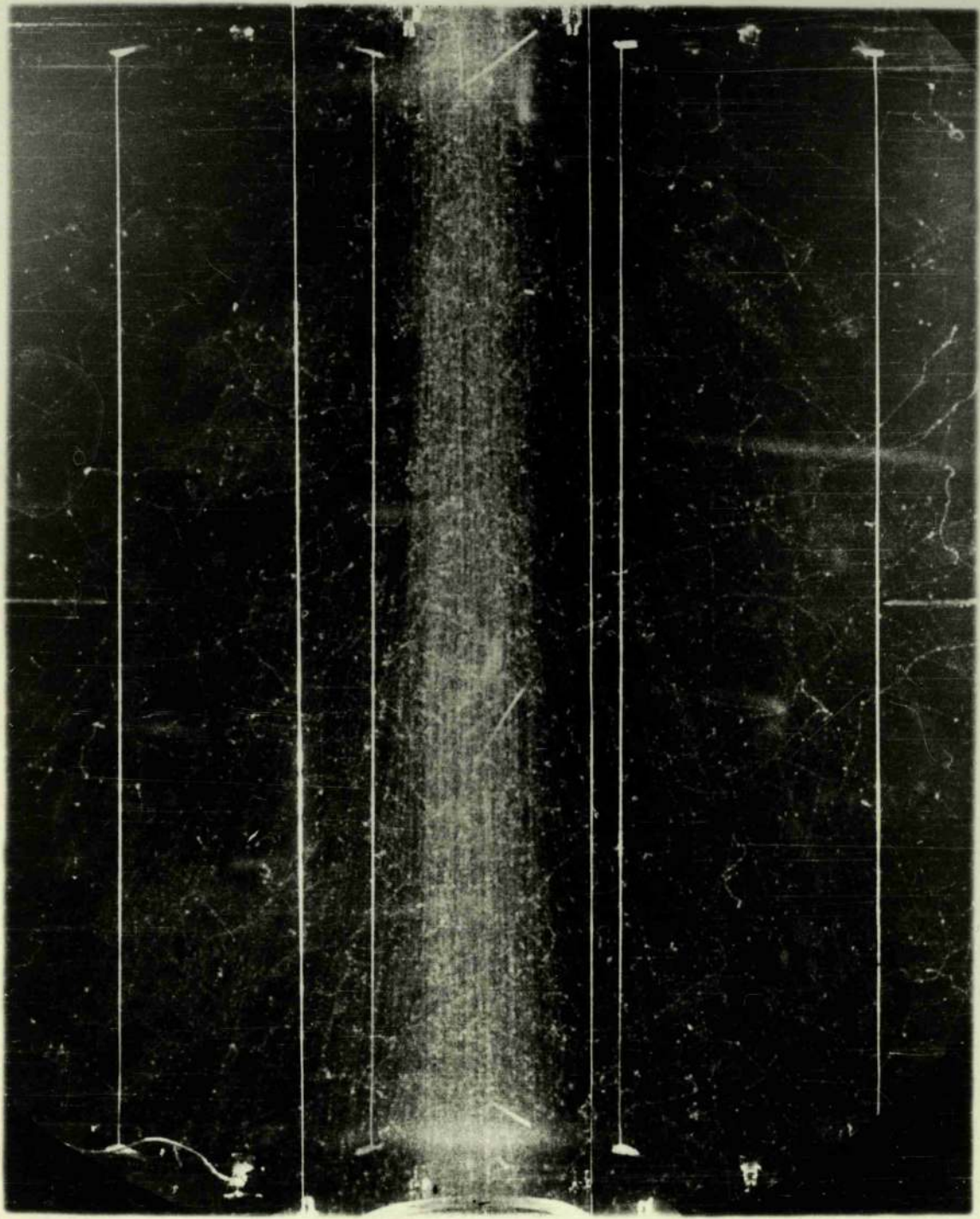
The first few photographs show that it is possible to see both the fast triggering proton and the short heavy recoiling nuclear fragments in the background of electrons produced by the gamma-ray beam. The photographs shown give a much inferior reproduction of the events than does the negative which is used for track measurement. It is much easier to pick out the dense black of a track in a negative than to distinguish the pure white in a print. In addition the range of tones available on printing paper is relatively limited.

The last few photographs show examples of 100 MeV protons scattering in the carbon analyser in the cloud chamber. In this case the lamp delay used was much longer and "fully grown" electron tracks can also be seen.

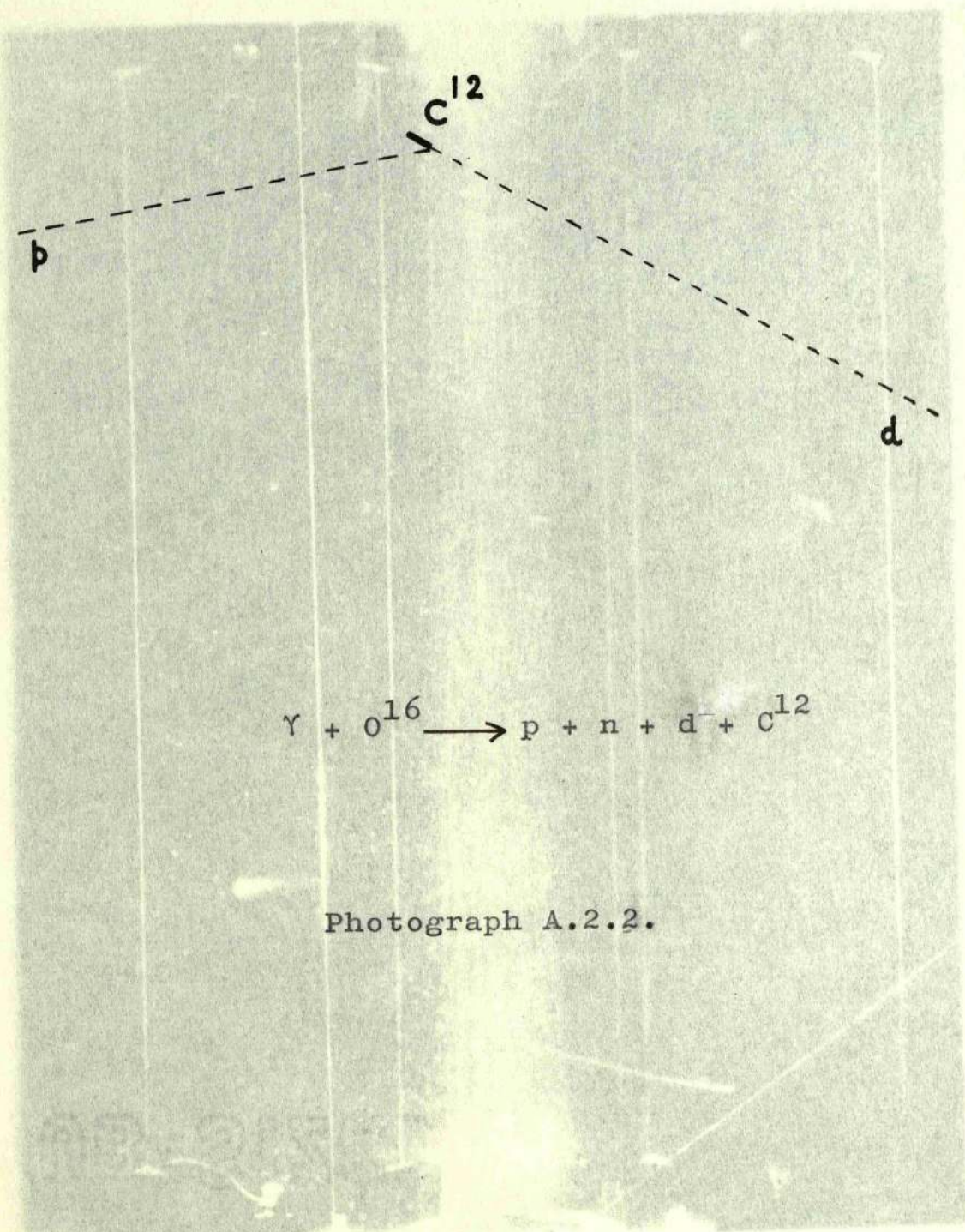
↓ BEAM DIRECTION



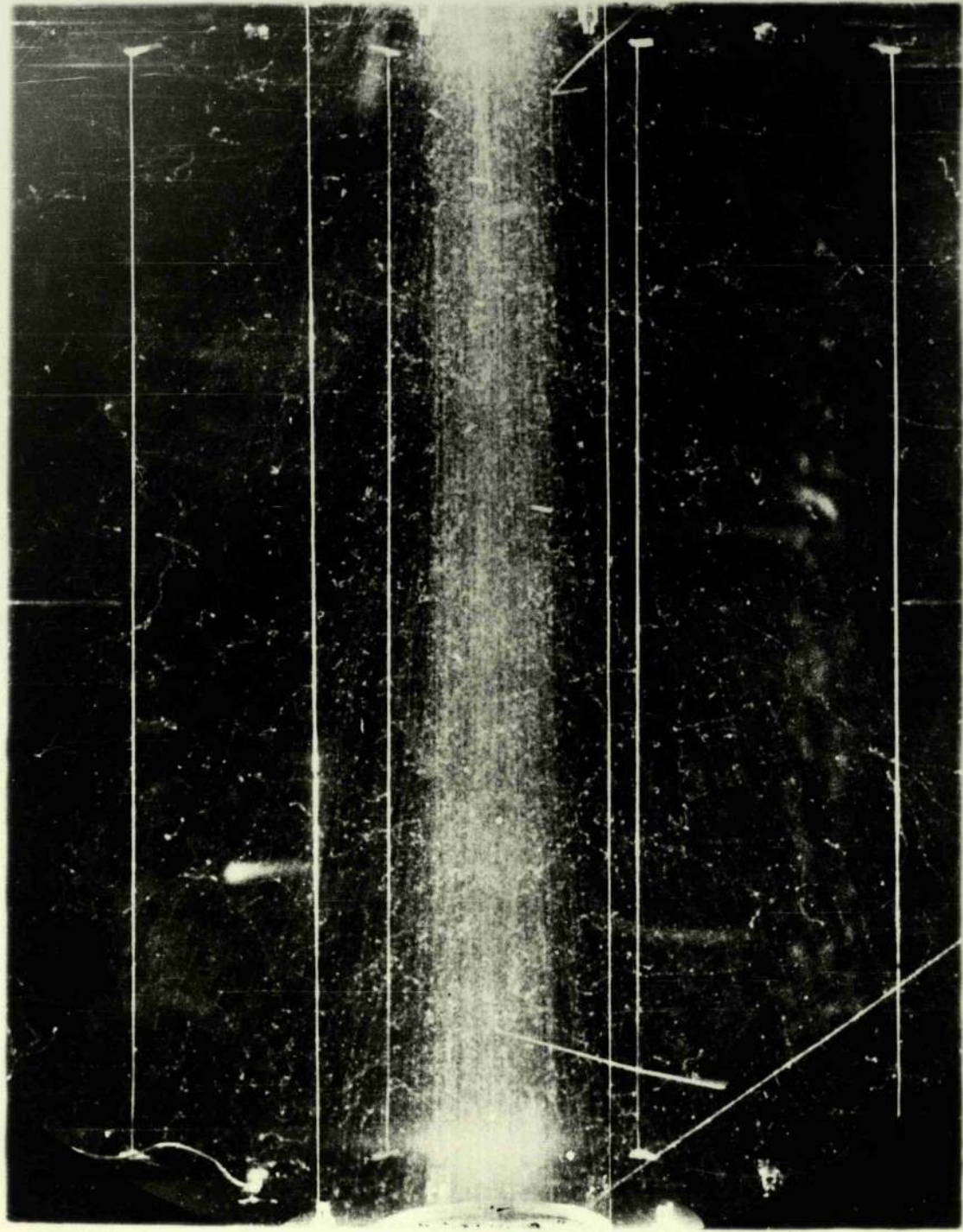
Photograph A.2.1.



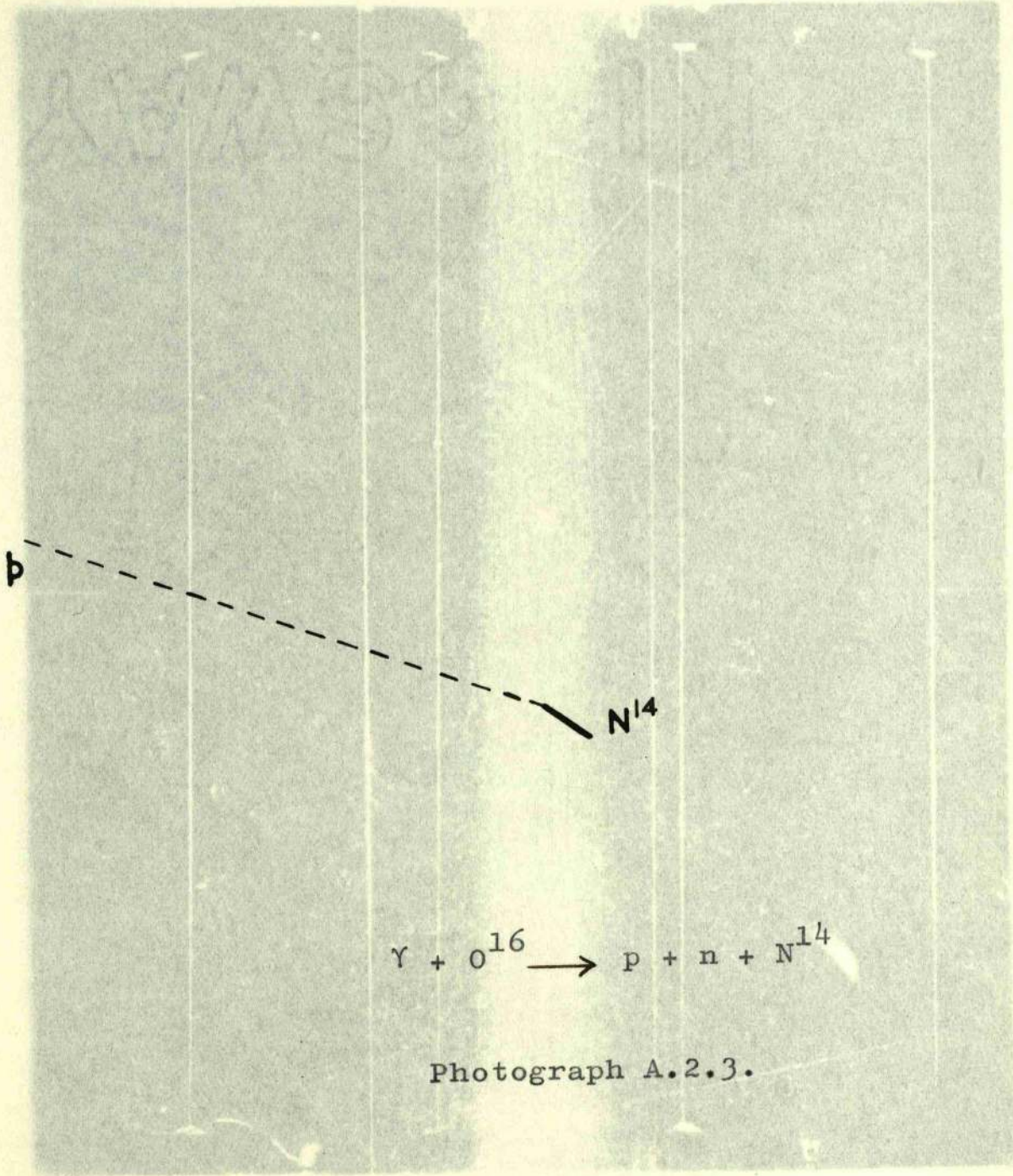
BEAM  
DIRECTION  
↓



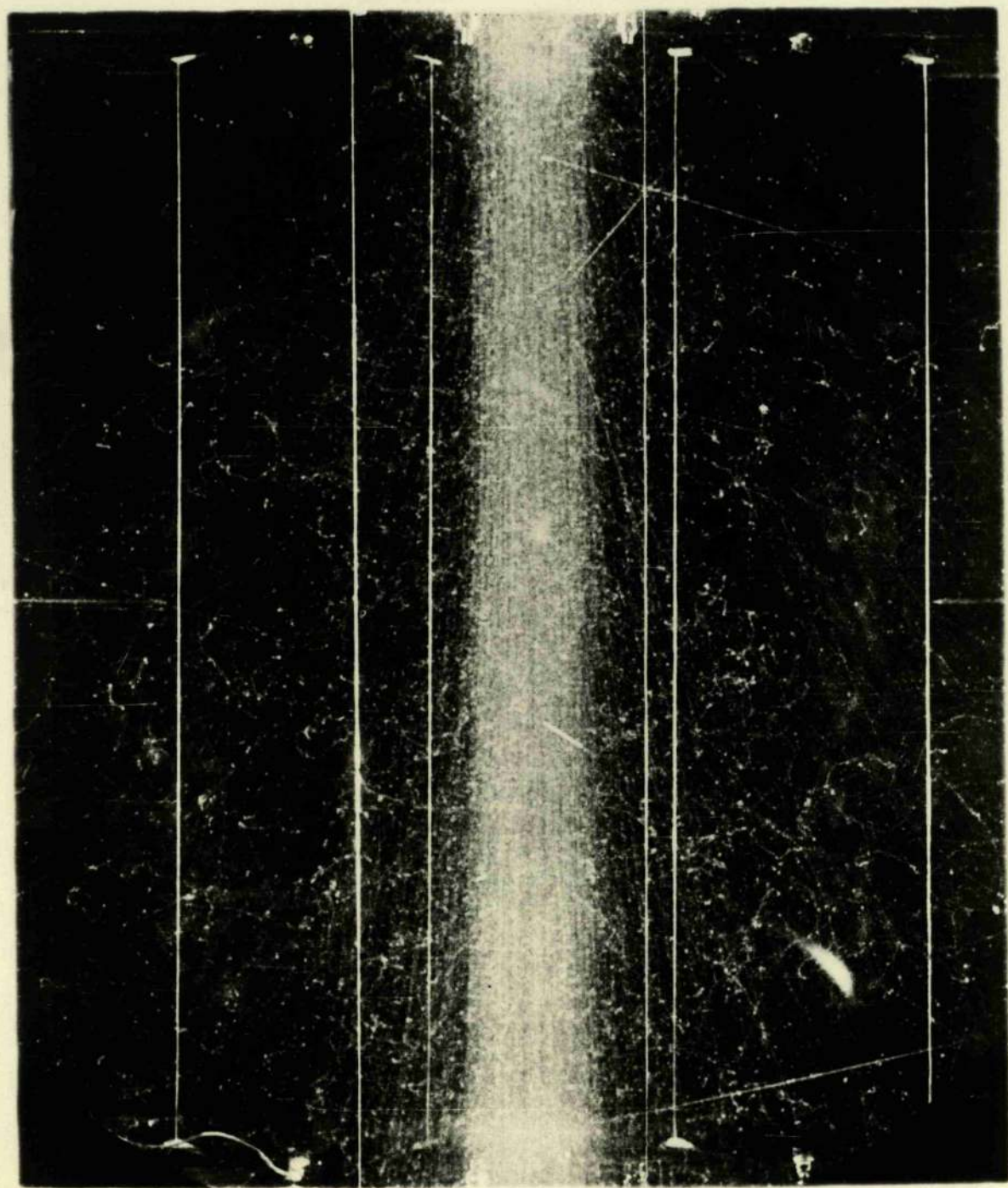
Photograph A.2.2.



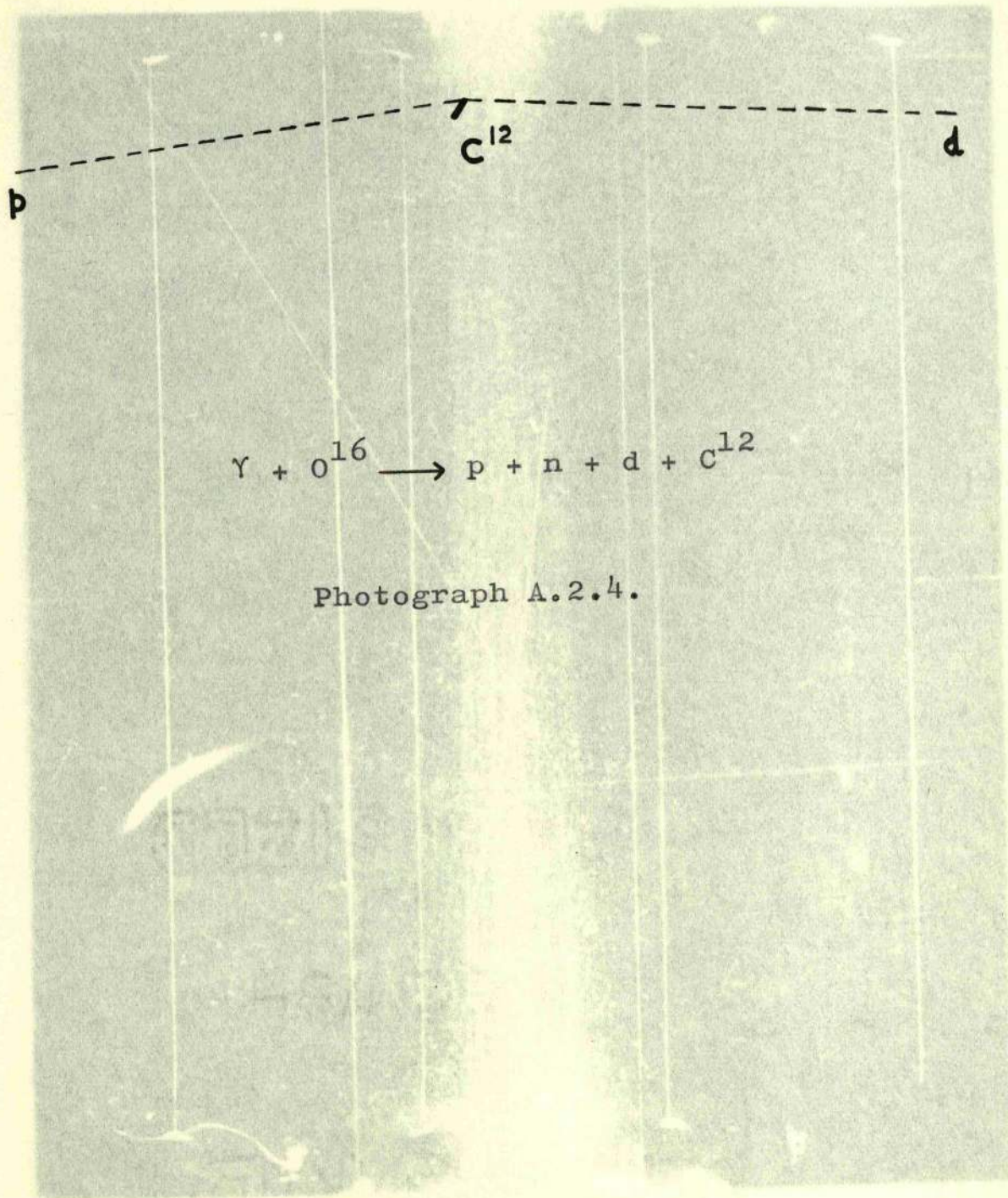
BEAM  
DIRECTION  
↓

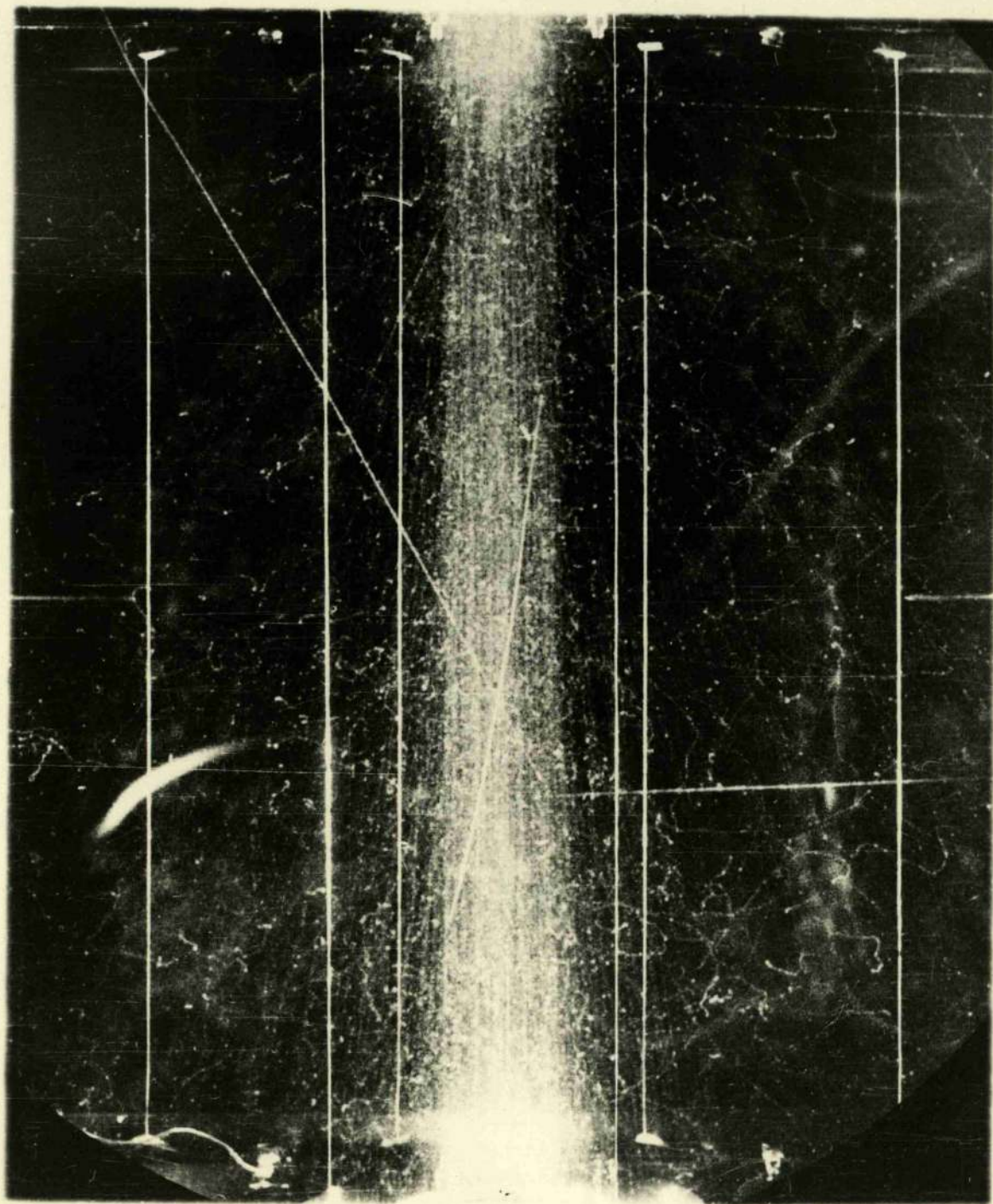


Photograph A.2.3.

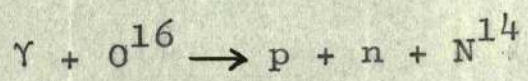
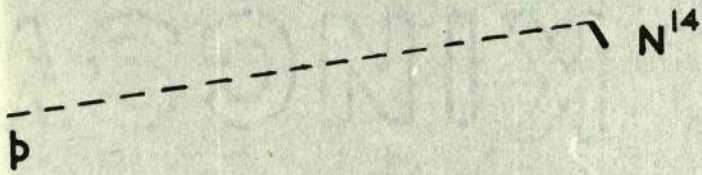


BEAM  
DIRECTION  
↓

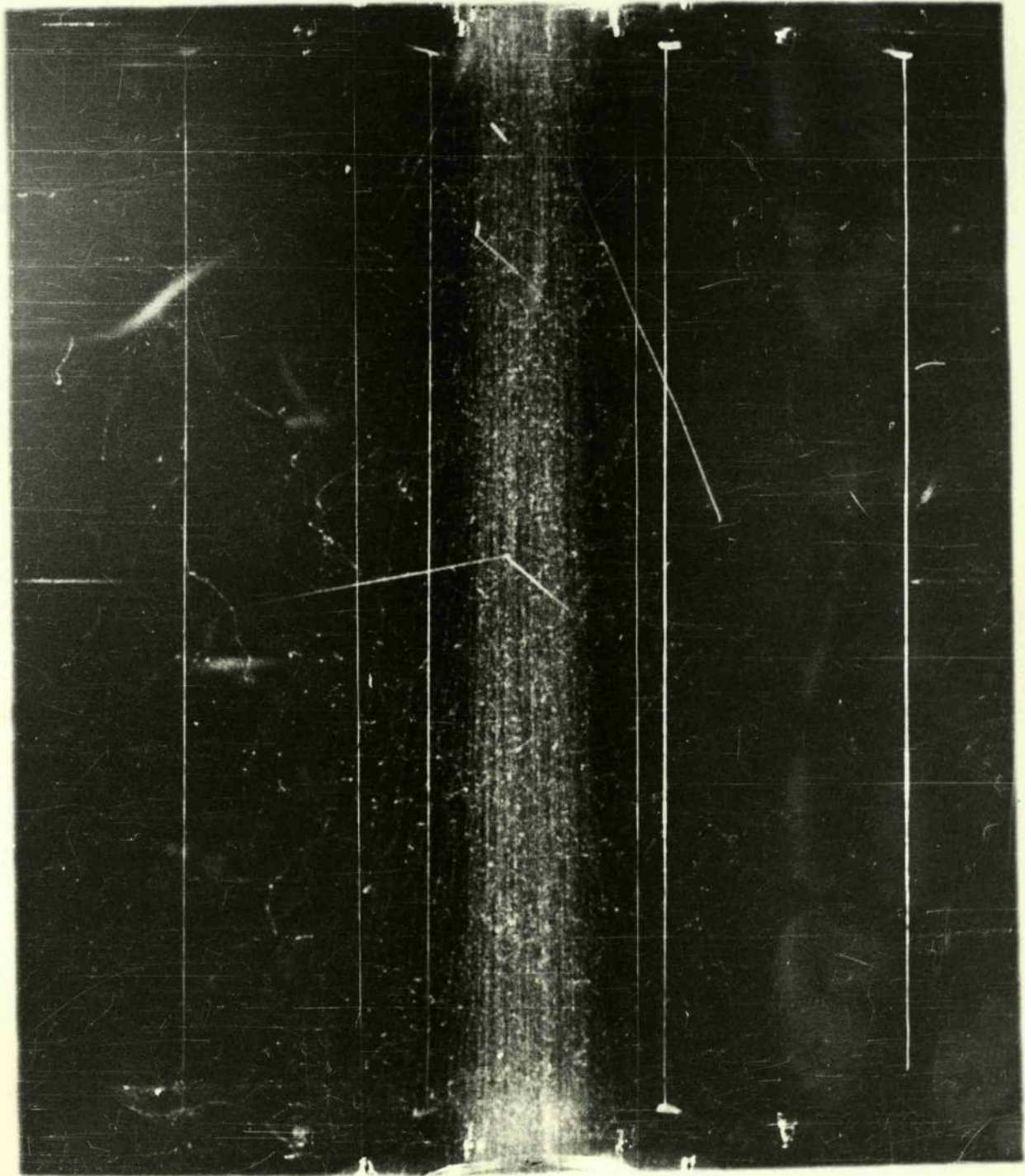




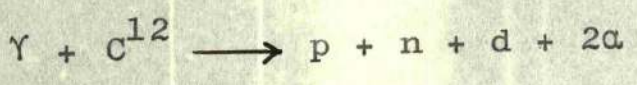
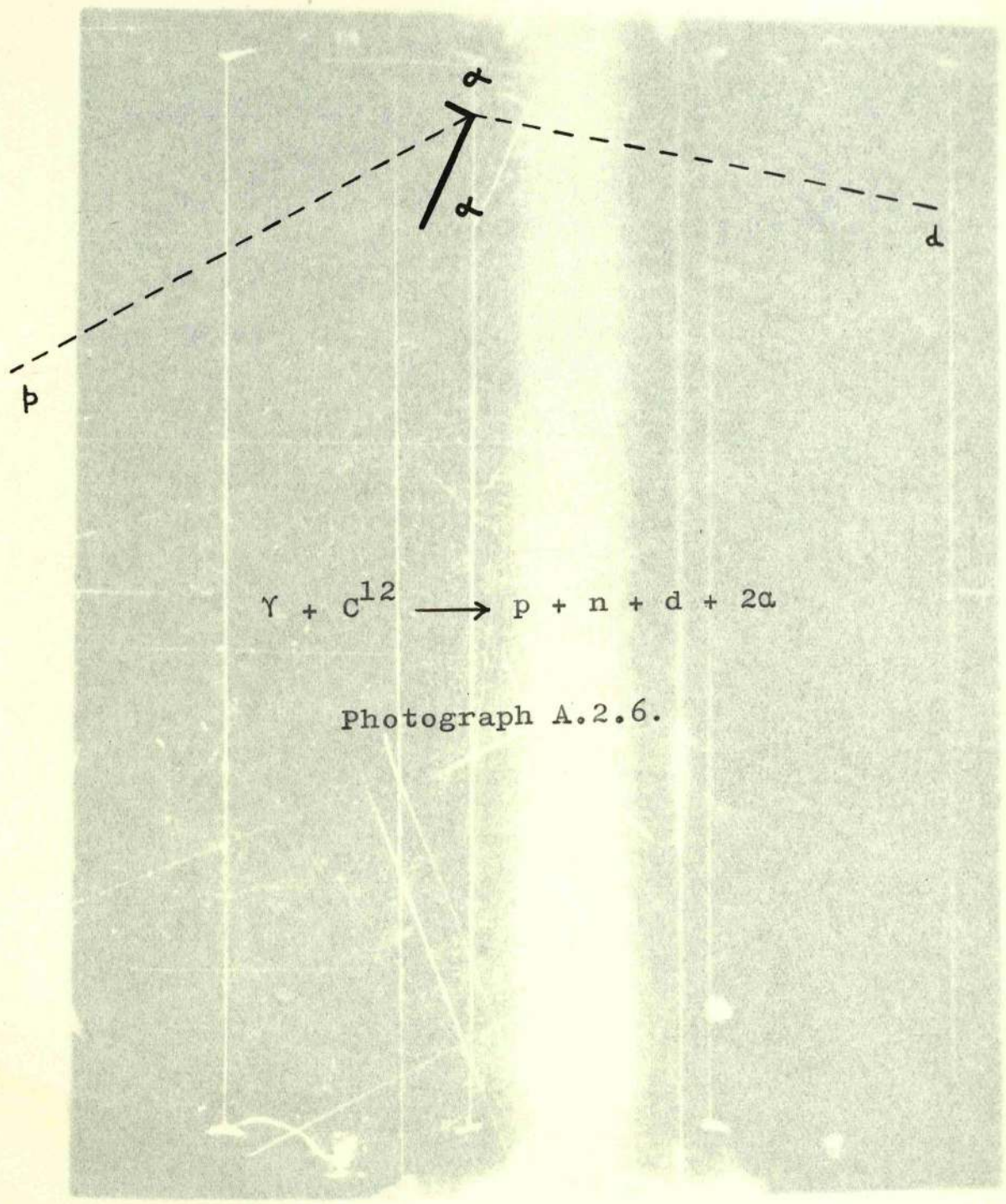
BEAM  
DIRECTION



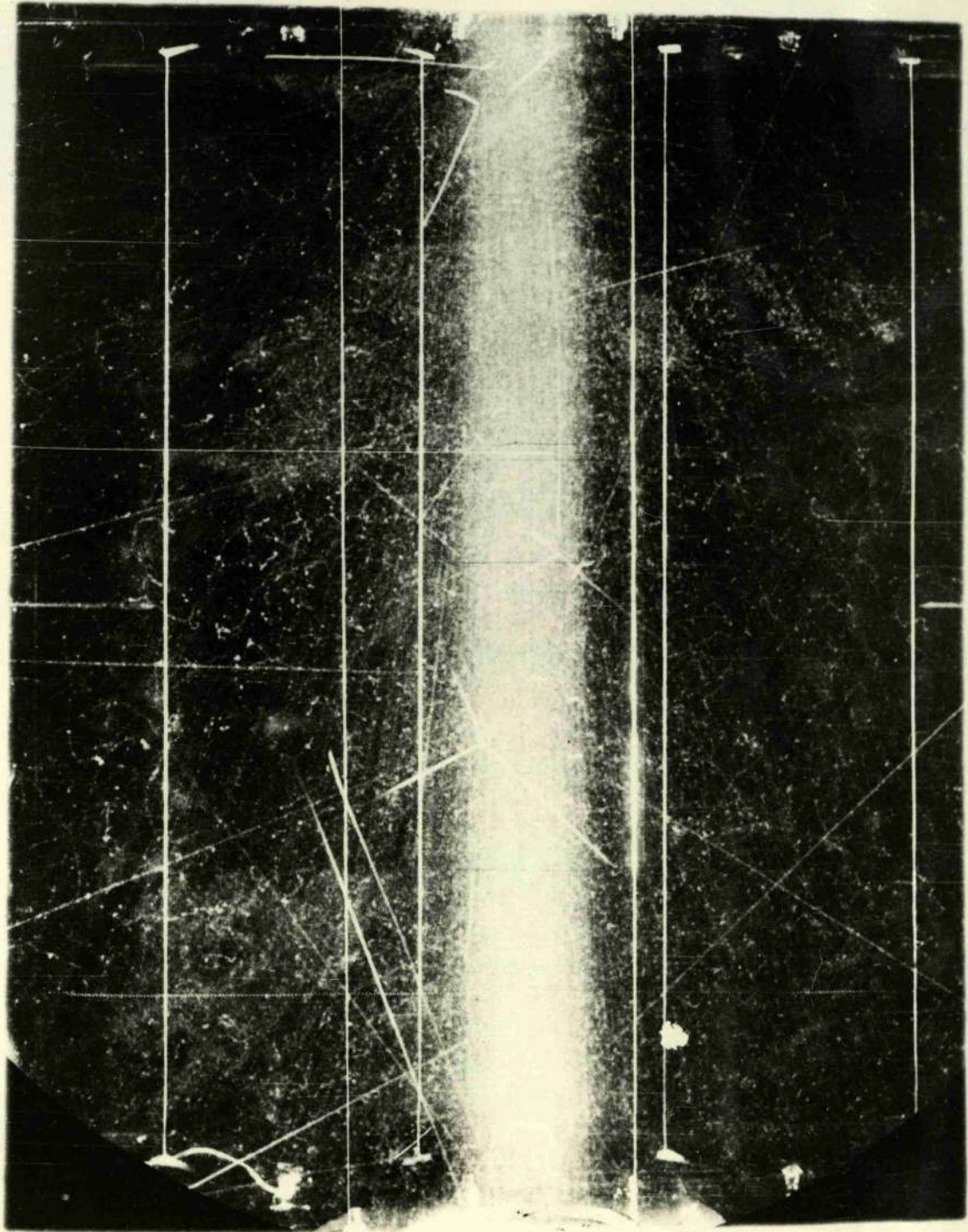
Photograph A.2.5.



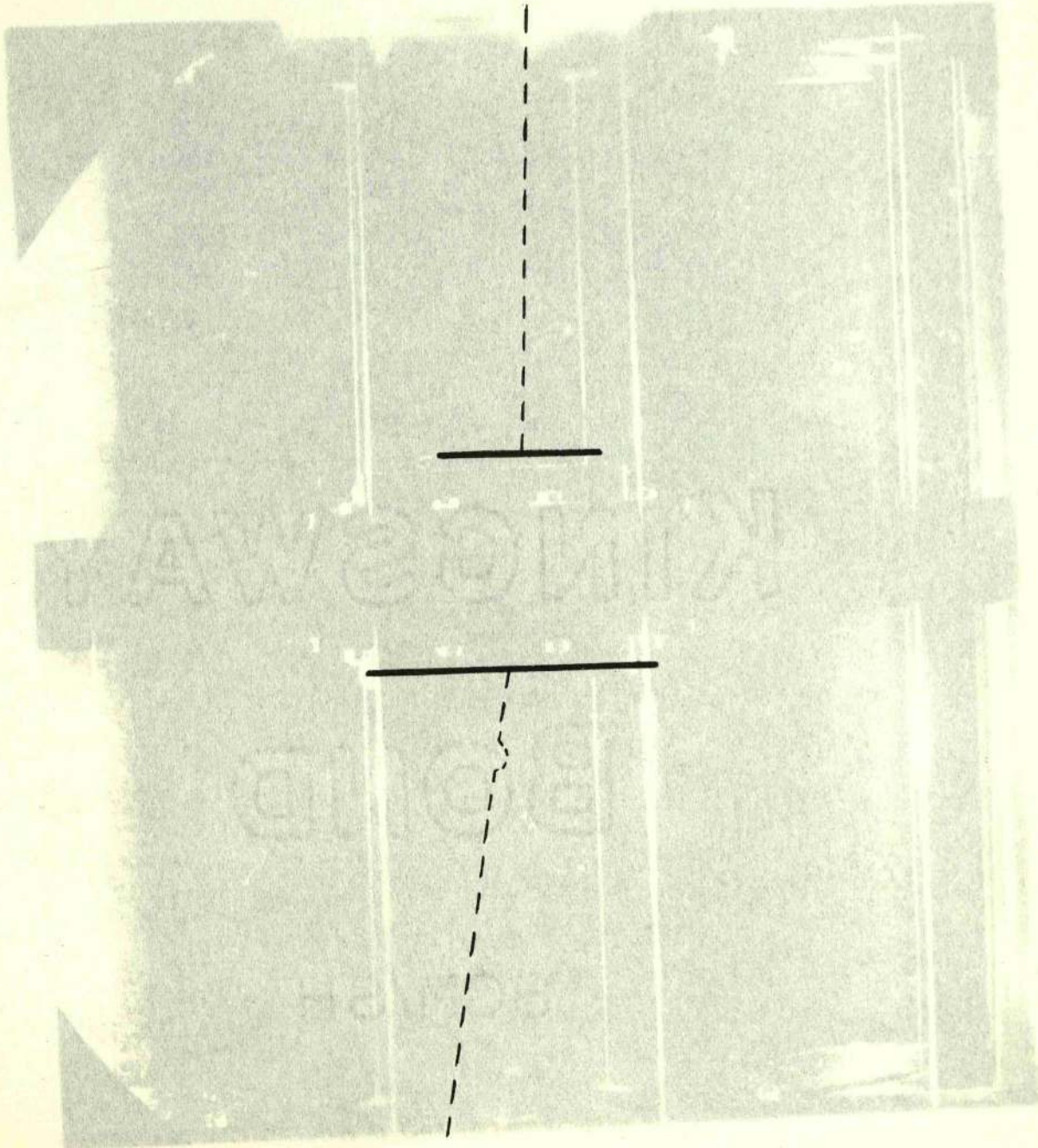
BEAM  
DIRECTION



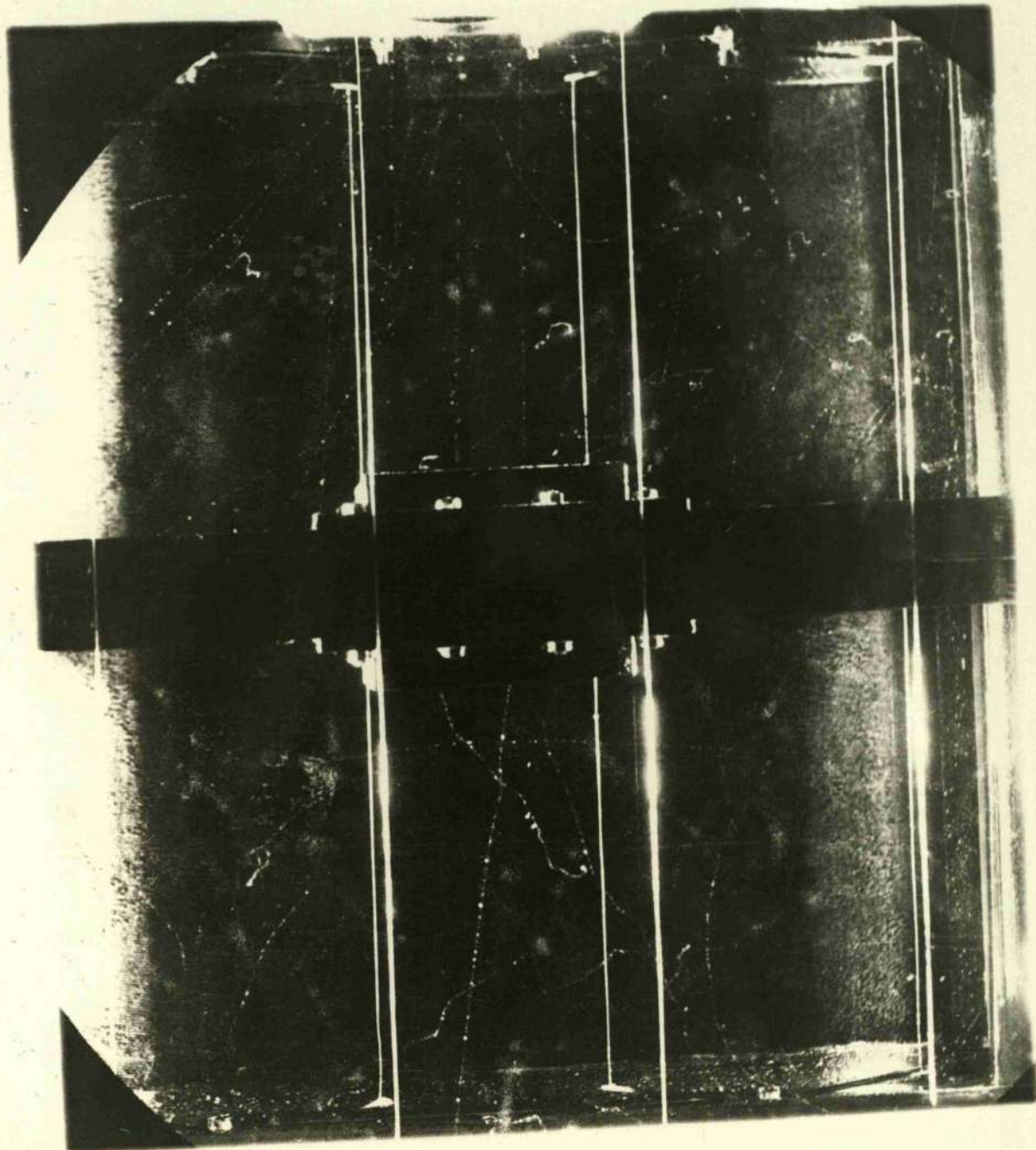
Photograph A.2.6.



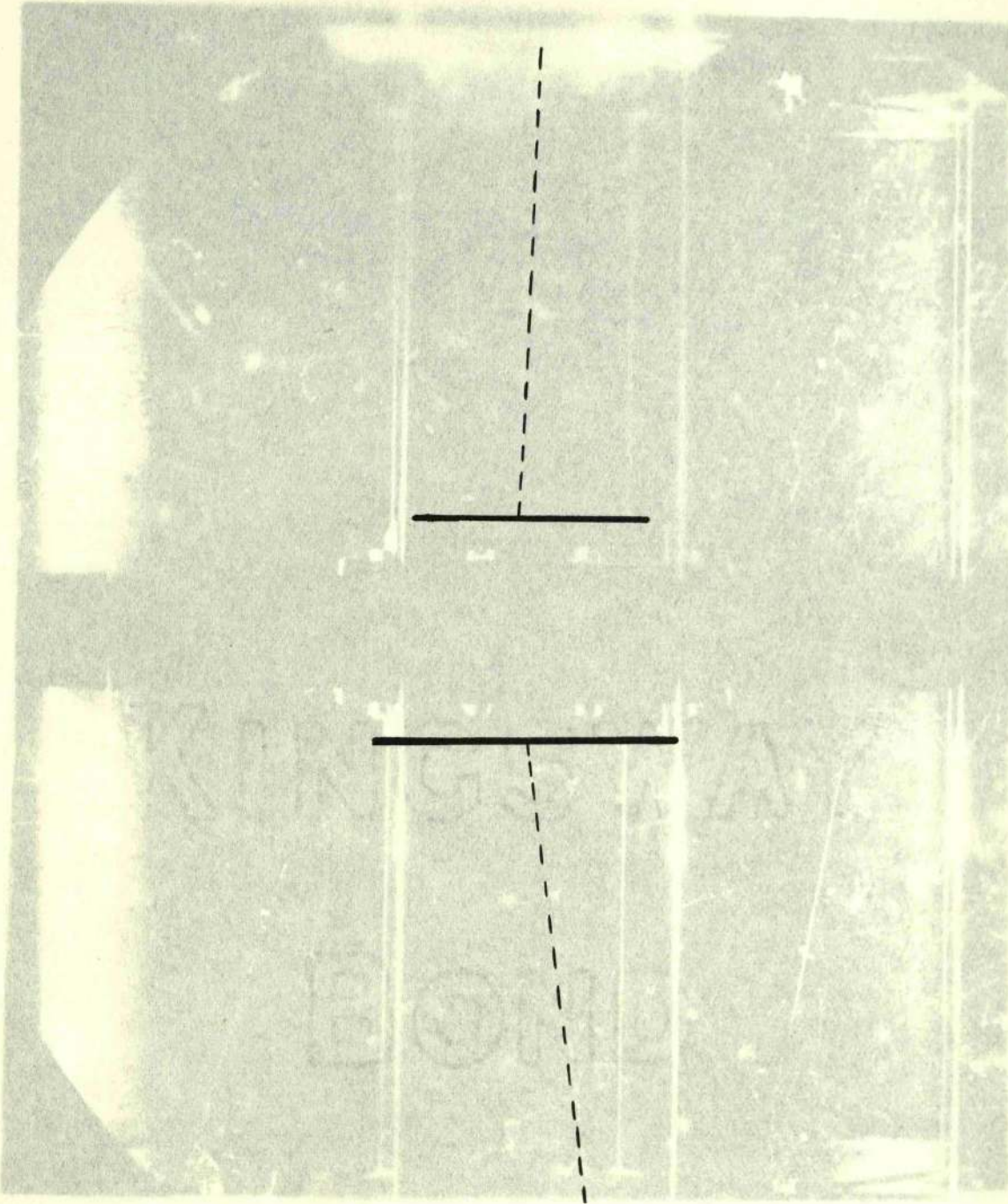
PROTON  
DIRECTION



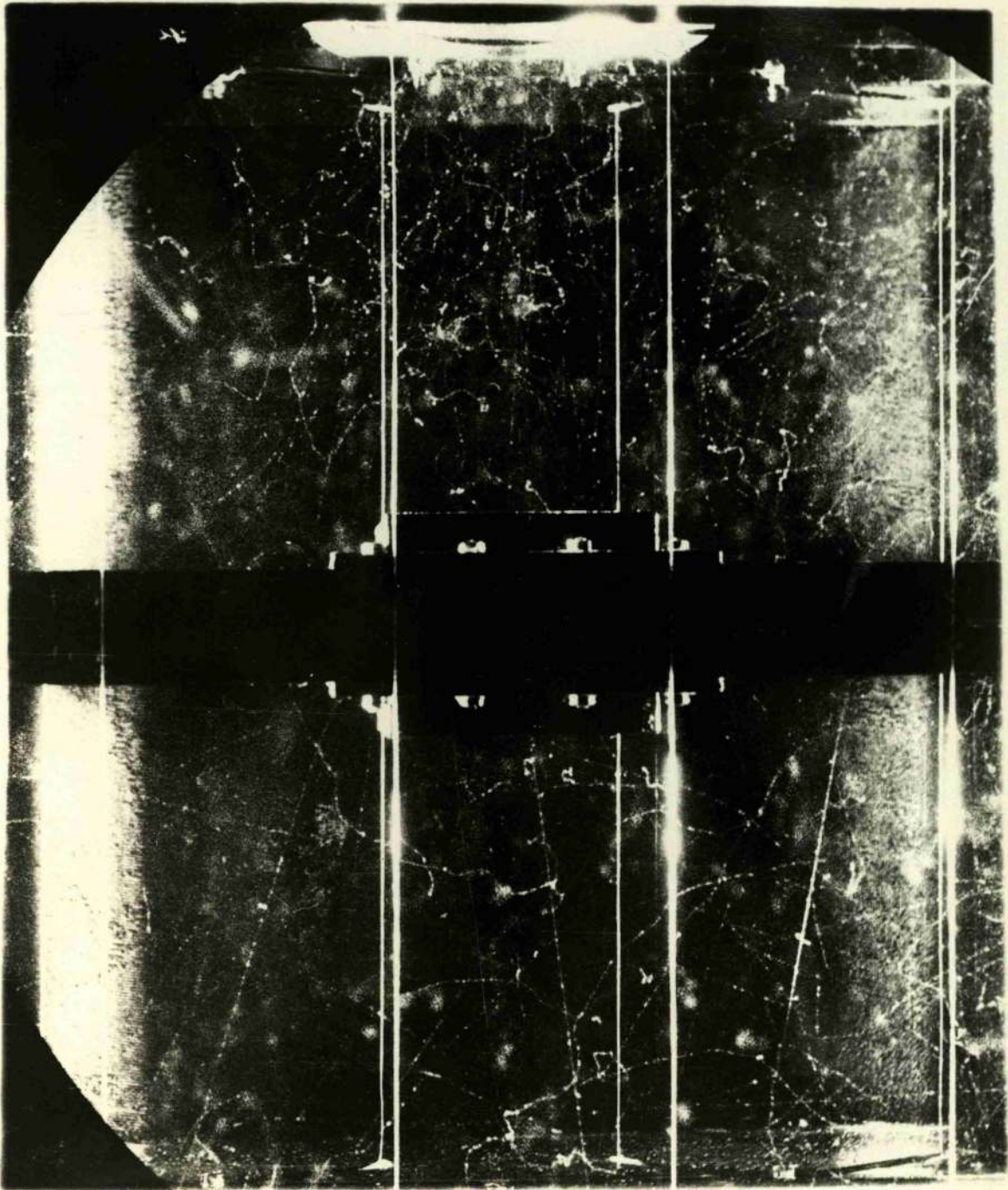
Photograph A.2.7.



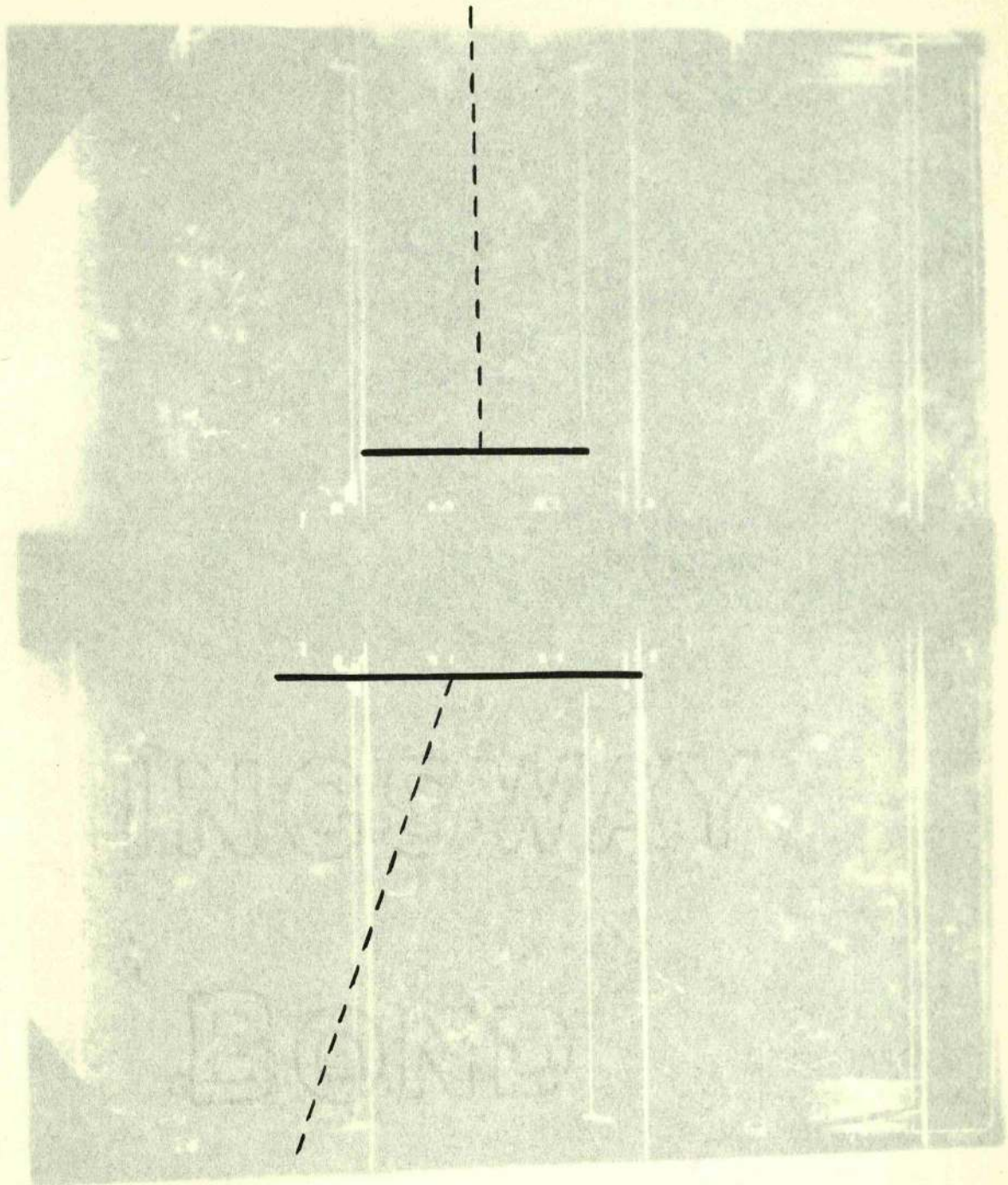
PROTON  
DIRECTION



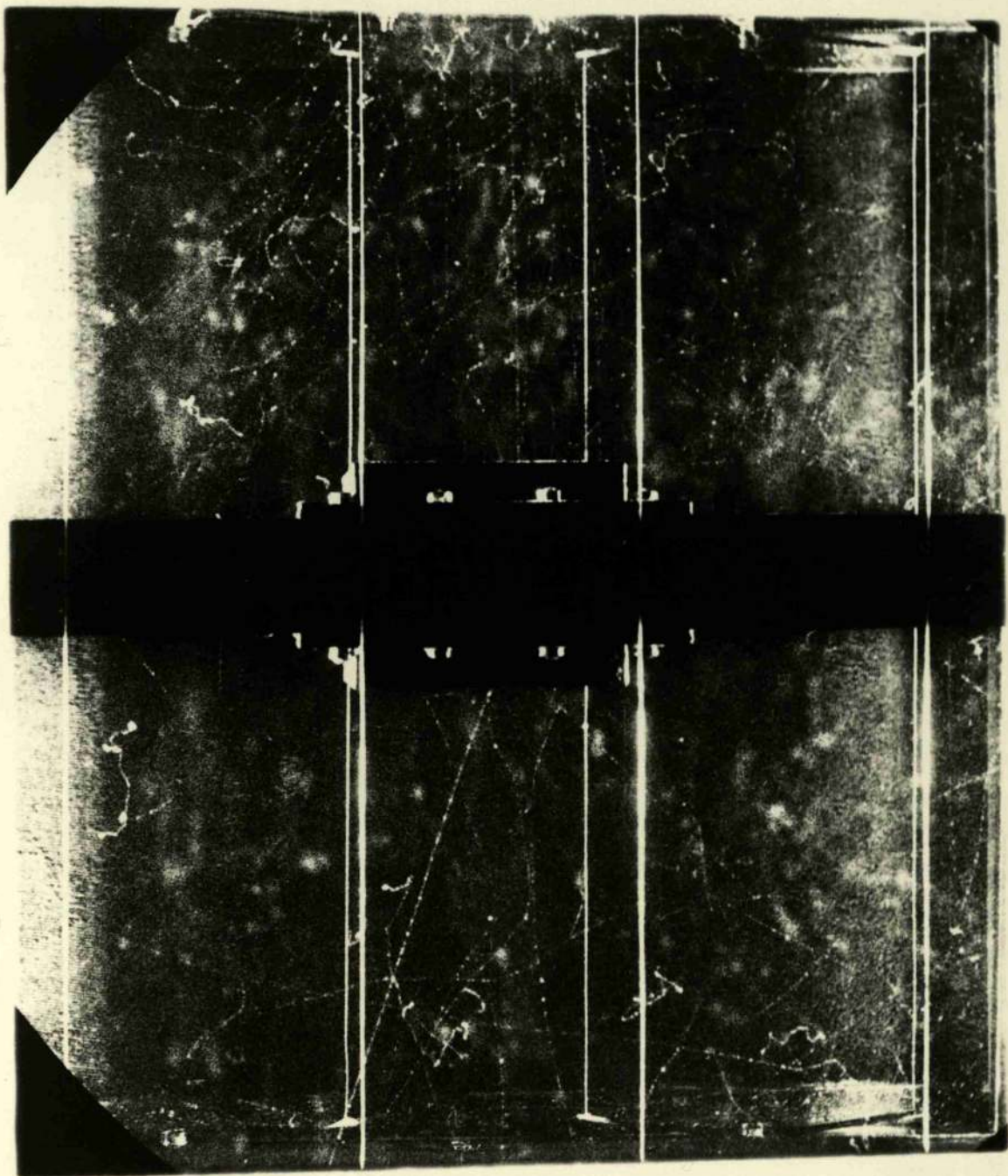
Photograph A.2.8.



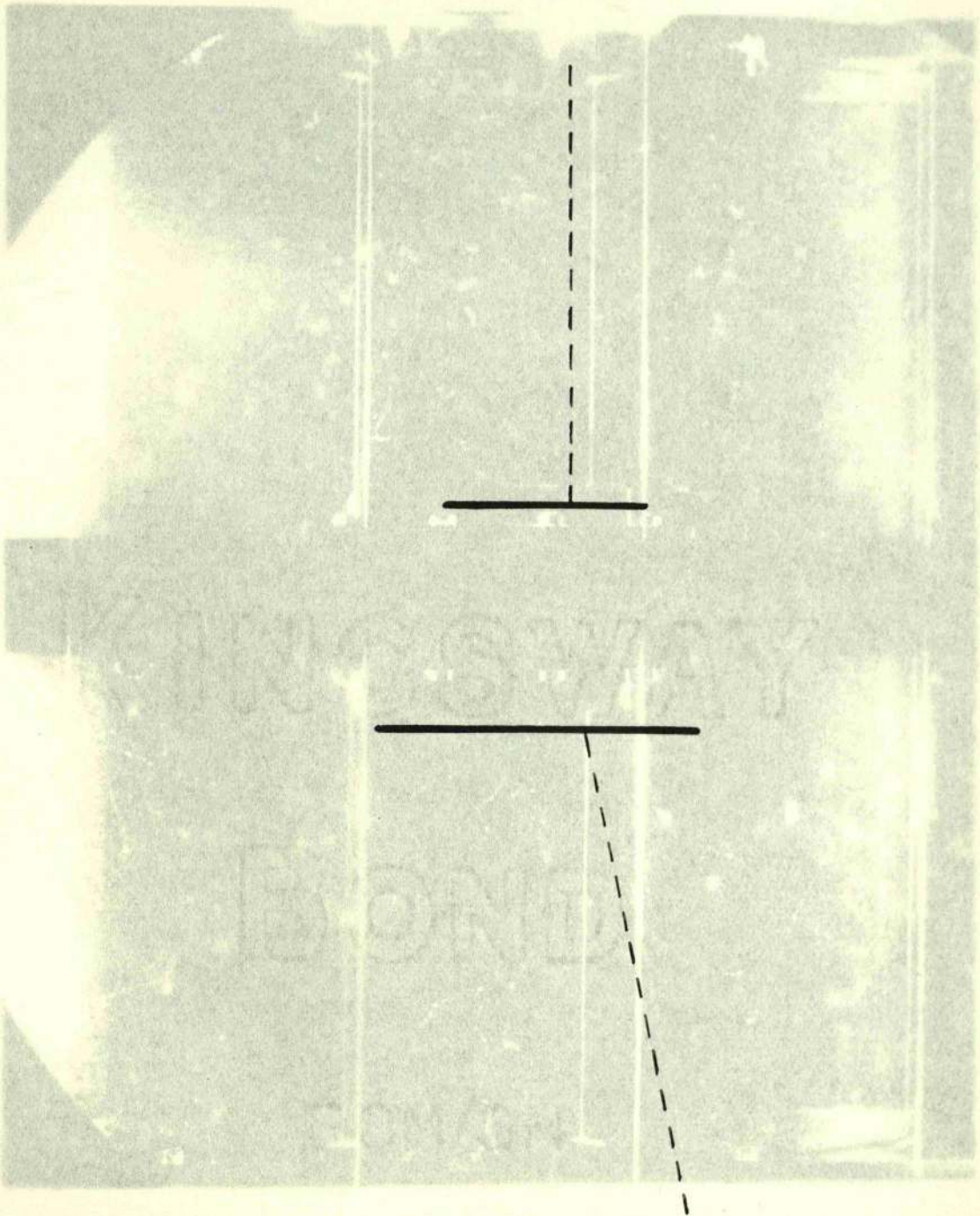
PROTON  
DIRECTION



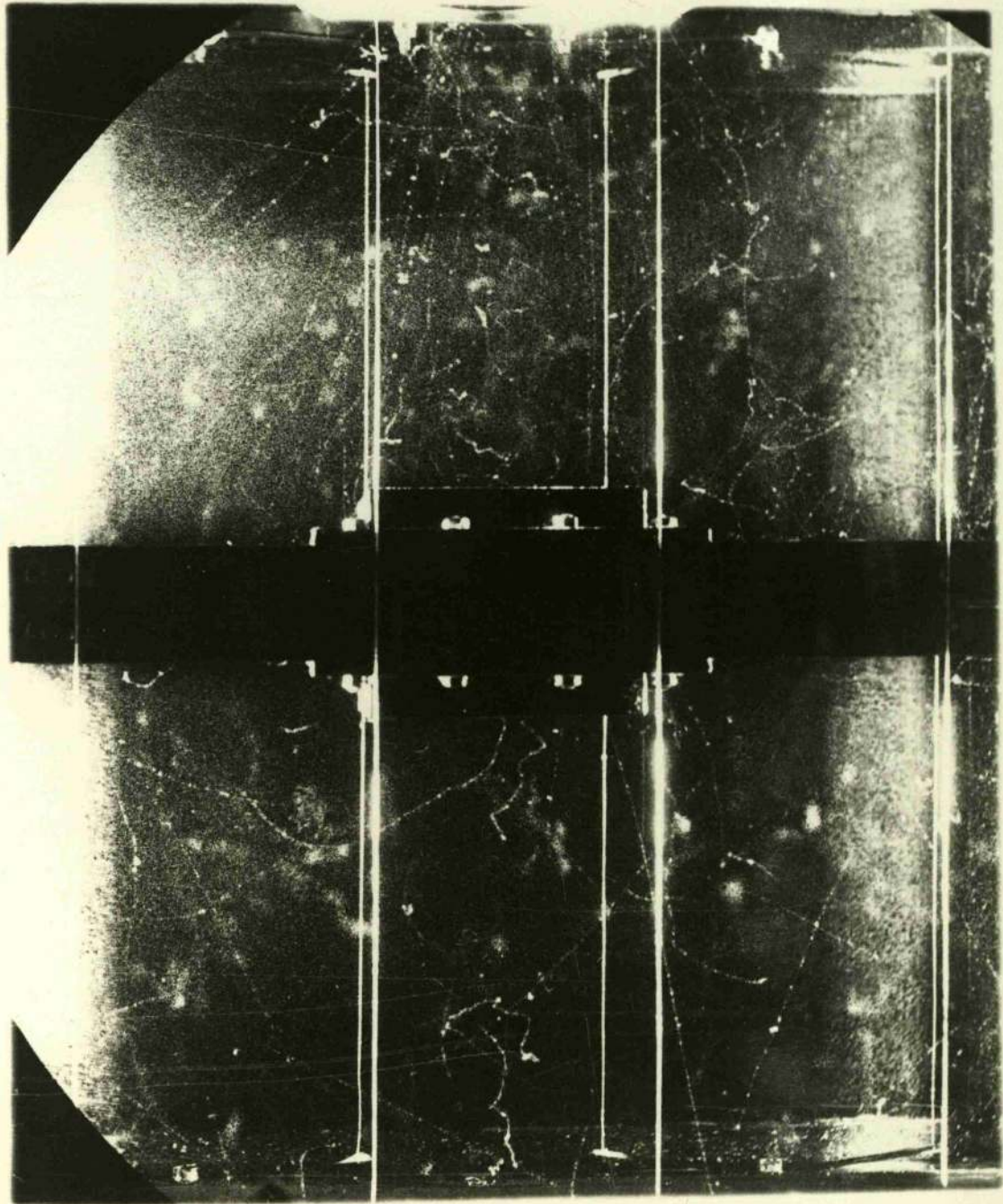
Photograph A.2.9.



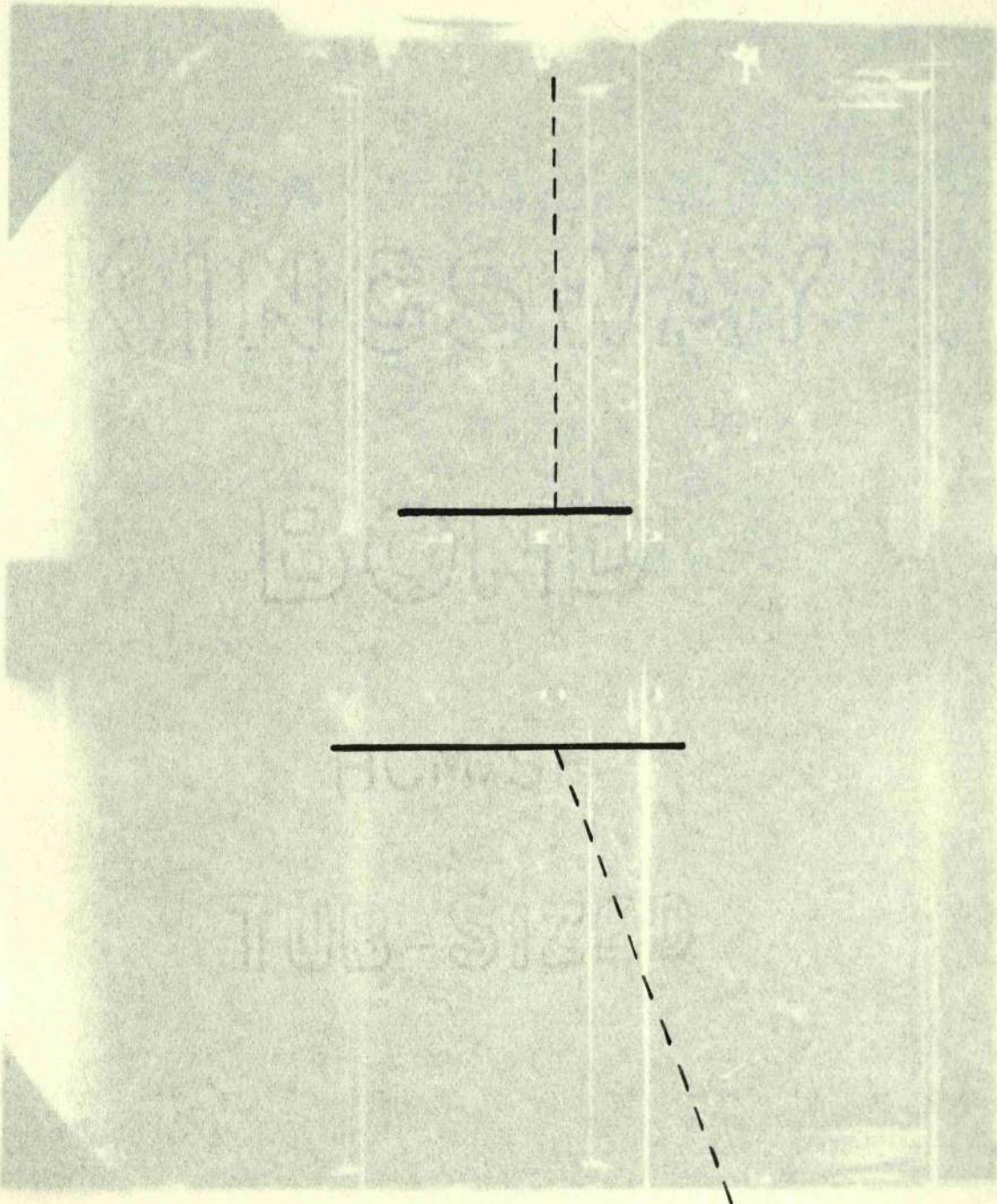
PROTON  
DIRECTION  
↓



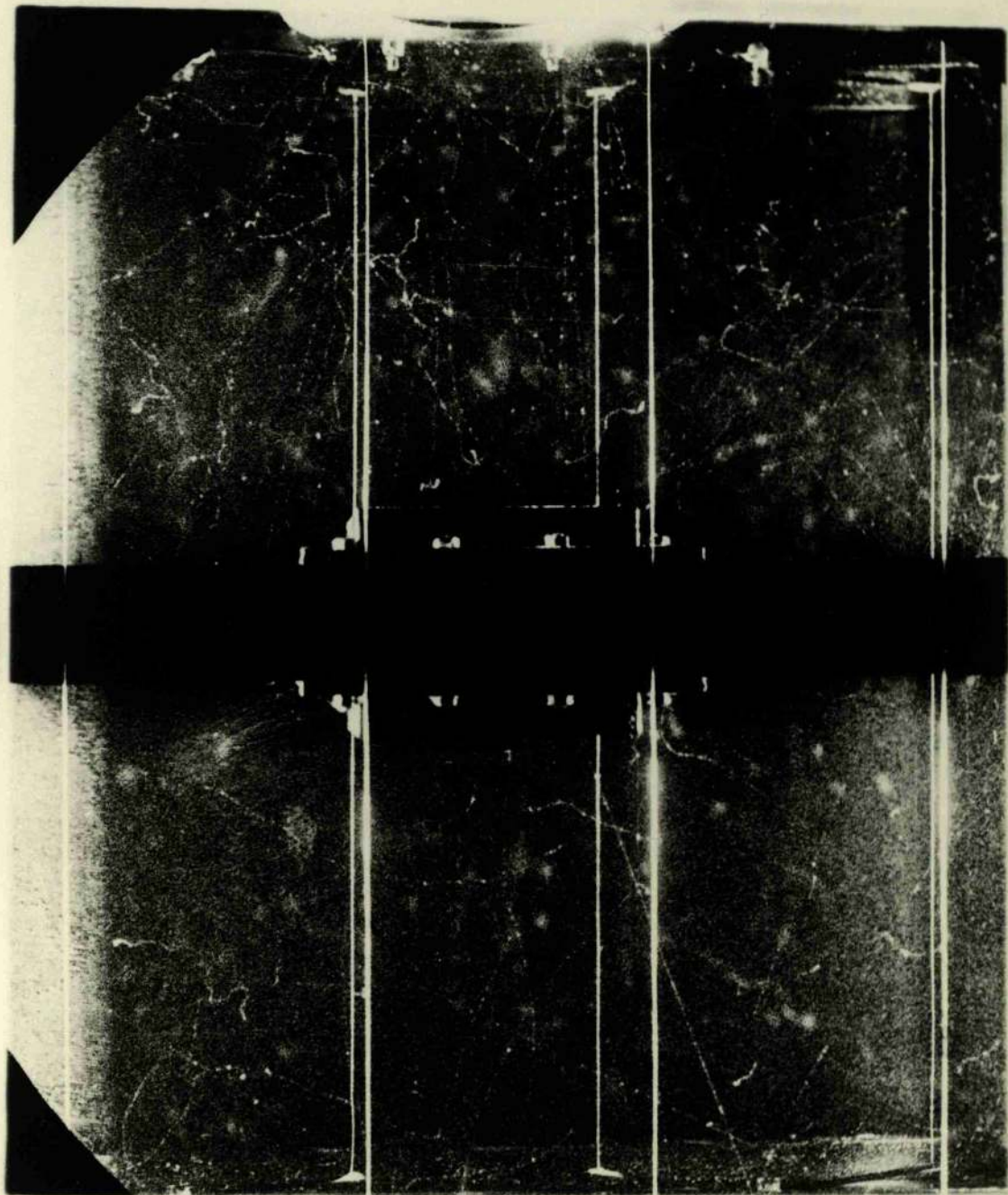
Photograph A.2.10.



PROTON  
DIRECTION



Photograph A.2.11.



- (1) Chadwick, J. *Ann. Entomol. Soc. Am.* 1934, 27, 1034.
- (2) Sailer, L. *Ann. Entomol. Soc. Am.* 1934, 27, 1034.
- (3) ... .. *Ann. Entomol. Soc. Am.* 1934, 27, 1034.

References.

- (1) ... .. *Ann. Entomol. Soc. Am.* 1934, 27, 1034.
- (2) ... .. *Ann. Entomol. Soc. Am.* 1934, 27, 1034.
- (3) ... .. *Ann. Entomol. Soc. Am.* 1934, 27, 1034.
- (4) ... .. *Ann. Entomol. Soc. Am.* 1934, 27, 1034.
- (5) ... .. *Ann. Entomol. Soc. Am.* 1934, 27, 1034.
- (6) ... .. *Ann. Entomol. Soc. Am.* 1934, 27, 1034.
- (7) ... .. *Ann. Entomol. Soc. Am.* 1934, 27, 1034.
- (8) ... .. *Ann. Entomol. Soc. Am.* 1934, 27, 1034.
- (9) ... .. *Ann. Entomol. Soc. Am.* 1934, 27, 1034.
- (10) ... .. *Ann. Entomol. Soc. Am.* 1934, 27, 1034.

- (1) Chadwick, J. and Goldhaber, M. : Nature 134, 237, 1934.
- (2) Szilard, L. and Chalmers, T.A. : Nature 134, 494, 1934.
- (3) Bothe, Wand Gentner, W. : Zeit. f. Physik 106, 236, 1937.
- (4) Kerst, D.W. : P.R. 60, 47, 1941.
- (5) Huber, O, Leinhard, O, Scherrer, P., and Waffler, H. : Helv. Phys. Acta 17, 139, 1944.
- (6) Baldwin, G.C. and Klaiber, G.S. : P.R. 70, 289, 1946.
- (7) Baldwin, G.C. and Klaiber, G.S. : P.R. 73, 1156, 1948.
- (8) Weinstock, E. and Halpern, J. : P.R. 94, 1651, 1954.
- (9) Okamoto, K. : Prog. Theor. Phys. 15, 75, 1956.
- (10) Okamoto, K. : P.R. 110, 143, 1958.
- (11) Ferrero, F., Malvano, R, and Tribuno, C. : N.C. 6, 385, 1957.
- (12) Carver, I.H. and Turchinetz, W. : Proc. Phys. Soc. 73, 69, 1959.
- (13) Toms, M.E. and Stephens, W.E. : P.R. 92, 362, 1953.
- (14) Reid, J.M., Swinbank, P. and Atkinson, J.R. : Physica 22, 1142A, 1956.
- (15) Montalbetti, R., Katz, L. and Goldemberg, J. : P.R. 91, 659, 1953.
- (16) Waffler, H. and Younis, S. : Helv. Phys. Acta 22, 614, 1949.
- (17) Stephens, W.E., Mann, A.K., Patton, B.J. and Winhold, E.J. : P.R. 98, 839, 1955.

- (18) Spicer, B.M. : P.R. 99, 33, 1955.
- (19) Johansson, S.A.E. and Forkman, B. : P.R. 99, 1031, 1955.
- (20) Stephens, W.E. : Physica 22, 1143, 1956.
- (21) Johansson, S.A.E. : Physica 22, 1144, 1956.
- (22) Livesey, D.L. : Can. Journ. Phys. 34, 1022, 1956.
- (23) Cohen, L, Mann, A.K., Patton, B.J., Reibel, K, Stephens, W.E., Winhold, E.J. : P.R. 104, 108, 1956.
- (24) Brix, P. and Maschke, E.K.: Z. Naturforsch 12a, 1013, 1957.
- (25) Johansson, S.A.E. and Forkman, B. : Arkiv Fur Physik 12, 359, 1957.
- (26) Milone, C, Ricamo, R. and Rinzivillo, R. : N.C. V, 532, 1957.
- (27) Milone, C. and Ricamo, R. : N.C. V, 1338, 1957.
- (28) Milone, C. Milone-Tamburino, S., Rinzivillo, R., Rubbino, A. and Tribuno, C.: N.C. 7, 729, 1958.
- (29) Brix, P. and Maschke, E.K.: Z. Phys. 155, 109, 1959.
- (30) Horsley, R.J., Haslam, R.N.H. and Johns, H.E. : Can. Journ. Phys. 30, 159, 1952
- (31) Montalbetti, R., Katz, L. and Goldemberg, J. : P.R. 91, 659, 1953.
- (32) Haslam, R.N.H., Horsley, R.J., Johns, H.E. and Robinson, L.B. : Can. Journ. Phys. 31, 636, 1953
- (33) Montalbetti, R. and Katz, L: Can. Journ. Phys. 31, 798, 1953
- (34) Katz, L, Haslam, R.N.H., Horsley, R.J, Cameron, A.G.W. and Montalbetti, R.: P.R. 95, 464, 1954.

- (35) Spicer, B.M. and Penfold, A.S. : P.R. 100, 5, 1377, 1955.
- (36) Spicer, B.M. : Austr. Journ. Phys. 10, 326, 1957.
- (37) Siddiq, A.K.M. and Haslam, R.N.H. : Can. Journ. Phys. 36, 963, 1958.
- (38) McElhinney, J., Bendel, W.L., Tobin, R.A. : P.R. 111, 1297, 1958.
- (39) Penfold, A.S. and Garwin, E.L. : P.R. 114, 1324, 1959.
- (40) Sadeh, R. : C.R. Acad. Sci. 249, 2313, 1959.
- (41) Campbell, J.G. : Austr. Journ. Phys. 8, 449, 1955.
- (42) Cohen, S.G., Fisher, P.S. and Warburton, E.K. : P.R. Letters 3, 433, 1959.
- (43) Tanner, N.W., Thomas, G.C. and Meyerhof, W.E. : N.C. XIV, 257, 1959.
- (44) Millar, C.H. and Cameron, A.G.W. : P.R. 78, 76, 1950.
- (45) Millar, C.H. and Cameron, A.G.W. : Can. Journ. Phys. 31, 723, 1953.
- (46) Stoll, P. : Helv. Phys. Acta 27, 395, 1954.
- (47) Goward, F.K. and Wilkins, J.J. : Proc. Phys. Soc. A65, 671, 1952.
- (48) Livesey, D.L. and Smith, C.L. : Proc. Phys. Soc. A65, 758, 1952.
- (49) Hsiao, C.A. and Telegdi, V.L. : P.R. 90, 494, 1953.
- (50) Svantesson, N.L. : N.P. 3, 273, 1957.
- (51) Penfold, A.S. and Garwin, E.L. : P.R. 116, 120, 1959.
- (52) Jones, K.W., Lidofsky, L.J. and Weil, J.L. : P.R. 112, 1252, 1958.
- (53) Elliott, J.P. and Flowers, B.H. : Proc. Roy. Soc. A242, 57, 1957.

- (54) Levinger, J.S. and Bethe, H.A.: P.R. 78, 115, 1950.
- (55) Levinger, J.S. and Bethe, H.A.: P.R. 85, 577, 1952.
- (56) Levinger, J.S. and Kent, D.C. : P.R. 95, 418, 1954.
- (57) Levinger, J.S. : P.R. 97, 122, 1955.
- (58) Goldhaber, M and Teller, E. : P.R. 74, 1046, 1948.
- (59) Steinwedel, H. and Jensen, J.H.D. : Zeits. f. Naturforsch 5a, 413, 1950.
- (60) Danos, M. : Ann. de. Phys. 10, 265, 195<sup>2</sup><sub>k</sub>
- (61) Danos, M. : N.P. 5, 23, 1958.
- (62) Danos, M. and Steinwedel, H. : Zeits.f.Naturforsch 6a, 217, 1951.
- (63) Wilkinson, D.H. : Proc. Glasgow Conf. on Nuc. and Meson Phys. 161, 1954.
- (64) Wilkinson, D.H. : Physica 22, 1039, 1956.
- (65) Courant, E.D. : P.R. 82, 703, 1951.
- (66) Brink, D.M. : N.P. 4, 215, 1957.
- (67) Levinger, J.S. : N.P. 8, 428, 1958.
- (68) Brown, G.E. and Levinger, J.S.: Proc. Phys.Soc.71, 733, 1958
- (69) Sugarman, N. and Peters, R. : P.R. 81, 951, 1951.
- (70) Levinger, J.S. : P.R. 82, 300, 1951.
- (71) Levinger, J.S. : P.R. 84, 43, 1951.
- (72) Gilbert, W. and Rose, J. : P.R. 85, 766, 1952.
- (73) Benedict, T.S. and Woodward, W.M. : P.R. 85, 924, 1952.
- (74) Benedict, T.S. and Woodward, W.M. : P.R. 86, 629, 1952.

- (75) Kikuchi, S. : P.R. 85, 1062, 1952.
- (76) Gilbert, W.S. and Rosengren, J.W. : P.R. 88, 901, 1952.
- (77) Keck, J.C. and Littauer, R. : P.R. 86, 1051, 1952.
- (78) Keck, J.C. and Littauer, R. : P.R. 87, 195, 1952.
- (79) Keck, J.C. and Littauer, R. : P.R. 88, 139, 1952.
- (80) Keck, J.C., Littauer, R.M., O'Neill, G.K., Perry, A.M. and Woodward, W.M. : P.R. 93, 827, 1954.
- (81) Whalin, E.A., Schriever, B.D. and Hanson, A.O. : P.R. 94, 763, 1954.
- (82) Whalin, E.A. : P.R. 95, 1362, 1954.
- (83) Whalin, E.A., Schriever, B.D. and Hanson, A.O. : P.R. 101, 377, 1956.
- (84) Keck, J.C., Tollestrup, A.V. and Smythe, W.R. : P.R. 96, 850, 1954.
- (85) Allen, L. and Hanson, A.O. : P.R. 95, 629, 1954.
- (86) Allen, L. : P.R. 98, 705, 1955.
- (87) Aleksandrov, I.A., Delone, N.B., Slovokhotov, L.I., Sokol, G.A., and Shtarkov, L.N. : JETP 6, 472, 1958.
- (88) Yamagata, T., Barton, M.Q., Hanson, A.O. and Smith, J.H. : P.R. 95, 574, 1954.
- (89) Keck, J.C. and Tollestrup, A.V. : P.R. 101, 360, 1956.
- (90) Dixon, D.R. and Bandtel, K.C. : P.R. 104, 1730, 1956.
- (91) Tatro, C.A., Palfrey, T.R., Whaley, R.M. and Haxby, R.O. : P.R. 112, 932, 1958.
- (92) Bethe, H.A. and Peierls, R. : Proc. Roy. Soc. A148, 146, 1935
- (93) Marshall, J.F. and Guth, E. : P.R. 76, 1879, 1949.
- (94) Marshall, J.F. and Guth, E. : P.R. 76, 1880, 1949.

- (95) Marshall, J.F. and Guth, E. :P.R. 78, 738, 1950.
- (96) Schiff, L.I. :P.R. 78, 733, 1950.
- (97) Austern, N. :P.R. 85, 283, 1952.
- (98) Austern, N. :P.R. 108, 973, 1957.
- (99) Berger, J.M. :P.R. 94, 1698, 1954.
- (100) Levinger, J.S. :P.R. 97, 970, 1955.
- (101) Meyer, P. :Ann.de Phys. 2, 498, 1957.
- (102) Varshin, Y.P. :Nature 182, 1726, 1958.
- (103) De Swart, J.J. and Marshak, R.E. :P.R. 111, 272, 1958.
- (104) Nicholson, A.F. and Brown, G.E. :Proc. Phys.Soc. 73, 221, 1959.
- (105) Huddleston, R.H. and Lepore, J.V. :P.R. 87, 207, 1952.
- (106) Nagahara, Y. and Fujimura, J. : Prog. Theor. Phys. 8, 49, 1952.
- (107) Fujimura, J. :Prog. Theor. Phys. 9, 132, 1953.
- (108) Bruno, B. and Depken, S. : Arkiv. Fysik 6, 177, 1953.
- (109) Austern, N. :P.R. 87, 208, 1952.
- (110) Austern, N. :P.R. 100, 1522, 1955.
- (111) Feld, B.T. :N.C. 2, Suppl.1, 145, 1955.
- (112) Ito, D., Ono, M., Kato, T. and Takahashi, Y. : Prog. Theor. Phys. 15, 74, 1956.
- (113) Suzuki, R. : Prog. Theor. Phys. 15, 536, 1956.
- (114) Yamaguchi, Y. :P.R. 95, 1628, 1954.
- (115) Yamaguchi, Y. and Yamaguchi, Y. :P.R. 95, 1635, 1954.

- (116) Yamaguchi, Y. and Yamaguchi, Y: P.R. 98, 69, 1955.
- (117) Wilson, R.R. : P.R. 86, 125, 1952.
- (118) Wilson, R.R. : P.R. 104, 218, 1956.
- (119) Zachariassen, F. : P.R. 101, 371, 1956.
- (120) Zernik, W., Rustgi, M.L. and  
Breit, G. : P.R. 114, 1358, 1959.
- (121) Siegert, A.J.F. : P.R. 52, 787, 1937.
- (122) Levinthal, C. and Silverman, A.: P.R. 82, 822, 1951.
- (123) Walker, D. : P.R. 81, 634, 1951.
- (124) Walker, D. : P.R. 82, 300, 1957.
- (125) Walker, D. : P.R. 84, 149, 1951.
- (126) Keck, J.C. : P.R. 85, 410, 1952.
- (127) Keck, J.C. and Perry, A.M. : P.R. 86, 629, 1952.
- (128) Weil, J.W. and McDaniel, B.D. : P.R. 86, 582, 1952.
- (129) Weil, J.W. and McDaniel, B.D. : P.R. 90, 380, 1953.
- (130) Weil, J.W. and McDaniel, B.D. : P.R. 92, 391, 1953.
- (131) Rosengren, J.W. and Dudley, J.M.: P.R. 89, 603, 1953.
- (132) Wattenberg, A., Feld, B.T.,  
Godbole, R.D. : P.R. 90, 380, 1953.
- (133) Wattenberg, A., Feld, B.T.,  
Godbole, R.D., Odian, A.,  
Scherb, F. and Stein, P.C. : P.R. 94, 1000, 1954.
- (134) Murray, P.C., Scace, R.I.,  
Haxby, R.O., and Palfrey, T.R. : P.R. 94, 764, 1954.

- (135) Haxby, R.O., Whaley, R.M.,  
Matheson, W.E., Carlson, C.R.,  
and Matthews, F.S. : P.R. 96, 826, 1954.
- (136) Kikuchi, S. : P.R. 80, 492, 1950.
- (137) Kikuchi, S. : P.R. 81, 1060, 1951.
- (138) Kikuchi, S. : P.R. 83, 1255, 1951.
- (139) Kikuchi, S. : P.R. 86, 41, 1952.
- (140) Kikuchi, S. : P.R. 86, 126, 1952.
- (141) Miller, R.D. : P.R. 82, 260, 1951.
- (142) George, E.P. : Proc. Phys. Soc. A69, 110,  
1956.
- (143) Peterson, V.Z. : P.R. 96, 850, 1954.
- (144) Peterson, V.Z. and Roos, C.E. : P.R. 105, 1620, 1957.
- (145) Kerst, D.W. and Price, G.A. : P.R. 79, 725, 1950.
- (146) Kerst, D.W., Penfold, A.S.,  
Koester, L.J. and Smith, J.H. : P.R. 87, 197, 1952.
- (147) Terwilliger, K.M., Jones,  
L.W. and Jarmie, W.N. : P.R. 82, 820, 1951.
- (148) Jones, L.W. and Terwilliger,  
K.M. : P.R. 91, 699, 1955.
- (149) Baranov, P.S. and Goldanskii,  
V.I. : J.E.T.P. 1, 613, 1955.
- (150) Baranov, P.S., Goldanskii, (J.E.T.P. 6, 865, 1958.  
V.I. and Roganov, V.S. : (P.R. 109, 1801, 1958.
- (151) Tamor, S. : P.R. 77, 412, 1949.
- (152) Heidmann, J. : P.R. 80, 171, 1950.
- (153) Khoklov, Ju.K. : Zh. eksper. teor. fiz.  
23, 241, 1952.

- (154) Levinger, J.S. : P.R. 107, 554, 1957.
- (155) Myers, H., Odian, A., Stein, P.C. and Wattenberg, A. : P.R. 95, 576, 1954.
- (156) Odian, A., Stein, P.C., Wattenberg, A., Feld, B.T. and Weinstein, R. : P.R. 102, 837, 1956.
- (157) Wattenberg, A., Odian, A.C., Stein, P.C., Wilson, H., and Weinstein, R. : P.R. 104, 1710, 1956.
- (158) Barton, M.Q. and Smith, J.H. : P.R. 95, 573, 1954.
- (159) Barton, M.Q. and Smith, J.H. : P.R. 110, 1143, 1958.
- (160) Butler, S.T. : P.R. 87, 1117, 1952.
- (161) Weinstein, R.M., Odian, A., Stein, P.C. and Wattenberg, A. : P.R. 99, 1621, 1955.
- (162) De Wire, J.W., Silverman, A., and Wolfe, B. : P.R. 92, 519, 1953.
- (163) De Wire, J.W., Edwards, D.A., Wolfe, B. and Silverman, A. : P.R. 95, 629, 1955.
- (164) Dedrick, K.G. : P.R. 100, 58, 1955.
- (165) Yoshida, S. : Prog. Theor. Phys. 6, 1032, 1951.
- (166) Gottfried, K. : N.P.5, 557, 1958.
- (167) Brueckner, K.A., Eden, R.J. and Francis, N.C. : P.R. 98, 1445, 1955.
- (168) Hendel, H. : Zeit. f. Physik, 135, 168, 1953.
- (169) Johansson, S.A.E. : P.R. 97, 434, 1955.
- (170) Chuvilo, I.V. and Shevchenko, V.G. : J.E.T.P. 5, 1090, 1957.
- (171) Chuvilo, I.V. and Shevchenko, V.G. : J.E.T.P. 7, 410, 1958.

- (172) Bazhanov, E.B., Volkov, I.M.  
and Kul'chitskii, L.A. : J.E.T.P. 8, 224, 1958.
- (173) Gorbunov, A.N. and Spiridinov,  
V.M. : J.E.T.P. 6, 16, 1958.
- (174) Gorbunov, A.N. and Spiridinov,  
V.M. : J.E.T.P. 7, 596, 1958.
- (175) Gorbunov, A.N. and Spiridinov,  
V.M. : J.E.T.P. 7, 600, 1958.
- (176) Whitehead, C., McMurray, W.R.,  
Aitken, M.J., Middlemas, N.  
and Collie, C.H. : P.R. 110, 941, 1958.
- (177) Weinstein, R., Stein, P.C.,  
Ozaki, S., Rankin, W., and  
Wattenberg, A. : M.I.T. Progress Report  
: August 1956. P.64.
- (178) Lalovic, B. : Thesis - Glasgow University  
1959.
- (179) Meyer, B and Stodiek, W. : Rev. Sci. Inst. 24, 76, 1953.
- (180) Atkinson, J.R., McFarlane,  
W., Reid, J.M. and Swinbank,  
P. : Nucl. Inst. 1, 152, 1957.
- (181) Menzies, D. : Thesis - Glasgow University  
1959.
- (182) Cence, R.J. : U.C.R.L. Report 8921.
- (183) Reid, J.M. and Lalovic, B. : Proc. Phys. Soc. 76, 65,  
1960.
- (184) Smith, J. and Larson, A. : Private communication.
- (185) Stein, P.C., Odian, A.C.,  
Wattenberg, A. and Weinstein,  
R. : P.R. 119, 348, 1960.
- (186) Serber, R. : P.R. 72, 1114, 1947.
- (187) Oxley, C.L., Cartwright,  
W.F., Rouvina, J., Baskir,  
E., Klein, D, Ring, J and  
Skillmann, W. : P.R. 91, 419, 1953.
- (188) Wolfenstein, L. : Ann. Rev. Nucl. Sci. 6,  
43, 1956.

- (189) Rosentsveig, L.N. : J.E.T.P. 4, 280, 1957.
- (190) Guth, E. and Mullin, C.J. : P.R. 76, 234, 1949.
- (191) Czyz, W. and Sawicki, J. : N.C. 3, 864, 1956.
- (192) Czyz, W. and Sawicki, J. : N.C. 5, 45, 1957.
- (193) Clementel, E. and Villi, C. : Private communication to  
Czyz, W. and Sawicki, J.
- (194) Hsieh, S.H. : N.C. 4, 138, 1956.
- (195) Hsieh, S.H. : Prog. Theor. Phys. 16,  
68, 1956.
- (196) Austern, N. : P.R. 108, 973, 1957.
- (197) Czyz, W. and Sawicki, J. : P.R. 110, 900, 1958.
- (198) De Swart, J.J. : Physica 25, 233, 1959.
- (199) De Swart, J.J. and Marshak, R.E: Physica 25, 1001, 1959.
- (200) Signell, P.S. and Marshak, R.E: P.R. 109, 1229, 1958.
- (201) De Swart, J.J., Czyz, W. and  
Sawicki, J. : P.R. Letters 2, 51, 1959.
- (202) Kawaguchi, M. : P.R. 111, 1314, 1958.
- (203) Zernik, W., Rustgi, M.L. and  
Breit, G. : P.R. 114, 1358, 1959.
- (204) Feld, B.T. : N.C. 12, 425, 1954.
- (205) Fermi, E. : P.R. 91, 947, 1953.
- (206) Yang, C.N. : Private communication to  
E. Fermi.
- (207) Watson, K.M., Keck, J.C.,  
Tollestrup, A.V. and Walker,  
R.L. : P.R. 101, 1159, 1956.
- (208) Wilson, R.R. : P.R. 110, 1212, 1958.

- (209) Peierls, R.F. : P.R. Letters 1, 174, 1958.
- (210) Sakurai, J.J. : P.R. Letters 1, 258, 1958.
- (211) Daniels, J.M., Grace, M.A.,  
and Robinson, F.N.H. : Nature 168, 780, 1951.
- (212) Gorter, C.J., Poppema, O.J.,  
Steenland, M.J. and Beun, J.A.: Physica 17, 1050, 1951.
- (213) Bleaney, B., Daniels, J.M.,  
Grace, M.A., Halban, H., Kurti,  
N., and Robinson, F.N.H. : P.R. 85, 688, 1952.
- (214) Bleaney, B., Daniels, J.M.,  
Grace, M.A., Halban, H., Kurti, Proc. Roy. Soc. A221,  
N., Robinson, F.N.H, Simon, F.E.:170, 1954.
- (215) Gorter, J., Tolhoek, H.A.,  
Poppema, O.J., Steenland,  
M.J. and Beun, J.A. : Physica 18, 135, 1952.
- (216) Poppema, O.J., Beun, J.A.,  
Steenland, M.J. and Gorter, C.J: Physica 18, 1235, 1952.
- (217) Poppema, O.J., Steenland, M.J.,  
Beun, J.A. and Gorter, C.J. : Physica 21, 233, 1955.
- (218) Wheatley, J.C., Huiskamp, W.J.,  
Diddens, A.N., Steenland, M.J.  
and Tolhoek, H.A. : Physica 21, 841, 1955.
- (219) Stein, P.C. : P.R. Letters 2, 473, 1959.
- (220) Connolly, P.L. and Weill, R. : Bull. Am. Phys. Soc.  
Ser. II, 4, 23, 1959.
- (221) Dickson, J.M., Rose, B. and Proc. Phys. Soc. A68,  
Salter, D.C. : 361, 1955.
- (222) Dickson, J.M. and Salter, D.C.: N.C. 6, 235, 1957.